Effect of Crosslinking on Carbon Nanotube Materials through Chemical Treatment and Irradiation

A Dissertation Presented for the

Doctor of Philosophy

Degree

The University of Tennessee, Knoxville

Xinyi Lu

May 2017

DEDICATION

In memory of my beloved father, Dr. Lianhai Lu.

ACKNOWLEDGEMENTS

The work in this dissertation would not have been possible without the kind assistance and endless support from a number of people. First and foremost, I would like to thank my advisor Dr. Jimmy Mays for his technical guidance and his patience with me in the past few years, his philosophy will always inspire me. I am also extremely grateful to Dr. Namgoo Kang who spent hours and hours sharing his knowledge and walking me through the techniques. I thank both of them for guiding me through the graduate school.

In addition, I would like to thank the rest of my committee members, Dr. Alexei P. Sokolov, Dr. Bin Zhao, Dr. Sheng Dai, Dr. Gajanan S. Bhat and Dr. Joshua R. Sangoro for their valuable time and suggestions to my work.

I would like to thank Dr. Kunlun Hong and Dr. Weiyu Wang, the past group members who altruistically helped younger researchers as mentors as well as friends. Their encouragement and suggestions to me in research and career helped me through the hard times.

I am grateful to my collaborators, Dr. Maria C. Evora, Dr. Nitilaksha Hiremath, and Benjamin R. Ripy, it was a pleasure to work with them on the project, and the work would not have been completed without their contribution. Many thanks to Dr. Amit Naskar who generously provided assistance on mechanical properties, to Dr. Roberto Uribe for his guidance through electron beam radiation. I also would like to thank Dr. Wenwen Wang, Dr. Fei Fan and Dr. Yuewen Xu for giving me the opportunity to contribute to their work.

Characterization is one of the most important aspect in the research of nano materials. I would like to thank Mr. Tom Malmgren, Dr. Bradley Miller, and Ms. Katrina Pangilinan for maintaining polymer characterization lab, Dr. John Dunlap for his constant help with the electron microscopes, and Alexis Dale for setting up Raman Spectroscopy. I thank all of them for their patience in trainings, and their effort to keep the instruments always ready to use.

I would like to thank all the Mays' group members who made this journey enjoyable. All the best to the past members, including Dr. Vikram Srivastiva, Dr. Justin Roop, Dr. Sachin Bobade, Dr. Beom-Goo Kang, and Dr. Christopher Hurley. I thank the current members, including Dr. Pryank Shah, Dr. Kostas Misichronis, Hongbo Feng, Wei Lu, Huiqun Wang, for their sweet companion, and best of luck to all of them. Thanks to my friend Le Yu who accompanied me through the writing process in the library.

The experience as a mass spectrometry student operator was important for my career as well as personal growth. I would like to thank the department for giving me the opportunity, and I thank Dr. Liguo Song, Dr. Shawn Campagna, Dr. Hector Castro, Carson Prevatte for their help and discussion on the technical details of mass spectrometry.

I would like to extend my thanks to everyone behind the scene, that made the graduate program run smoothly. I thank Dr. Frank Vogt for his patience and prompt response to my questions. I thank Ms. Julie R. Harden for dealing with my graduation process. I am also grateful to Rhonda Wallace, Shelby Chasity, Pam

Roach and Rachel Rui for their administrative work; Beverly Adams, Gail Cox, and Jessica VanBrunt for keeping chemstore convenient; Johnny Jones, Tim Free and Bo Bishop for their technical support on electronics, machinery, and glassware. Special thanks to the past member of IT support, Bill Gurley, for helping me install a copy of Origins on my MacBook, which made data processing even possible through the rest of my graduate study.

I extend my thanks to Dr. Yang Li, Dr. Lingling Wu and all the other researchers in the Li's group at Dalian University of Technology. Without their help, I would not have started my life at UTK.

Finally, I would not be here today without the tireless unconditional support from my fiancé, Yongchi Xiao, thank you for your encouragement, strategic planning, and all your love. To my mother, Ms. Yue Wang, my sister Xinran Lu, my grandmother Ms. Yajuan Guo, and everyone else in the family, my sooon-to-be parents in law, you should know that your support was worth more than I can express on paper.

ABSTRACT

Carbon nanotubes (CNTs) exhibit a variety of exceptional properties, especially their ultrahigh tensile strength on the order of 100GPa show promise for constituting the next-generation carbon fiber. However, challenges remain to translate these properties into useful technology, primarily due to the sliding of the tubes past one another under tensile loading. The work presented in this dissertation is focused on enhancing the interaction between the CNTs and their bundles in a macro-assembly, in order to improve the tensile properties of the material.

Applying inter-tube crosslinks has been predicted to significantly enhance the stress transfer between the CNT components. We developed a novel chemical crosslinking method for reinforcement of carbon nanotube fibers (CNTFs) employing benzocyclobutene (BCB)-based polymers. This simple one-step mechanism achieves covalent functionalization of CNT surface and 3D crosslinking simultaneously, in the solid-state. The denser packing of CNTF, impregnated polymer and establishment of covalent crosslinking after the treatment all contributed to the enhancement of tensile strength by 250%.

Several process parameters were investigated for the BCB-induced crosslinking of CNTF. A series of poly(styrene-r-4-vinyl-benzocyclobutene) (PS-VBCB) with varying BCB/PS content were synthesized and the copolymer with PS content of 80% lead to the optimum result, possibly due to the BCB-BCB collapsing to form undesired defects at high percentage of BCB. The concentration of the

polymer solution for infiltration into CNTF was found to be critical in determining the amount of infiltrated PS-VBCB polymer. 0.05% wt or 0.1% wt results in highest mechanical properties. Pure heating of CNTF free from BCB degrades the load transfer, which further supports the positive effect of BCB crosslinking on CNTF.

Electron-beam (e-beam) induced crosslinking alters the morphology and properties of carbon structures. In this dissertation, the effect of e-beam irradiation on CNTF was observed, both positive and negative phenomena. At the presence of functional species, e-beam initiates functionalization by creating radicals on CNT. CNTF grafted with acrylic acid exhibited improvement in tensile strength by 77%. Finally, a preliminary attempt was made to combine the e-beam and BCB chemistry on the CNT materials.

TABLE OF CONTENTS

LIST OF TABLES

LIST OF FIGURES

LIST OF SCHEMES

CHAPTER I

INTRODUCTION TO PROPERTIES AND MODIFICATION OF CARBON NANOTUBE MATERIALS

1.1 Background

Carbon Fiber and related composites are of significant importance for wide applications in aerospace technologies, military armors, wind turbines and sporting goods. The exceptional properties of carbon fibers including high strength and chemical resistivity are primarily due to their unique structure: sp^2 hybridized carbon atoms organized in honeycomb-shaped crystals.[1]

Carbon nanotubes (CNTs) are perfect resemblance of perfect carbon fibers on the nanometer scale. CNTs are an allotrope of carbon in the form of seamless cylinders of sp^2 hybridized graphene sheets.[2] Depending on the number of walls, CNTs are classified into single-wall (SWNT) and multi-wall (MWNT), as illustrated in **Figure 1.1**. Diameters of SWNTs and MWNTs are typically 0.4[3] to 3 nm and 1.4 to 100 nm,[4] respectively, and the length of CNTs range from less than 100 nm to several centimeters.[2] The resulting aspect ratio is so high that it can be considered

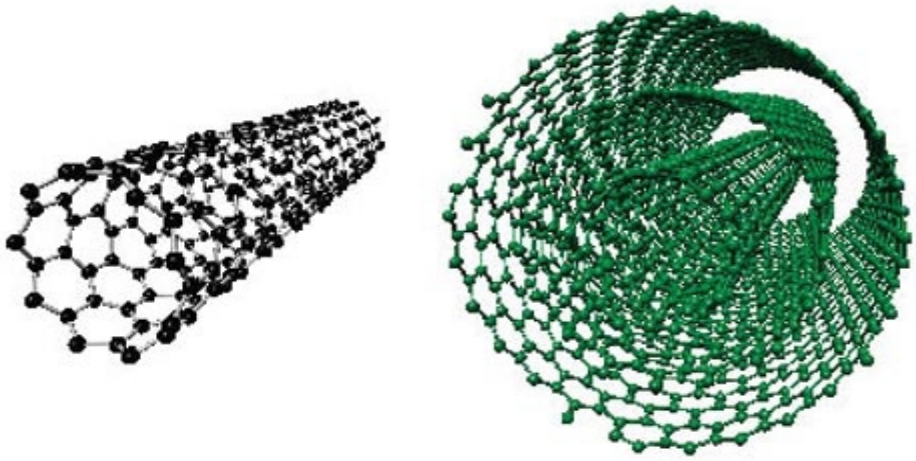

Figure 1.1 Illustration of SWNT(left) and MWNT(right), from physicsworld.com

from the electronic point of view as a one-dimensional structure.[5]

As a result of such unique structure, CNTs exhibit a group of exceptional physical properties. Both theoretical[6-8] and experimental[9-11] studies confirm superb mechanical properties of CNTs. SWNT bundles exhibit tensile modulus of 1.0TPa and strength of 50 GPa.[11] Individual MWNTs show tensile modulus of 1.0 TPa and strength of 100 GPa, when only the cross-sectional area of the CNT is considered.[12] The Young's modulus of 1 TPa is much higher than that of conventional carbon fibers (200-800GPa), and the tensile strength on the order of 100 GPa is over 10-fold higher than any industrial fiber. In addition, CNTs exhibit high electric and thermal conductivities. SWNTs can be metallic or semi-conductive depending on the chirality of the tube, which is orientation of the graphene sheet with respect to the CNT axis. MWNTs are typically metallic and can carry currents of up to 4×10^9 A cm^{-2}, which is more than 1000 times greater than those of metals such as copper.[13] Individual SWNTs can have a thermal conductivity of 3500 W m^{-1} K^{-1}, exceeding that of diamond.[14] Ever since the discovery of CNTs by Iijima in 1991,[15] the commercial production and application of CNTs have been continuously increasing in areas ranging from composites,[16] supercapacitors,[17, 18] sensors,[19] to field emission sources.[20] Most of the applications have been found in bulk composite materials and thin coatings,[2] where CNT fillers are randomly oriented throughout the material.

Incorporation of nanotubes as fillers into composites can dramatically increase the electrical conductivity and mechanical properties of the material.[4]

However, it is well known that untreated CNTs have poor compatibility with other materials. A general problem is that CNTs tend to form bundles of parallel tubes that contain up to hundreds of tubes arranged in a hexagonal lattice,[21] thus only part of the surface area is available for stress transfer with the matrix.[22] In addition, facile sliding of individual tubes and between concentric walls in MWNTs occurs.[10] Functionalization of CNTs has been found to significantly enhance the dispersion of CNT in various matrices at higher loading. In addition to covalent and noncovalent chemical functionalizations, high energy radiation provides a facile route toward modification of CNTs. Besides utilizing CNTs in composites, numerous well-aligned macroscopic forms of CNTs have been developed, such as horizontal and vertical CNT arrays, yarns and sheets. Unfortunately, the current mechanical, electrical, and thermal properties of these macrostructures remain a fraction of those of the individual CNTs. In this chapter, functionalization of CNTs for composites is briefly reviewed, radiation is introduced as a scalable functionalization method, and finally the fabrication and enhancement of pure CNT macrostructures is discussed, with an emphasis on the crosslinking of CNT assemblies.

1.2 Chemical Functionalization of CNTs

As mentioned above, pristine CNTs are difficult to disperse in water or common organic solvents,[23] thus making them difficult to process. Functionalization of CNTs, (essentially the attachment of chemical moieties onto the tubes) provide a promising path to overcome this barrier. Functionalization

allows the CNT to show improved solubility, and become easier to incorporate into the matrix to better utilize the excellent properties of CNTs. Selective functionalization is also capable of tuning the electrical and mechanical properties of CNTs since modification could result in different properties. The reactivity of carbon nanotubes is primarily driven by curvature of the tubular structure.[24] As displayed in **Figure 1.2**, for an sp^2 hybridized trivalent carbon, aplanar structure is highly favored, where the planar bond angle is 120° and pyramidalization angle is 0°. On the other hand, there is a 19.5° pyramidalization angle in sp^3 hybridized carbons.[25] Conversion of carbons on the nanotube from sp^2 to sp^3 thus directly relieves the local strain at the junction point and mitigates the strain at nearby carbons.[25] Since the curvature is even more severe at the end caps of CNTs, the reactivity of carbons at such locations is expected to be higher. Generally, there are several types of functionalizations, as illustrated in **Figure 1.3**. Noncovalent functionalization utilizes physical adsorption forces, such as Van der Waal's interactions (e.g. polymer wrapping) and π-π stacking. Covalent functionalization involves formation of stable chemical bonds between the introduced moiety and the nanotube scaffold. The hybridization of the carbon at the reaction site is then converted from sp^2 to sp^3. The local defects, such as terminals, open holes, pentagon-heptagon sites, can also be utilized for functionalization, and are usually further oxidized to carboxylic acid groups to allow subsequent reactions. In a few studies, insertion of small molecules in to the tubular holes have also been discovered.

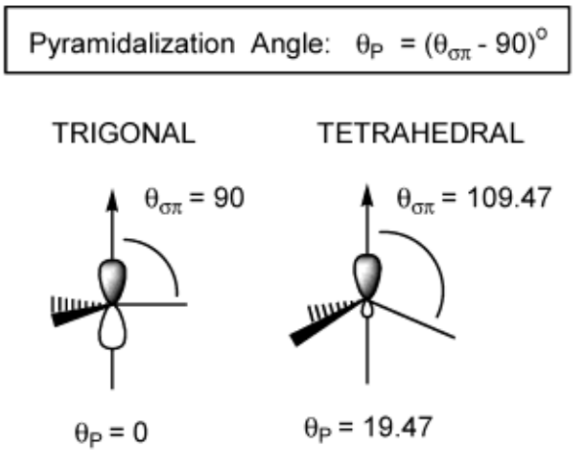

Figure 1.2 Diagram of pyramidizational angle (θ_p).[25]

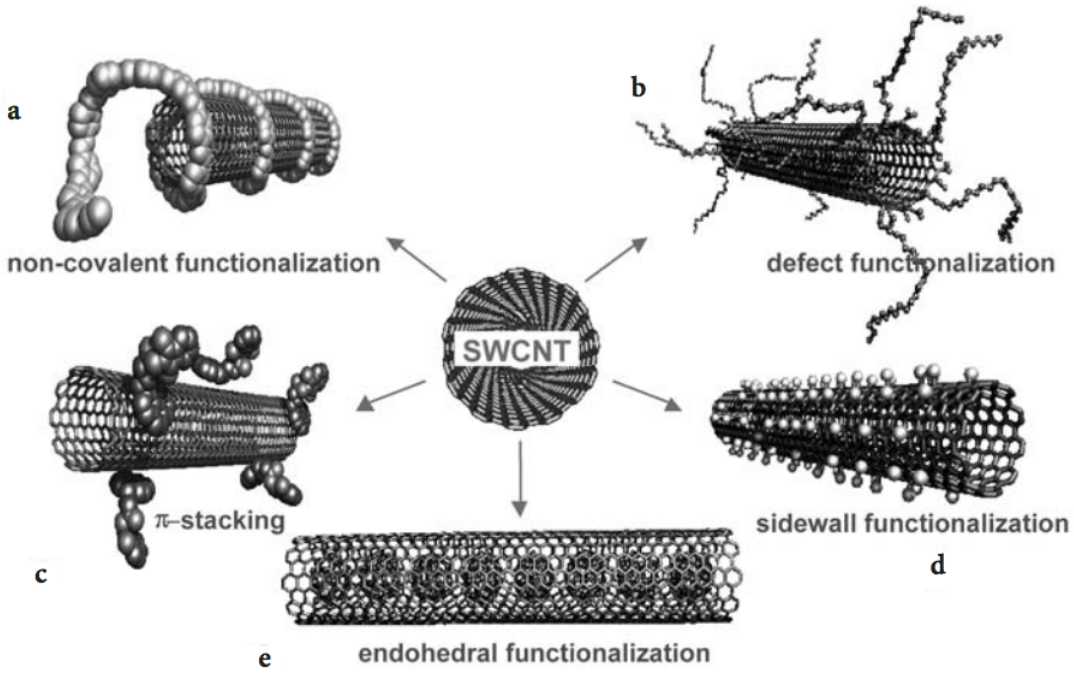

Figure 1.3 Different possibilities for the functionalization of SWCNTs. a) Noncovalent functionalization with polymers. b) Defect-group functionalization. c) Noncovalent functionalization with molecules through p-stacking. d) Sidewall functionalization. e) Endohedral functionalization, in this case C_{60}@SWCNT[26]

1.2.1 Non-covalent functionalizations

CNTs are able to form non-covalently functionalized complexes, typically through surfactant stabilization,[27-30] $\pi - \pi$ stacking with aromatic small molecules, physical wrapping with polar polymers, and direct interaction with biomolecules. The fact that the dispersibility of CNTs can be enhanced without sacrificing their extended π -network has attracted much interest on non-covalent functionalization.[31]

One of the initial attempts was the use of amphiphilic surfactants such as sodium dodecylsulfate (SDS) or benzylalkonium chloride to disperse CNTs in aqueous solutions.[27-29] This technique was applied to solvate and separate carbon nanotubes by their sizes or from fullerene impurities, with surfactant concentration at 0.1-2 wt.%. Through the process (typically involving sonication), it is believed that bundles of CNT have been disintegrated into individual CNTs and trapped in the hydrophobic interior of surfactant micelles. Near the critical micelle concentration (CMC) of the surfactant, most surfactant molecules are adsorbed onto the surface of graphitic carbon instead of forming individual micelles.[32, 33] The self-assembly of surfactants on the nanotube surface is speculated to be parallel to the axis of the tube, instead of along the cross-section, as illustrated in **Figure 1.4**.[34] In one study, the best surfactant to solvate CNTs was found to be sodium dodecylbenzene sulfonate (NaDDBS) which consists of an aromatic ring in addition to an alkyl chain and hydrophilic sulfonate headgroup.[34] The CNTs can be individually stabilized by NaDDBS up to 63% (determined by atomic force

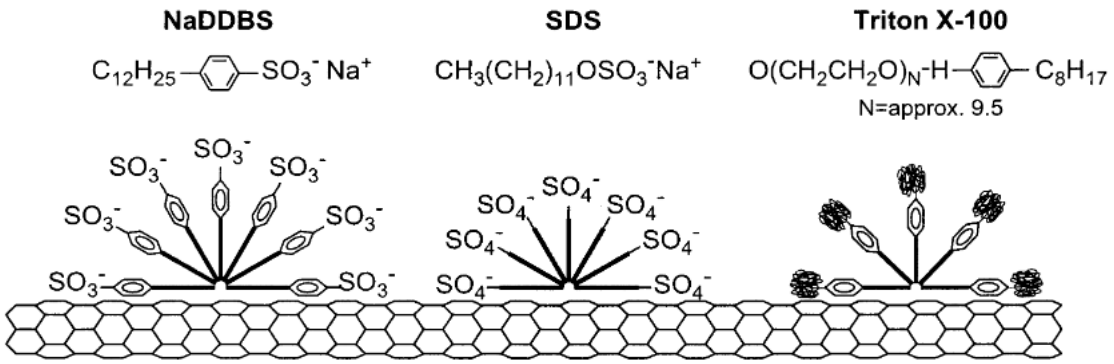

Figure 1.4 Scheme of the adsorption of surfactants onto the nanotube surface. Surfactant molecules are self-assembled on the tube surface parallel to the cylindrical axis.[34]

microscope, AFM) at 20 mg/mL in aqueous solution, while the capability of Triton-X is on the order of 2 mg/mL.[34] In a more recent study, the dispersion power of several surfactants has been compared, concluding that Triton-X100 performs better than sodium dodecyl sulfate (SDS) and CNT-to-surfactant ratio has been indicated as the most important parameter to optimize nanotube dispersion.[35] The downstream applications of surfactant-assisted CNT dispersions include fabrication of carbon paste electrode to determine the electrochemical behavior of biomolecules in pharmaceutical formulation,[36] and utilizing the negative charge provided by the surfactant for fabrication of multi-layer films.[37] In addition, this technique creates the possibility to spin CNT solutions into macroscopic assemblies using the traditional wet-spinning methods,[38-40] and the details will be further discussed in section 1.4.

Besides interaction with surfactants through Van der Waal's forces, π-π stacking with aromatic molecules is another important force to be utilized for solubilizing CNT. The most widely applied molecules under this category include pyrene and porphyrin. Simulation showed that the interaction between nanotubes and aromatic small molecules such as benzene and benzoquinone derivatives might be efficient for controlling electronic properties of CNTs through noncovalent functionalization.[41] Experiments show that the functionalization of pyrene onto CNT is irreversible, since no reduction in functional group was observed after redissolving of the functionalized material in solvents or aqueous solutions.[42] This is a fact that enables further modification of pyrene derivative with desired

moieties.[43] The functionalization of CNT with pyrene is demonstrated by modification of CNT surface using 1-pyrenebutanoic acid succinimidyl ester (the structure is illustrated in **Figure 1.5**.[44] The succinimidyl ester group is highly reactive and could be used to immobilize protein molecules through nucleophilic substitution reactions with amine moieties commonly observed on the surface of protein.[44] The immobilized biosystems introduces recognition properties to CNT materials, which is promising for the development of biosensors. Simmons et al. also studied the functionalization of CNT with a pyrene derivative, pyrene carboxylic acid (PCA).[45] Stable aqueous dispersion of CNT is obtained through the modification and composite was prepared with polycarbonate matrix.[45] This result shows that PCA enhances the CNT-polymer adhesion thus improving the dispersion of SWNT throughout the matrix.[45] Similarly, other forms of pyrene have

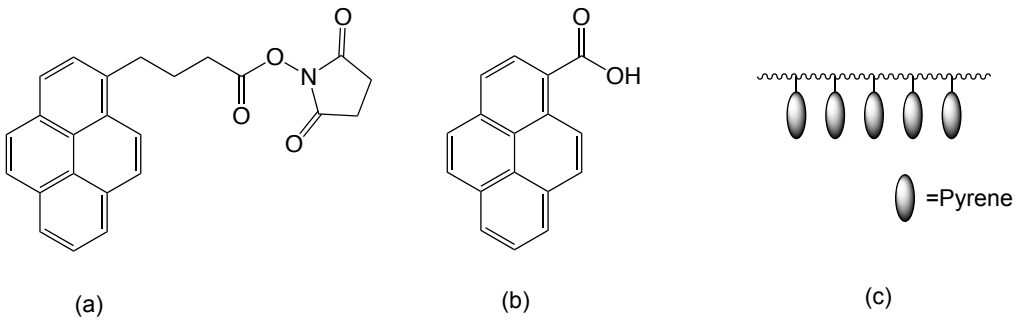

Figure 1.5 Pyrene derivatives for noncovalent functionalization of CNT. (a) 1-Pyrenebutanoic acid succinimidyl ester for immobilization of proteins through nucleophilic substitution of the succinimidyl group with amines on protein molecules. (b) Pyrene carboxylic acid to introduce versatile acid groups onto CNT as an alternative for oxidation. (c) Copolymer with pyrene as pendent group.

also been proved to enhance the solubility of CNT in solvents and water, such as polymers bearing pyrene pendent groups on the backbone, as illustrated in **Figure 1.5 (c)**.[42, 46] Pyrene-CNT interaction can also be utilized to introduce polymers onto the nanotube surface, which is beneficial for dispersion of CNT in the corresponding polymer matrix, as in the case that modifies CNT with pyrene endcapped polystyrene and subsequently dispersing it in a polystyrene matrix.[47] The noncovalent interaction of CNTs with pyrene and porphyrin derivatives leads to change transfer and altered electronic structure of CNTs,[48, 49] which can be utilized as novel electron donor-acceptor nanohybrids.[50-52] The same π-π stacking between pyrene derivative [17-(1- pyrenyl)-13-oxa-heptadecanethiol (PHT)] and CNTs is also applied by Liu et al. to coat a layer of gold nanoparticle on the nanotube surface (see **Figure 1.6**).[53]

Conjugate polymers carrying hydrophilic or hydrophobic groups are also capable of effectively dispersing CNTs in aqueous or organic media through establishment of specific and directional π-π stacking with the graphitic surface of the nanotubes.[48, 54, 55] Interestingly, polymers such as poly(m-phenylene vinylene) (PmPV) and poly(3-hexylthiophene) (P3HT) exhibit helical wrapping around the tube, as evidenced by atomic force microscope (AFM) and scanning tunneling microscope (STM).[56, 57] The unspecific physical adsorption of non-conjugate random-coil type polymers such as polystyrene and polypyrrolidone onto the nanotubes is also considered a form of non-covalent functionalization.[58, 59] Baskaran et al. suggested the functionalization is based on π -H interaction.[60] The

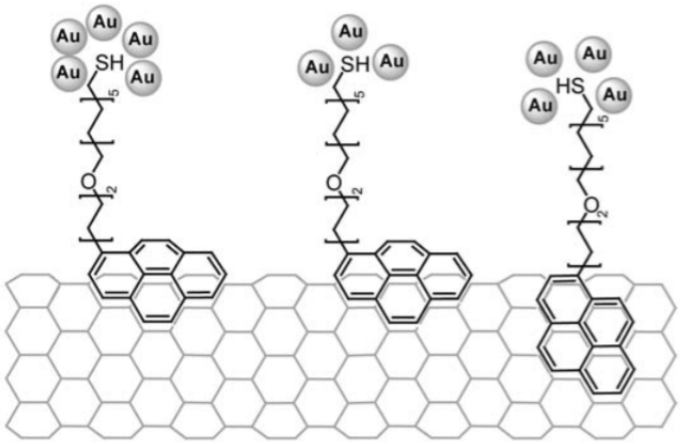

Figure 1.6 π-π stacking of 17-(1-pyrenyl)-13-oxa-heptadecanethiol (PHT) with CNTs and self-assembly of gold nanoparticles[53, 61]

adsorption is thermodynamically favored because of the large reduction of CNT surface energy.[62]

Similarly, biomolecules are employed to enhance the dispersion of CNTs both in aqueous and organic solutions. These biomolecules include saccharides,[63, 64] proteins,[44] enzymes and DNA.[43, 65, 66]

1.2.2 Covalent Functionalization

Covalent chemistry allows for attachment of functional groups through formation of stable chemical bondings, converting sp^2 hybridized carbons on the graphitic cylinder into sp^3 configuration. In contrast to noncovalent functionalization, covalent chemistry enhances the dispersion and miscibility of CNTs throughout various media at a price: inevitable disruption of the honeycomb structure and decrease in electrical/ electronic properties.[67] However, covalent functionalization on CNT does have one advantage over its counterpart, given that chemical bondings are generally considered more stable to thermal treatment than labile non-covalent forces. The most commonly applied covalent functionalization reactions are summarized in **Figure 1.7**. They include defect oxidation, halogenation, carbine/nitrene addition, diaozium arylation, 1,3-dipolar cycloaddition, [4+2] cycloaddition, and many others will be discussed in detail.

Oxidation of CNT introduces oxygen-containing functional groups onto the nanotube surface, such as carboxylic acid, hydroxyl, carbonyl, ester, and epoxy moieties. The introduced functional groups significantly enhance the dispersion of

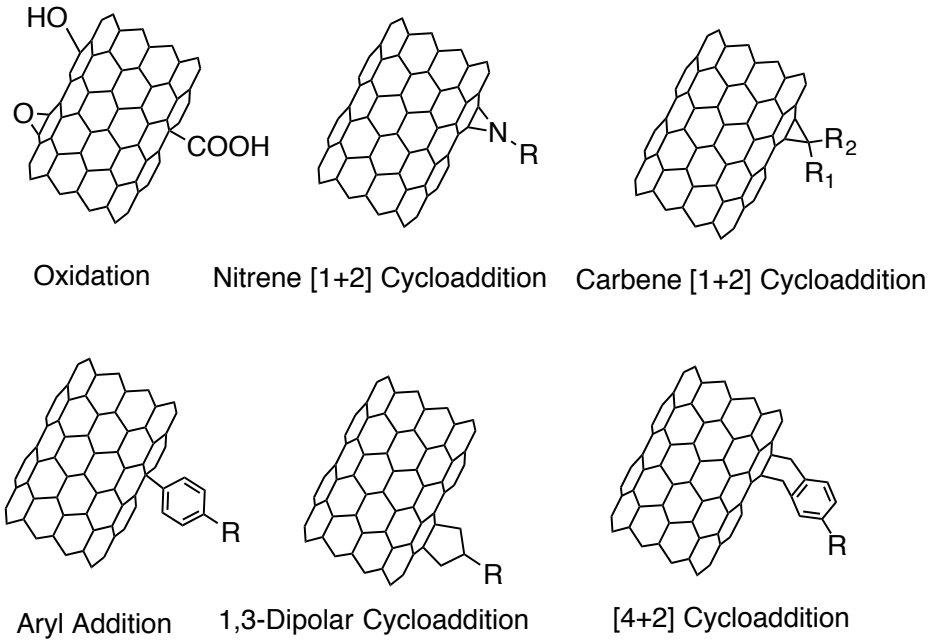

Figure 1.7 The most commonly applied Covalent functionalization reactions, including oxidation, nitrene and carbine addition, aryl additions, 1,3-dipolar cycloaddition, and [4+2] cycloaddition.

CNT in aqueous solutions. On the other hand, oxidation typically requires harsh conditions, such as sonication in concentrated strong acid (nitric acid[68, 69] and its mixture with sulfuric acid[70]), and exposure to oxidative gases (e.g. ozone[71]). The reactions typically occur at defect sites, such as curvature, dangling bonds, and open ends of the tube, therefore the functional groups are unevenly distributed along the axis of the tube. The extreme environment inevitably results in cleavage of the tube,[72] and opening of tube tips,[73] which potentially sacrifices the properties of CNTs. The oxidation chemistry is very versatile, in terms of the possibility of many further modifications on the carboxylic acid groups, including amidation and esterification. In such cases, the carboxylic acid is first activated by thionyl chloride ($SOCl_2$),[73, 74] followed by coupling with amines or alcohols using dicyclohexyl-carbodiimide (DCC) as dehydrating agent.[54, 75, 76]

Nitrene and carbene based additions was first achieved by Holzinger and coworkers, and the resulting material was characterized by NMR, electronic absorption spectroscopy, and AFM.[77] Several bifunctional crosslinkers based on nitrene chemistry have been applied to link bundles of CNTs in a buckypaper.[78] Spectroscopy results revealed that the electronic properties of the CNTs did not change on a large scale, indicating successful functionalization at low degree of perturbation to the graphitic network.[79]

Aryl addition onto CNT can be achieved by heating aniline derivative to 60°C in the presence of a catalyst generating aryl diazonium intermediate insitu, as illustrated in **Scheme 1.1**.[80] An alternative way to perform this type of

functionalization is applying preformed diazonium salt.[81] Significant amount of functional groups can be attached through this method, estimated as high as one out of 20 carbons.

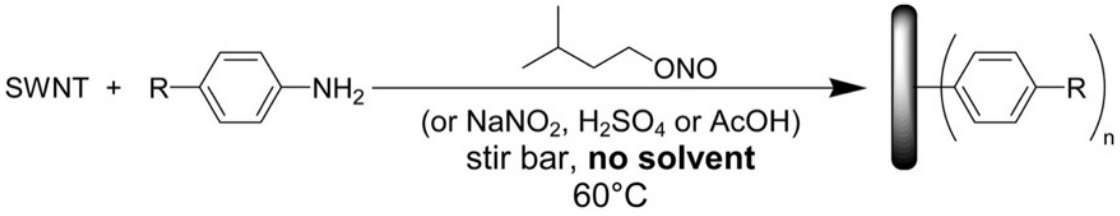

Scheme 1.1 Solvent-Free aryl addition Functionalizations of CNT using 4-Substituted Anilines and catalysts[80]

1,3-dipolar cycloaddition on carbon nanomaterials is also referred to as Prato reaction. It was first widely applied in the functionalization of fullerenes.[82] In this reaction, azomethine ylides is generated insitu by condensation of an α-amino acid and an aldehyde, which then forms pyrrolidine rings on CNT surface, as shown in **Scheme 1.2**.[83]

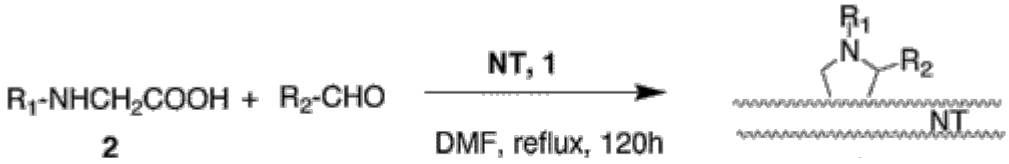

Scheme 1.2 1,3-dipolar cycloaddition of azomethine ylides, generated by condensation of an α-amino acid and an aldehyde[83]

Benzocyclobutene (BCB) is a class of molecules that undergoes Diels-Alder [4+2] Cycloaddition with carbon double bonds. The first application of this molecule in covalent functionalization of CNTs is demonstrated by Sakellariou et al, as

illustrated in **Scheme 1.3**.[84] The highly strained 4-membered ring on BCB is susceptible to thermal ring-opening to form a o-quinodimethane intermediate and readily reacts with aromatic carbons on CNTs. Versatile moieties can be introduced to CNTs by using corresponding BCB derivative. The advantage of this functionalization include: 1) functionalization sites afford relatively statistical distribution along the axis of the CNTs as opposed to oxidation, 2) not requiring catalyst, and 3) no small molecule byproducts released.

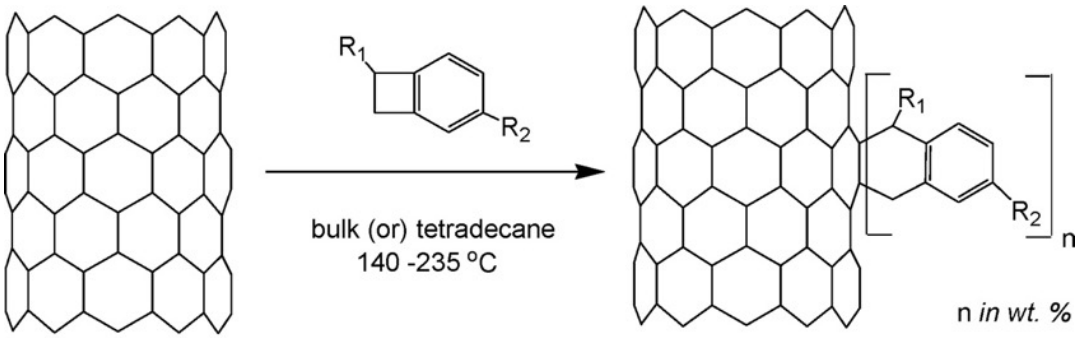

Scheme 1.3 Diels-Alder [4+2] Cycloaddition of BCB derivatives with CNT in bulk or tetradecane with temperature elevated to 140-235°C[84]

1.3 Radiation Effects on Carbon Nanostructures

The effects of particle irradiation (such as electron and ions) in solids has been subject to investigation since the 1950s due to interest in irradiation-induced degradation of metals, semiconductors and graphitic components of fission and fusion reactors.[85, 86] Modification of carbon materials using radiation has thus been an intense field of research with graphite being a reactor material. As the new

graphitic carbon materials emerged, namely fullerene, carbon nanotubes, and graphene, the need for research on their behavior under particle irradiation has continued.

In most cases, the carbon nanostructures were first discovered with the aid of transmission electron microscopes (TEM), where the sample specimens were subject to electron of energy around 100-300 keV. This instrument is the most powerful tool in investigating the structures on the nanometer scale, but the structure could be inevitably altered by electron radiations and this sometimes lead to misinterpretation of observations. Extensive research has been performed on imaging electron irradiation-induced defect on carbon structures.[87-90]

Although traditional studies mainly focused on damaging effect of radiation on solid matter, more recent reports on high energy particle or electromagnetic wave irradiation demonstrated that irradiation can have beneficial effects on nanostructures. Under certain circumstances, the structure of carbon nanotubes can be deliberately engineered using irradiation, such as generation of inter-tube connections, or merging in a controllable way. As a result, irradiation can be used to mediate the mechanical[91], electronic[92, 93] and magnetic[94, 95] properties of carbon nanostructures.[96]

This section briefly reviews the effect and application of radiation on carbon nanostructures beginning with a touch on the basics in the radiation physics.

1.3.1 High-energy particle radiation on solid matter

The effect of highly energetic particle (such as an electron or ion) irradiation on an atom involves several mechanisms on different scales and dimensions.[97] The most important primary radiation effects are[97]:

-electronic excitation or ionization of individual atoms

-electronic excitation of collective atoms such as formation of plasmons

-breakage of bonds or crosslinking

-mechanical movement that lead to heating of the target

-sputtering of atoms from the surface

Secondary effects include[97]:

-emission of photons (x-rays or visible light)

-emission of secondary or Auger electrons

Depending on the energy of the radiating particle, and the specific type of material being radiated, the effect of each interaction mentioned above on the damage of the sample could vary significantly. Considering carbon material, these interactions could be divided into those that lead to a displacement of atoms (knock-on effects) and those that do not (excitations). It is intuitive that the importance of excitations decreases with higher particle energy, whereas the knock-on effects become more significant. Insulators are subject to all kinds of damage induced by irradiation. In metals, the excitations such as ionization are readily quenched due to the existence of free electrons. This makes the metals relatively stable under low energy irradiation, and only subject to damages when

knock-on effects take place at high energy irradiation. Similarly, knock-on atom displacement is the major source of radiation induced alteration of carbon nanostructures due to the semi-metal properties of their graphitic basic units.

The knock-on displacement event is completed in the following sequence[97]:

-energy transfer from the projectile to the nucleus (primary knock-on)

-interatomic collisions (cascade)

-transfer of energy above the threshold level to form stable defects that do not spontaneously recombine

-thermal migration of point defects

If highly energetic electron was considered as projectile, the collision with an atom could be described by the following model. The energy transfer is minute due to great difference in masses of the two colliding objects, and the change in direction of the electron accounts of almost all of the momentum transfer, as shown in **Figure 1.8**.

The energy transferred to the nucleus depends on the angle between the initial direction of the particle and the direction in which the knocked nucleus is scatterd (θ), and the maximum energy (T_{max}) will be transferred if a head-on collision takes place, as in the following equation[97]

$$T(\theta) = T_{max} \cos^2 \theta$$

The maximum energy transferred from the electron to the atom (mass M) from the relativistic electron (energy E, mass m) can be calculated from[97]

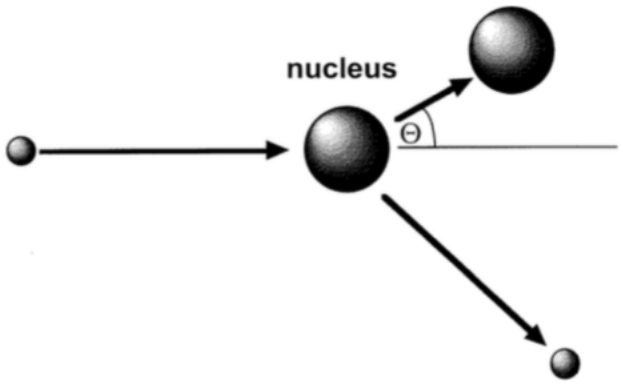

Figure 1.8 Scattering of a light particle (electron) by a nucleus[97]

$$T_{max} = \frac{2E(E + 2mc^2)}{Mc^2}$$

In addition, upon absorption of energy above the threshold level (T_d), the irradiated atom produces a vacancy-interstitial pair (Frenkel pair) that does not spontaneously recombine. Substituting T_d into the equation, one can estimate the minimum energy of impinging electron required to displace an atom.[98]

$$E_{th} = \frac{T_d(m + M)^2}{4mM}$$

These interstitials and vacancies either annihilate or become stable when the interstitial-vacancy separation exceeds the recombination radius. The radius displays highest along closely packed direction, and lower along rather open direction. When recombination is difficult, the defects tend to aggregate with their similar parties to form clusters.

In addition to forming Frenkel pairs, radiation could have other possible effects. When a surface atom is knocked by a highly energetic particle or when secondary particle generated from collision cascades intersects a surface atom, the atom could be ejected from the specimen, which is called sputtering.[99] Under certain circumstances, irradiation can also lead to the self-organization of a solid structure. [100, 101]

1.3.2 Effect of high-energy particle radiation on carbon

The irradiation effects in nanoscale carbon materials are somewhat different from that observed in most other densely packed bulk solids. For example, a stable interstitial-vacancy pair can be formed in carbon nanotube upon

energy absorption slightly above the threshold level (T_d), and the open structure of the nanoscale material makes it more difficult for the pair to recombine. [98]

The atom displacement threshold energy (T_d) is even different between carbon allotropes, as it depends on not only the bond energy but also the local chemical bonding as well as the availability of open space in vicinity. [98] In graphite, the basic unit structure underlying all carbon nanostructures, the threshold energy perpendicular to the basal plane (15-20 keV) is much lower than that of in-plane displacement, presumably 30 keV.[97] In an isolated SWNT with a diameter over 1nm, the T_d on the direction perpendicular to the tube surface is about 15-17 keV, which is close to the value for graphite, and the tangential direction had T_d of 30-50 keV.[102, 103]

The irradiation-induced defects in carbon nano-systems include point defects such as Frenkel pairs and defects on a higher dimension such as change in nanotube chirality.[89] The point defects on the atomic scale include single vacancy, multivacancies, and interstitials.[98]

In the carbon nanostructures, the vacancies do not just stay as missing atom in the sp^2 lattice, instead, the atoms near the vacancy exhibit strong tendency to reconstruct, as illustrated in **Figure 1.9**. The single vacancies (SV), divacancies(DV) and multivacancies can undergo reconstructions to form pentagons, heptagons, octagons, and saturate the undesired dangling bonds.[104, 105] The reconstruction is more favorable in nanotubes compared to graphite[106, 107] due to the curvature of the system. Therefore, carbon nanotubes can be

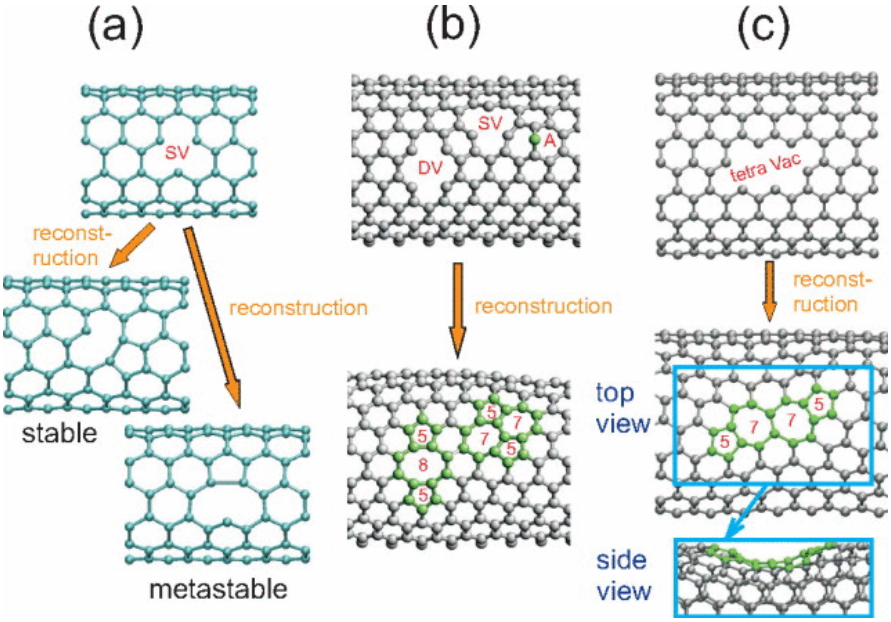

Figure 1.9 Reconstructions of the atomic network near vacancies in single-walled carbon nanotubes. (a) Reconstruction of a single vacancy in a 6,6 armchair carbon nanotube. (b) Reconstructions of the atomic network of a 10,10 carbon nanotube with several point defects. A DV transforms to an agglomeration of five- and eight-membered rings. A SV and an adatom may form a metastable SW 5757 defect. (c) Reconstruction of a tetravacancy.[98]

considered as a self-healing materials under irradiation.

Corresponding to the vacancy defects, there are also interstitial-type defects, which are additional carbon atoms adsorbed on the sp^2 carbon nanostructures. Similar to vacancy defects, the interstitial atoms on carbon nanotube have lower adsorption energy on C-C bonds oriented perpendicular to the axes of the tube than parallel positions.[108] Interestingly, in contrast to the vacancy defects, migration of interstitial atoms is easier (barrier energy about 0.4 eV) over the graphene plane than on the surface of carbon because curvature decreases adatom diffusivity.[108, 109]

In MWNTs or bundles of SWNTs, irradiation can cause more complex interstitial defects, such as intershell[110, 111] and intertube[91] covalent bonds. This type of defect can have significant effect on the mechanical properties of the nanotube, and will be elaborated in section 1.6.

1.3.3 Basics of electron beam facility

When electron beam is applied to radiate a material, the most important parameters of the facility are beam energy, and current. Beam energy provides information on how far the radiation will penetrate into the material. Generally speaking, the denser the material (higher Z number, higher subatomic particles in a material), the greater the likelihood the radiation will interact with the material and lose energy. Similarly, the higher the radiation energy, the more it will penetrate into the same material before being stopped. The penetration depth of electron radiation in carbon can be calculated from the NIST database. For

example, a carbon fiber composite with density of 1.6 g/cm^2 can be penetrated to 24mm using a 10 MeV beam.[112] Beam current is correlated to electron fluence thus can be associated with dose rate of the radiation. The amount of exposure to electrons of a material is called the absorbed dose, characterized in the International System (SI) as the gray (Gy). A more commonly used unit in industry is kilogray (kGy), where 1 kGy=1J/g absorbed energy per mass.[113]

In reality, there are two major methods to determine the absorbed dose of a material upon electron beam radiation: 1) Calculation from area throughput equations which is typically applied in research-oriented low energy small accelerators; and 2) referring to a dosimeter that has been proved of the reliability and stability in terms of irradiation response and this is widely applied in continuous industrial facilities with high beam energy.[113] The most widely applied dosimeters are based on analine, an aminoacid that gives the highest degree of precision upon exposure to electron beam irradiation.[114] Alanine forms a very stable free radical that exhibits long-term stability to most environmental challenges.[115] The irradiation-response radicals can be subsequently detected by electron paramagnetic resonance(EPR). An analine coated film (**Figure 1.10**) is placed near the target material through irradiation, and exposed dose can be obtained by inserting the film into the EPR device with instant temperatures measured. A bench-top EPR is displayed in **Figure 1.11**.

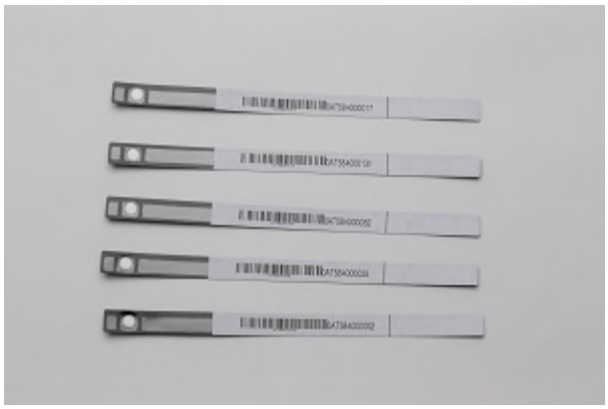

Figure 1.10 Analine coated film dosimeter

Figure 1.11 Bruker bench-top EPR e-scan series

1.3.4 Radiation graft polymerization

Radiation graft polymerization is a well established technique dating back to the 1950s and initially applied to polymeric substrates to form “graft copolymers”.[116, 117] The technique is briefly illustrated in **Figure 1.12**. The most important example is the functionalization of fluoropolymers, since this type of polymers show excellent chemical and thermal resistance and are difficult to functionalize through chemical methods. Currently, radiation graft polymerization is extended to wider applications, such as carbon nanomaterials.[118, 119] When substrate “A” is exposed to ionizing radiation, such as electron beam, X-ray, and γ-ray, active radicals are generated randomly across the surface of the substrate, which act as initiators for radical polymerization of monomer “B”. Unlike chemically initiated polymerizations, radiation grafting leaves no contamination from the initiators and reduces the cost of production.[120] This method is applicable to many incompatible monomer/polymer combinations to impart interesting properties to the resulting material.[121] Radiation is also capable of initiating polymerizations at low temperatures with various states of monomer, even in the solid-state.[116, 122]

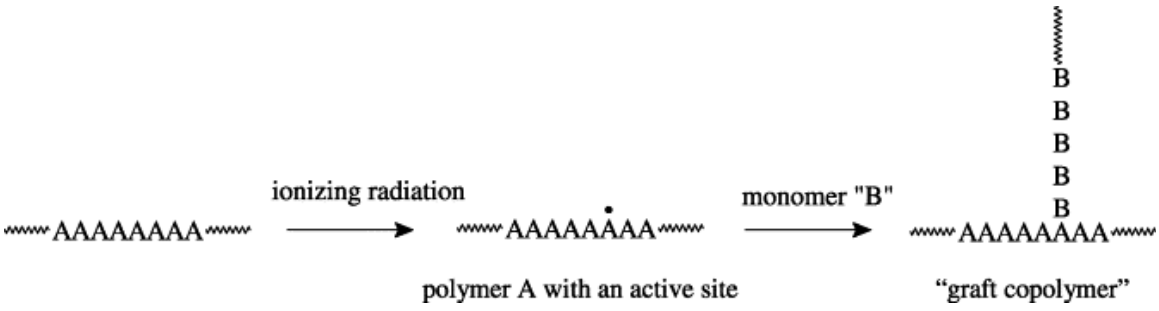

Figure 1.12 The use of ionizing radiation to graft monomer “B” on to polymer “A”[123]

There are two major types of radiation grafting polymerization methods developed: (1) simultaneous irradiation, where the substrate A and monomer are both subject to radiation; and (2) pre-irradiation, where only substrate A is irradiated and subsequently allowed in contact with monomer B.

Simultaneous irradiation is also referred to as mutual or direct irradiation. Monomer B can be present in the form of vapor, liquid, as well as solution. The irradiation may take place in air, but more preferably in inert atmosphere in order to form active radicals resulting in graft polymerization. As in the following mechanism, S is for substrate material while M stands for monomer unit.

$$S \xrightarrow{\text{e-beam}} S^{\bullet} \quad \text{(Irradiation to form primary radicals)}$$

$$S^{\bullet} + M \longrightarrow SM^{\bullet} \quad \text{(Initiation)}$$

$$SM^{\bullet} + nM \longrightarrow SM_{n+1}^{\bullet} \quad \text{(Propagation)}$$

$$SM_n^{\bullet} + SM_m^{\bullet} \longrightarrow SM_{n+m} \quad \text{(Termination)}$$

This is the most straightforward method since the grafting can occur as soon as the radicals are produced. In the mean time, however, the monomers can form radicals upon irradiation, and exhibit strong tendency of homo-polymerization. This would lead to an unfavorable gel effect, also known as Trommsdorf effect which eventually limit the degree of grafting. There are a number of methods to overcome this problem and ensure the grafting efficiency through keeping the formation of radicals on the substrate at higher rate than in the monomers. These approaches include adding polymerization inhibitors to the system such as Fe^{2+} salts, using

good solvents, as well as maintaining at low dose rate to suppress rapid termination of growing grafted chains.[120]

Pre-irradiation method generally involves two steps: (1) irradiation of the substrate to form active radicals; and (2) placing the activated substrate in contact with the monomer. If the substrate material was irradiated under inert atmosphere or vacuum, and preserved until in contact with monomers, the generated radicals would directly initiate the monomer units under a similar mechanism to the simultaneous method. If the irradiation was carried out in air, the radicals react with oxygen to form peroxide or hydroperoxides, which can be thermally initiated to react with the monomers.

$$\text{S-H} + \text{O}_2 \xrightarrow{\text{e-beam}} \text{SOOH} \quad \text{(Irradiation to form hydroperoxides)}$$

$$\text{SOOH} \longrightarrow \text{SO}^{\bullet} + \text{OH}^{\bullet} \quad \text{(Thermal decomposition)}$$

$$\text{SO}^{\bullet} + \text{M} \longrightarrow \text{SOM}^{\bullet} \quad \text{(Initiation)}$$

$$\text{SOM}^{\bullet} + \text{nM} \longrightarrow \text{SOM}^{\bullet}_{\text{n+1}} \quad \text{(Propagation)}$$

The advantage of pre-irradiation over simultaneous irradiation method is that there is less concern for homopolymerization since the monomer was not subject to radiation.[124]

Application of radiation graft polymerization in carbon materials range from gas sensors[125], biosensors[118] to composites. γ-ray from ^{60}Co source has been applied in many studies as ionizing radiation source. For example, polymethylmethacrylate (PMMA) was grafted onto MWNTs by a two-step technique: radiolysis of ethanol in presence of MWNTs to create trapped radicals

followed by polymerization of acrylic acid from these active sites.[126] Polystyrene grafted MWNTs were obtained by one-step γ-ray irradiation of the tubes in pure styrene.[127] The effect of absorbed radiation dose and concentration of monomer solution on the grafting of styrene was further discussed by Jung and coworkers.[128] In order to improve the compatibility of MWNT with nylon-6 polymer matrix, Yu et al. grafted glycidyl methacrylate-maleic acid onto MWNT using a single-step radiation method and observed higher mechanical strength in the resulting composite.[129] Yang et al. functionalized MWNTs with several vinyl monomers including 4-vinylphenylboronic acid (VPBAc) through γ-ray irradiation to obtain glucose sensors.[118] Effect of electron beam irradiation on carbon materials have been widely studied,[103, 130, 131] but has not been utilized as the source of radiation graft polymerization on carbon, to the best of our knowledge.

1.4 Fabrication of Neat CNT Materials

In addition to using CNTs as fillers in composites, the exceptional properties of individual CNTs also lead to researches on developing macroscopic neat CNT assemblies, such as mats and fibers that could potentially exhibit the properties of their CNT building block in useful materials. Unlike traditional carbon fibers, CNT fibers are very flexible and could be bent or tied into a knot without breaking, which becomes an impetus for development of CNT fibers.[39] In CNT fibers, the individual CNTs are mostly aligned to one another and parallel to the axis of the fiber. The degree of alignment has significant impact on the mechanical performance of the resulting fiber, thus has been a key issue in fabrication of these materials.[132] To

date, there are three major routes to manufacture CNT fibers: (1) wet-spinning from CNT dispersions, (2) dry-spinning from vertically aligned CNT arrays grown on a substrate, and (3) direct dry-spinning from CNT aerogel produced in a chemical vapor deposition (CVD) reactor. Other less commonly seen methods will not be discussed in this dissertation, but can be found in this review.[132]

1.4.1 Wet-spinning from CNT dispersion

The wet-spinning technique has been widely applied in production of commercial polymeric fibers, such as Kevlar, acrylic, and polyacrylonitrile (PAN). In the process, a solution of the polymer is injected and lead through a coagulation bath that precipitates the polymer into a fiber while rinsing away the excess solvent.[133] Similar idea can be applied to CNTs as long as a stable dispersion of CNT is prepared, which can be achieved through various means mentioned in section 1.2.1 (considering noncovalently functionalized nanotubes only). A typical process for making CNT fiber is illustrated in **Figure 1.13** below.

Vigolo et al. first utilized this approach to fabricate macroscopic CNT fibers in 2000.[39] The SWNTs are dispersed in an aqueous solution with the help of sodium dodecyl sulfate (SDS) surfactant. The noncovalent functionalization of aliphatic chains of the amphiphile with graphitic network of CNT successfully separated the tubes from Van der Waal's interaction. The dispersion is then introduced to a co-flowing coagulation bath, i.e. polyvinylalcohol (PVA) solution. The resulting SWNT fiber inevitably carries small percentage of PVA. Similarly,

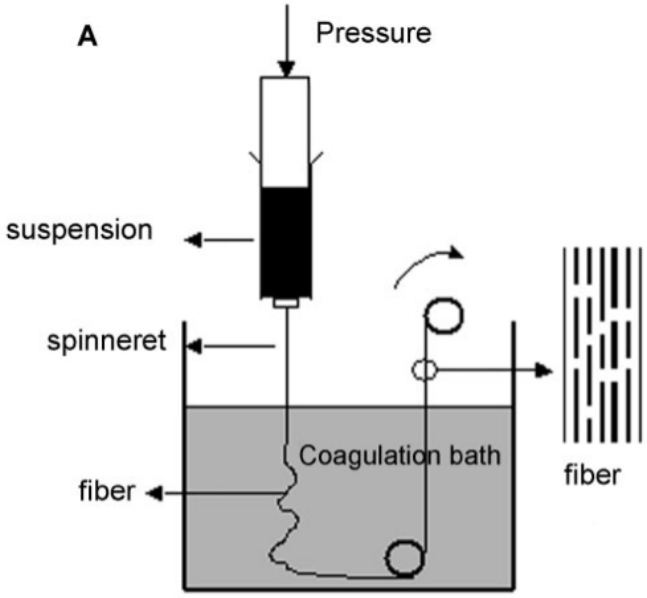

Figure 1.13 Illustration of typical wet-spinning CNT fibers.[133]

Dalton et al. further optimized the process by modifying the spinning set up and using a different surfactant, lithium dodecyl sulfate (LDS).[134] The advantage of PVA present in the fiber enhanced load transfer between CNTs, however, the electrical conductivity of the fiber will be decreased from pure CNT fibers because of the non-conductive nature of the PVA polymer.

As an alternative approach to PVA wet-spinning, pure CNT fibers can be produced through acid-assisted wet spinning. In a report by Ericson and coworkers, the purified SWNTs were suspended in and thoroughly mixed with 102% sulfuric acid, then extruded into coagulation bath through a small capillary tube.[135] Continuous SWNT fiber is formed with length of up to 30m. The thermal and electrical conductivities are much higher than PVA-containing CNT fibers.

A wet-spinning method without involvement of superacid has been developed to avoid protonation of CNTs caused by highly concentrated sulfuric acids.[136] The dispersion of SWNT in LDS surfactant was allowed in contact with an acidic/ basic flocculation bath where continuous fibers are formed. Interestingly, the fiber structure can be hollow in addition to commonly observed solid fibers.[136] In addition, Zhang et al. developed another approach that does not require superacid nor incorporation of polymers.[133] MWNTs are first dispersed in ethylene glycol to form a lyotropic liquid crystalline phase then coagulated in ether bath. The fibers spun through this approach exhibit high level of alignment, which may be due to the liquid crystalline phase. A comparison of the methods mentioned above is presented in **Table 1.1**.

Table 1.1 Comparison of CNTF spun from various wet-spinning methods

Suspension Solvent	Coagulation Bath	Tensile Modulus	Tensile Strength	Electrical Conductivity	Comment
H_2O, LDS[134]	5% wt PVA solution	80 GPa	1.8 GPa	<10 S/cm	PVA in fiber
102% H_2SO_4[135]	Ether/5% H_2SO_4/ H2O	120 GPa	0.12 GPa	500 S/cm	Potentially protonated
Ethylene glycol[133]	Ether	70 GPa	0.15 GPa	80 S/cm	Pure CNT fiber

1.4.2 Dry-spinning from vertically aligned CNT forest

Resembling fabrication of wool, cotton and silk fibers, CNT fibers can also be produced by dry-spinning from vertically aligned arrays.[132, 137, 138] Typically the CNTs are grown vertically from catalyst deposited on a substrate through chemical vapor deposition (CVD), then drawn at perpendicular direction to CNTs to form a fiber. The morphology of such arrays shows great impact on the degree of their spinnability.[139] **Figure 1.14** illustrates the spinning of CNT fiber, where the fiber, drawing wedge, and the array are presented. The diameter of the resulting fiber is determined by the width of the forest sidewall originally used to form the wedge.[138] Despite tremendous effort on modifying this approach in order to improve the properties CNT fiber, the mechanism of the process is insufficiently understood. Several groups proposed structural models for the dry-drawing process. Kuznetsov and coworkers suggest that a network of individual CNTs or thin CNT bundles are peeled off from large vertical CNT bundles during drawing and accumulate at the ends of the large bundles. [140] These networks joint the ends of nearby large bundles, which ensures continuous drawing.[140] Zhu et al. used SEM to monitor the pulling process in-situ and suggested a similar mechanism.[141]

1.4.3 Dry-spinning from aerogel produced in CVD reactor

Another method to fabricate CNT fiber is through direct spinning from furnace that produces CNT.[142, 143] As illustrated in **Figure 1.15**, carbon feedstock (such as ethanol, acetone and hexane) and catalyst (e.g. ferrocene and thiophene) are mixed into a solution that was pumped into the CVD furnace with H_2 as the

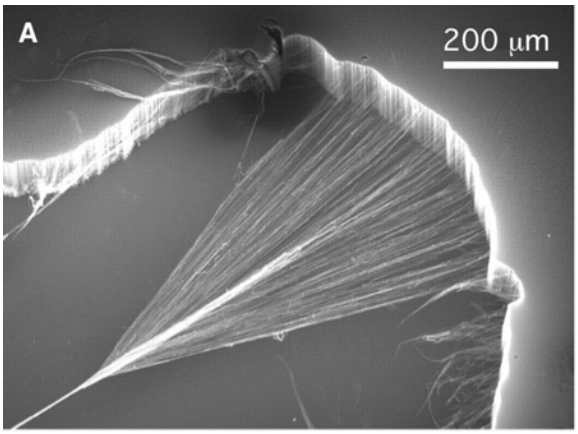

Figure 1.14 SEM images of a carbon nanotube yarn in the process of being simultaneously drawn and twisted during spinning from a nanotube forest[138]

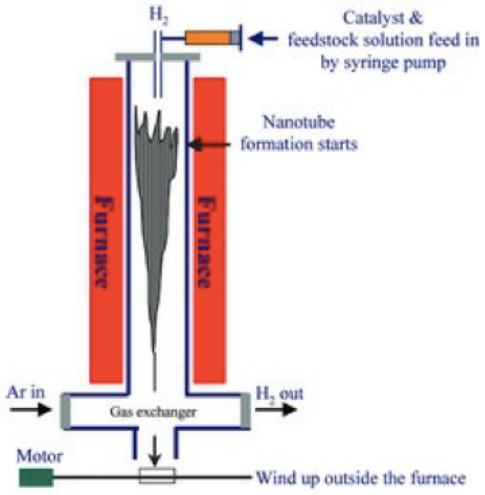

Figure 1.15 Schematic view of spinning fiber from CNT aerogel[132, 142, 143]

carrier gas. An aerogel of CNT is then formed within the heating chamber which is subsequently captured and wound into continuous fiber.

Compared to the first two approaches, CNT fiber directly spun from aerogel exhibit higher mechanical strength and stiffness, with the highest values reported so far reaching 8.8 GPa and 357 GPa, respectively, which are competitive with current commercial high-strength fibers.[144] The properties of the as-spun fibers can be tuned through process parameters such as catalyst concentration and winding rate. It has been confirmed that lower catalyst concentration promotes formation of thin-walled CNTs which leads to higher mechanical performance of the fibers.[145] In addition, higher winding-rate is favored in the process because of higher compactness and alignment between the CNT building blocks.[143]

The assembly of CNT into macroscopic materials is considered a “top-down” approach to take advantage of CNTs as compared to the application in composites, yet many challenges remain to commercialize the CNT fibers and mats. One essential problem is the scale-up of CNT fiber fabrication at controlled cost. Though CNT fibers with acceptable performance are successful produced through wet-spinning on a laboratory scale, it is an expensive process in industry. The spinning-from-array process is only as difficult to scale up if not more, because of the limitation in size of the array and lack of continuity. Direct-spinning from aerogel is the most promising method for scaling up since the fibers can be produced continuously as long as the feedstock is provided into the furnace. Still, it is difficult to control the consistency of the fiber, as Koziol reported, the high and

low strength of the fibers produced from the same set-up could differ greatly (8.8 GPa and lower than 1GPa).[144] Though it is commonly acknowledged that the tensile strength of stiff fibers (such as carbon fiber and glass fiber) is inherently statistical,[132] the variation in CNT fiber strength should have been smaller than commercial carbon and glass fibers, as observed by Zu et al..[146]

1.5 Mechanical Properties of Neat CNT Materials and Their Post-Treatments

Unfortunately, the mechanical properties of CNT fibers synthesized by far are well below that of individual CNTs. From another perspective, the stress transfer efficiency of individual CNTs to fibers on the micrometer scale is also an order of magnitude lower than that of traditional textile fibers.[147] In general, the factors affecting the mechanical properties of CNT fibers lies on different length scales. On the nanometer scale, the structural parameters of individual nanotubes are key factors, such as wall thickness, tube length, and diameter. Longer nanotubes result in higher fiber strength due to increased contact area and entanglement.[148] Smaller wall thickness (fewer number of concentric walls in each nanotube) and greater diameter indicates higher chance of tube collapsing (cross-sectional flattening, resembling the shape of “dog-bone”), which results in greater inter-tube contact area and thus higher efficiency of mechanical load transfer.[143, 145, 149] On the micrometer scale (bundle scale), the nanotube alignment, entanglement, and inter-tube load transfer are the contributing factors.[150] Finally, on the macroscopic scale, fiber twist angle,[148] diameter, and compactness of the

fiber become key factors. This section will begin with introduction to a CNT fiber fracture model, then mainly focus on the factors on the macroscopic scale and discuss post-treatments that are capable of tuning these factors.

1.5.1 Model of CNT fiber undergoing tensile fracture

The simplified model of CNT fiber fracture is demonstrated in **Figure 1.16**.[149] CNT fiber can be considered as a bundle of aligned rigid rods that can slide past one another, as in **Figure 1.16**(a). When tensile stress is applied to the end of the fiber at a certain gauge length, the fibril building blocks slide with respect to the nearby elements, as illustrated in **Figure 1.16**(b). The fracture of the fiber occurs at a stress value far below the failure strength of individual fibril elements, which, in this case, are CNTs. The actual CNT fiber that have undergone tensile fracture is examined under SEM (**Figure 1.16**(c)) which agrees with the model. It also indicates that the strength of the fiber originates from resistance to sliding of the CNTs and depends on the contact area between the tubes.[149] According to the model by Vilatela et al., the tensile strength of a CNT fiber can be calculated through a simple equation considering the length of CNTs, inter-tube contact area, and the interfacial shear strength.[149]

Koziol et al. suggested that for production of high-strength CNT fibers, the CNTs are required to be as structurally perfect as possible, free from defects that lead to kinks and aggregation into bundles.[144] In addition, the CNTs need to be aligned as perfectly as possible to the axis of the fiber.[144] However, a more recent research proposed that imperfect orientation of CNTs in the fiber and the presence

Figure 1.16 (a) Simple model of the fiber as collection of fibrous elements, (b) tensile fracture of fiber involving failure in shear between the fibrous elements, and (c) SEM micrograph of actual CNT fiber having undergone failure in tensile test (scale bar is 10 μm).[149]

of amorphous carbonaceous particles within the fiber serving as defects, can act as positive factors for increasing load transfer.[151]

1.5.2 Solvent densification

Solvent densification is a post treatment that effectively increases fiber density.[152] It involves immersion or exposure of the fiber to a liquid and subsequent evaporation of the liquid. After this process, the fiber is densified due to the surface tension of the solvent and the diameter of the fiber is decreased. Though the orientation of CNTs has not been increased, the load transfer between the bundles as well as between individual CNTs is improved, thus the mechanical properties of the resulting fiber is enhanced.[144]

Liu et al. studied the effect of liquid densification (referred to as “shrinking”) on the dimension and mechanical properties of CNT fibers.[152] The shrinking process does not have any effect of the strain at break of the CNT fiber, but improved the stiffness as well as the toughness, illustrated in **Figure 1.17**(a). They have observed a near direct correlation between shrinkage of diameter and maximum load at failure of the resulting CNT fiber, as shown in **Figure 1.17**(b). Several common solvents have been tested for their “shrinking ability”. Among water, ethanol, and acetone, Liu concluded that acetone exhibited the best effect of densification.[152]

More recently, Li et al. studied the densification effect of a wider range of solvents on CNT fibers.[153] They have found that rather than volatility, the polarity of the solvent is the key factor the affect the solvent’s ability to enhance the

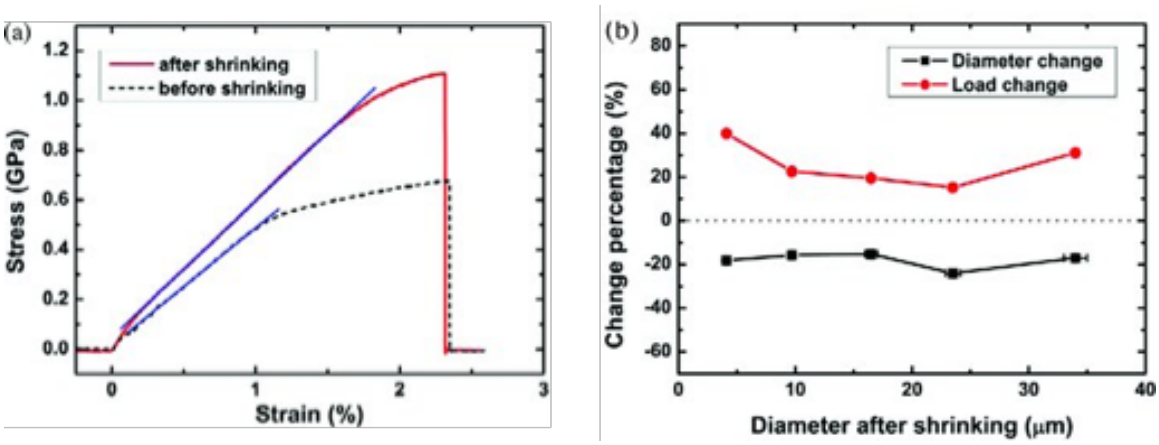

Figure 1.17 (a) Stress–strain curves of a typical CNT yarn before and after acetone densification. The diameter of the yarn changed from 11.5 μm to 9.7 μm due to the shrinking effect. (b) Correlation of percentage change in diameter and change in maximum loads of the yarns due to the shrinking effect.[152]

mechanical performance of the CNT fiber. Threatment of fiber with highly polar organic solvents, such as N,N-dimethylformamide (DMF), dimethyl sulphoxide (DMSO), and N-methyl-2-pyrrolidone (NMP) leads to much better results than densification with less polar solvents such as acetone and ethanol. It has been concluded that ethylene glycol is the most efficient solvent due to its –OH polar groups.[153]

1.5.3 Fiber twisting

In addition of solvent treatment, twisting is another approach to densify the fiber. Similar to the effect described in section 1.5.2, twisting the fibers effectively reduces the inter-tube spaces. The increased packing density results in a higher friction coefficient between the tubes, which is favorable for stress transfer.

Zhang et al. compared the mechanical properties of twisted and untwisted CNT fiber spun from the same 650 μm thick vertical array.[154] The overlay of the stress-strain curve is presented in **Figure 1.18**. The tensile strength of the fiber increased from 0.15 to 0.40 GPa, however, the the authors did not report the change in specific strength in order to rationalize the improvement to enhanced stress transfer rather than decrease in diameter.

Twisting the fiber at small angle contributes positively to the mechanical properties of the fibers. On the other hand, over-twisting the CNT fiber might lead to negative results. When the fiber is twisted at high degree, the applied tensile load is transferred to compress the CNT components rather than dissipated along the tube axis because of the misalignment.[155] Theoretically, there should be an

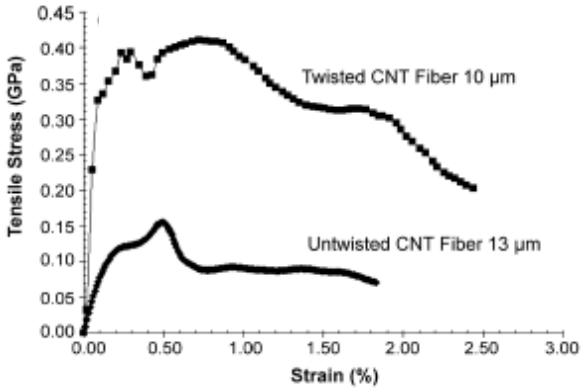

Figure 1.18 Stress-strain curve of as-spun and twisted CNT fiber fabricated from 650 μm thick array. The diameter of the fiber decreased from 13 to 10 μm.[154]

optimum value for twist angle of CNT fibers. The study by Fang et al. confirmed this assumption.[156] They have found that twist angle (helix angle as mentioned inthe original text) of 20° results in the highest strength of CNT fibers, while further increase in the angle will monotonously lower the mechanical properties.[156]

1.5.4 Infiltration of polymer

Polymers and CNTs have been incorporated in many composite materials to combine their properties. Unlike dispersing CNTs in a polymer matrix, infiltration of polymer into macroscopic CNT fibers is a “top-down” approach and greatly increased the percentage of CNT in the resulting material. As a post treatment for CNT fibers, the infiltration of polymer effectively improves the mechanical properties of CNT fiber, mainly through enhanced inter-tube load transfer and improved micro-structrure, rather than the loadbearing capacity of introduced polymer.[132, 157] The molecular level coupling of polymer chains with CNTs effectively constrains the deformation of CNT network, and enhance the strength of CNt junctions.[158] Many studies have been performed to investigated the effect of various polymers on the CNT fiber properties, and some of the representative work is discussed below.

The infiltration of polyvinylalcohol (PVA) into CNT fibers has been investigated by Liu et al.[159] It is presented that the tensile strength of PVA infiltrated CNT fiber (1.95 GPa) is 255% higher than that of simply twisted fiber (0.55 GPa). The improvement can be attributed both to reduction of fiber diameter as well as enhanced stress transfer between the tubes due to the presence of polymer chains.

Li et al. compared the effect of multiple polymers on the mechanical strength and electrical conductivity of CNT fiber.[153] Among dodecylamine oligomer, polyurethane (PU) and PVA, PVA show the highest improvement in ultimate tensile strength of the treated fiber. Two other polymers used in this study, polyimide, and bismaleimide resin (BMI), demonstrated even higher ability, but through a different mechanism. Unlike strengthening by simple linear polymer such as PVA, these two types of infiltrated yarns are made by infiltration of a precursor followed by thermoset curing. A 3D network is generated in the process, locking CNTs in place.[153]

More recently, Jung and coworkers [160] studied the role of polymer in altering the structures of CNT fiber by infiltrating polystyrene (PS), polyacrylonitrile (PAN) and PVA. The experiment showed that PVA yielded the highest improvement in tensile properties of the fibers. The effective strengthening was correlated to the large bundle size of PVA infiltrated CNT fiber, which is resulted by poor affinity of polar PVA with graphitic material.[160]

1.5.5 Crosslinking

Along with the above mentioned methods, crosslinking is also an important post treatment for CNT fibers. Since it is the major problem of investigation of this dissertation, a separate section (1.6) will be devoted to it.

1.6 Crosslinking CNT Fiber

Crosslinking of CNT was first observed under electron microscopes. It refers to formation of inter-tube bridges between the individual CNTs or concentric cylinders in a MWNT. As discussed in section 1.5, the mechanical failure of CNT fiber and bundles is mainly due to weak friction forces between the tubes. It is intuitive that introducing crosslinks to these systems should effectively prevent sliding and thus lead to higher mechanical strength.

Theoretical simulations suggest irradiation-induced crosslinking of CNT fibers and mats could lead to improvement of 1-2 order of magnitude.[161] Cornwell et al. demonstrated via molecular dynamics simulation that tensile strength of 60 GPa could be achieved if appropriate interstitial crosslinking is employed.[162] In practice, such high improvement has only been demonstrated on a bundle scale, within the electron microscope.[91, 163] E-beam irradiation of SWNT bundles resulted in a 30-fold increase in bending modulus.[91] MWNT bundles exhibited tensile strengths as high as 100 GPa after e-beam irradiation in the microscope.[163] On the macroscopic scale, crosslinking of CNT fibers and mats have been performed through various means, as discussed below in detail. Despite some improvement shown resulted in each crosslinking method, there is still a huge gap between current results and the potentials of CNT.

1.6.1 Mechanical Interlocking of CNT in macroscopic material

Some reports claim that crosslinking of CNTs has been achieved through infiltration of a precursor followed by curing/self-crosslinking of the impregnated

material to trap the CNTs in a rigid network. Since no covalent bond is established on the graphitic carbons where the chemical status of CNT remain unchanged, this type of post-spinning treatment should be regarded as “mechanical interlocking” rather than the term “crosslinking”.

Boncel and coworkers [164] demonstrated a chemical treatment to enhance the mechanical properties of CNT fiber. The fiber is first densified by acetone vapor then coated with 1,5-hexadiene monomer. After subsequent exposure to UV light, the diene crosslinked and enhanced the bundle inter-connectivity. An increase of 100% in specific tensile strength was observed.

Inspired by mussel adhesives, Ryu et al. developed a post-treatment for CNT fibers to improve their mechanical properties.[165] Catecholamine containing polymer capable of self-crosslinking is first impregnated into a CNT fiber after spinning at around 8% wt.. After curing at 120°, the specific tensile strength of the fiber is improved by up to 284%. With addition of Fe(III) salt, catechol-Fe coordination lead to even higher improvement, 337% on specific tensile strength.[165]

Cui et al. have used PAN polymer as a precursor to reinforce CNT fibers and films.[166] Upon carbonization at 1000 °C, the infiltrated PAN forms crosslinks to mechanically lock CNTs in a rigid network. A 30% increase in tensile strength has been observed for CNT fibers infiltrated with PAN from a 1 %wt. solution after thermal graphitization.[166]

Similarly, Tran et al. infiltrated epoxy into mechanically densified CNT ribbons.[167] After curing of the epoxy matrix, the tensile strength of the ribbon increased by 120%, and modulus by over 300%. Interestingly, the electrical conductivity also exhibited a large improvement, from 1657 S/cm to 4887 S/cm, which was caused by highly compact microstructure after the combined treatment, despite that epoxy is a non-conductive material.

Infiltration of graphene oxide (GO) into CNT fibers has been studied as an inter-locking approach because of the higher friction coefficient of GO surface for sliding than those found for pristine graphene sheets.[168] The high mechanical properties of GO particles and their size perfectly matching the void size between CNT bundles in the fiber are reasons for choosing these GO particles. Ultimate tensile strength has been improved by 56% through this method.[168]

1.6.2 Chemical crosslinking of CNT assembly

Different from the interlocking discussed in section 1.6.1, the actual crosslinking should involve establishment of direct covalent bonds on the CNT surface. Most ideally, this calls for reagents that bear multiple reactive sites to attach to CNT wall. Holzinger et al. first demonstrated chemical crosslinking of SWNT powder by applying single-step [2+1] cycloaddition reactions. Bi-functional crosslinkers at different length were synthesized that can covalently attach to two different SWNTs.[78] The single-step crosslinking of macroscopic CNT assembly is achieved through cross-dehydrogenative coupling.[169]

More commonly, crosslinking is achieved through multiple chemical modifications, as illustrated in **Figure 1.19**. First a surface functionalization of CNT is carried out to introduce an active moiety. Subsequently, a crosslinking reaction is triggered, either the coupling of the introduced functional groups, or an additional reaction with a multi-functional crosslinker.

In a study by Chen et al., a bucky paper is crosslinked through multi-step chemical treatment and improved in both mechanical and electrical properties.[170] The sample is first oxidized by strong acid to introduced carboxylic acid groups onto the nanotube surface. The acid groups are subsequently coupled with 10,12-pentacosadiyn-1-ol, a long-chain alcohol bearing two alkyne groups in the middle of the molecule. After UV irradiation is applied to the sample, the alkyne groups afford conjugational crosslinking. The tensile strength of MWNT bucky paper is increased by 100%, while SWNT alternatives exhibits higher improvement, by 300%.

Zhang and coworkers [171] crosslinked the CNT bucky paper in-situ during the film fabrication step. CNT powder is first functionalized with -NH_2 moieties, then

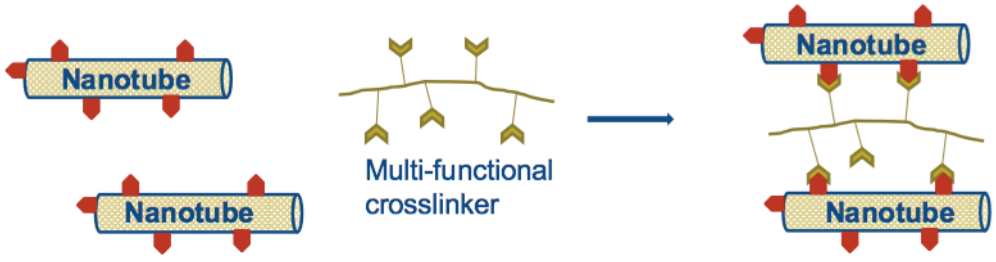

Figure 1.19 Multi-step chemical crosslinking of CNTs in close vicinity[172]

suspended in benzoquinone while being filtered from micromembrane. During the process, the amine groups on CNT reacts with benzoquinone where inter-tube crosslinking can be established. The tensile strength and electrical conductivity of in-situ crosslinked buckypaper is 49% and 120% higher than its non-crosslinked counterpart, respectively.

Similar strategy has also been performed using CNT fibers.[173] Min et al. first functionalized CNT fiber with –OH groups through diazonium addition. In the next step, a multi-functional ester is introduced as a crosslinker. The combined treatment increased the tensile strength of the fiber by 80%, yet only 30% is attributed to crosslinking. The authors attribute this effect to insufficient infiltration of the crosslinkers because of the densified fiber structure after the acid functionalization.

1.6.3 Irradiation induced crosslinking of CNT assembly

High energy irradiation could lead to atom displacement and rearrangement to form interstitials, as discussed in section 1.3. Thus effective crosslinking on CNT macro assemblies can thus be generated through irradiation, including ^{60}Co γ-ray and electron beam.

Mial et al. first demonstrated γ-ray irradiation of CNt fiber in air to improve their mechanical properties.[174] At γ-ray dose of 670 kGy, the irradiated fibers exhibited highest improvement in breaking stress , 27% from 665 MPa to 846 MPa. The dose rate of 1.5 kGy/hr and 4.2 kGy/hr do not show a difference on their effect on the resulting fiber, while the structure of the fiber does. The improvement has

been observed to be greater on tightly structured yarns than loosely structure ones. The oxidation on carbon surface induced by irradiation also contributes to the improvement.

The researchers at NASA Glenn Research Center irradiated CNT fibers and Sheets using electron-beam.[175, 176] The irradiation treatment by itself at electron fluence of 2.2×10^{17} e/cm^2 yield a 140% increase in tensile strength of CNT yarns. When the irradiation is preceded with a chemical functionalization step to introduce -OH and -NH_2 groups, the combined treatment lead to even higher improvement, an additional of 60%.[175] More recently, the same group provided insight on a trade-off observed between mechanical properties and electrical conductivity of the CNT fibers treated by e-beam irradiation combining with a variety of functional groups.[176]

References

1. Chung, D., Butterworth-Heinemann: 2012.

2. De Volder, M. F.; Tawfick, S. H.; Baughman, R. H.; Hart, A. J., *Science* **2013,** *339* (6119), 535-539.

3. Tang, Z.; Zhang, L.; Wang, N.; Zhang, X.; Wen, G.; Li, G.; Wang, J.; Chan, C.; Sheng, P., *Science* **2001,** *292* (5526), 2462-2465.

4. Baughman, R. H.; Zakhidov, A. A.; de Heer, W. A., *science* **2002,** *297* (5582), 787-792.

5. Ebbesen, T. W., *Annual review of materials science* **1994,** *24* (1), 235-264.

6. Robertson, D.; Brenner, D. W.; Mintmire, J., *Physical Review B* **1992,** *45* (21), 12592.

7. Overney, G.; Zhong, W.; Tománek, D., *Zeitschrift für Physik D Atoms, Molecules and Clusters* **1993,** *27* (1), 93-96.

8. Treacy, M. J.; Ebbesen, T.; Gibson, J., **1996**.

9. Falvo, M.; Clary, G.; Taylor, R.; Chi, V.; Brooks, F.; Washburn, S.; Superfine, R., *Nature* **1997,** *389* (6651), 582-584.

10. Salvetat, J.-P.; Briggs, G. A. D.; Bonard, J.-M.; Bacsa, R. R.; Kulik, A. J.; Stöckli, T.; Burnham, N. A.; Forró, L., *Physical Review Letters* **1999,** *82* (5), 944.

11. Yu, M.-F.; Files, B. S.; Arepalli, S.; Ruoff, R. S., *Physical review letters* **2000,** *84* (24), 5552.

12. Yu, M.-F.; Lourie, O.; Dyer, M. J.; Moloni, K.; Kelly, T. F.; Ruoff, R. S., *Science* **2000,** *287* (5453), 637-640.

13. Wei, B.; Vajtai, R.; Ajayan, P., *Applied Physics Letters* **2001,** *79* (8), 1172-1174.

14. Pop, E.; Mann, D.; Wang, Q.; Goodson, K.; Dai, H., *Nano letters* **2006,** *6* (1), 96-100.

15. Iijima, S., *nature* **1991,** *354* (6348), 56-58.

16. Harris, P., *International Materials Reviews* **2004,** *49* (1), 31-43.

17. Lu, W.; Dai, L., INTECH Open Access Publisher: 2010.

18. Yu, C.; Masarapu, C.; Rong, J.; Wei, B.; Jiang, H., *Advanced Materials* **2009,** *21* (47), 4793-4797.

19. Yamada, T.; Hayamizu, Y.; Yamamoto, Y.; Yomogida, Y.; Izadi-Najafabadi, A.; Futaba, D. N.; Hata, K., *Nature nanotechnology* **2011,** *6* (5), 296-301.

20. Chopra, S.; McGuire, K.; Gothard, N.; Rao, A. M.; Pham, A., *Applied Physics Letters* **2003,** *83* (11), 2280-2282.

21. Journet, C.; Maser, W.; Bernier, P.; Loiseau, A.; De La Chapelle, M. L.; Lefrant, d. l. S.; Deniard, P.; Lee, R.; Fischer, J., *nature* **1997,** *388* (6644), 756-758.

22. Peigney, A.; Laurent, C.; Flahaut, E.; Bacsa, R.; Rousset, A., *Carbon* **2001,** *39* (4), 507-514.

23. Bahr, J. L.; Mickelson, E. T.; Bronikowski, M. J.; Smalley, R. E.; Tour, J. M., *Chemical Communications* **2001,** (2), 193-194.

24. Haddon, R., *Science* **1993,** *261* (5128), 1545-1550.

25. Niyogi, S.; Hamon, M.; Hu, H.; Zhao, B.; Bhowmik, P.; Sen, R.; Itkis, M.; Haddon, R., *Accounts of Chemical Research* **2002,** *35* (12), 1105-1113.

26. Hirsch, A., *Angewandte Chemie International Edition* **2002,** *41* (11), 1853-1859.

27. Bandow, S.; Rao, A. M.; Williams, K. A.; Thess, A.; Smalley, R. E.; Eklund, P. C., *The Journal of Physical Chemistry B* **1997,** *101* (44), 8839-8842.

28. Krstic, V.; Duesberg, G. S.; Muster, J.; Burghard, M.; Roth, S., *Chemistry of Materials* **1998,** *10* (9), 2338-2340.

29. S. Duesberg, G.; Burghard, M.; Muster, J.; Philipp, G., *Chemical Communications* **1998,** (3), 435-436.

30. Moore, V. C.; Strano, M. S.; Haroz, E. H.; Hauge, R. H.; Smalley, R. E.; Schmidt, J.; Talmon, Y., *Nano Letters* **2003,** *3* (10), 1379-1382.

31. Bilalis, P.; Katsigiannopoulos, D.; Avgeropoulos, A.; Sakellariou, G., *RSC Advances* **2014,** *4* (6), 2911-2934.

32. Wanless, E. J.; Ducker, W. A., *The Journal of Physical Chemistry* **1996,** *100* (8), 3207-3214.

33. Manne, S.; Cleveland, J.; Gaub, H.; Stucky, G.; Hansma, P., *Langmuir* **1994,** *10* (12), 4409-4413.

34. Islam, M. F.; Rojas, E.; Bergey, D. M.; Johnson, A. T.; Yodh, A. G., *Nano Letters* **2003,** *3* (2), 269-273.

35. Rastogi, R.; Kaushal, R.; Tripathi, S.; Sharma, A. L.; Kaur, I.; Bharadwaj, L. M., *Journal of colloid and interface science* **2008,** *328* (2), 421-428.

36. Sanghavi, B. J.; Srivastava, A. K., *Electrochimica Acta* **2010,** *55* (28), 8638-8648.

37. Zhang, M.; Su, L.; Mao, L., *Carbon* **2006,** *44* (2), 276-283.

38. Dalton, A. B.; Collins, S.; Munoz, E.; Razal, J. M.; Ebron, V. H.; Ferraris, J. P.; Coleman, J. N.; Kim, B. G.; Baughman, R. H., *Nature* **2003,** *423* (6941), 703-703.

39. Vigolo, B.; Penicaud, A.; Coulon, C.; Sauder, C.; Pailler, R.; Journet, C.; Bernier, P.; Poulin, P., *Science* **2000,** *290* (5495), 1331-1334.

40. Wu, Z.; Chen, Z.; Du, X.; Logan, J. M.; Sippel, J.; Nikolou, M.; Kamaras, K.; Reynolds, J. R.; Tanner, D. B.; Hebard, A. F., *Science* **2004,** *305* (5688), 1273-1276.

41. Zhao, J.; Lu, J. P.; Han, J.; Yang, C.-K., *Applied physics letters* **2003,** *82* (21), 3746-3748.

42. Petrov, P.; Stassin, F.; Pagnoulle, C.; Jérôme, R., *Chemical communications* **2003,** (23), 2904-2905.

43. Zhao, Y.-L.; Stoddart, J. F., *Accounts of chemical research* **2009,** *42* (8), 1161-1171.

44. Chen, R. J.; Zhang, Y.; Wang, D.; Dai, H., *Journal of the American Chemical Society* **2001,** *123* (16), 3838-3839.

45. Simmons, T. J.; Bult, J.; Hashim, D. P.; Linhardt, R. J.; Ajayan, P. M., *ACS nano* **2009,** *3* (4), 865-870.

46. Chao-Hua, X.; Ren-Jia, Z.; Min-Min, S.; Yan, G.; Gang, W.; Xiao-Bin, Z.; Hong-Zheng, C.; Mang, W., *Nanotechnology* **2008,** *19* (21), 215604.

47. Yan, Y.; Cui, J.; Pötschke, P.; Voit, B., *Carbon* **2010,** *48* (9), 2603-2612.

48. Zou, J.; Liu, L.; Chen, H.; Khondaker, S. I.; McCullough, R. D.; Huo, Q.; Zhai, L., *Advanced Materials* **2008,** *20* (11), 2055-2060.

49. Kim, K. K.; Yoon, S. M.; Choi, J. Y.; Lee, J.; Kim, B. K.; Kim, J. M.; Lee, J. H.; Paik, U.; Park, M. H.; Yang, C. W., *Advanced Functional Materials* **2007,** *17* (11), 1775-1783.

50. Guldi, D. M.; Rahman, G. M. A.; Zerbetto, F.; Prato, M., *Accounts of Chemical Research* **2005,** *38* (11), 871-878.

51. Guldi, D. M.; Rahman, G.; Jux, N.; Tagmatarchis, N.; Prato, M., *Angewandte Chemie* **2004,** *116* (41), 5642-5646.

52. Ehli, C.; Rahman, G. A.; Jux, N.; Balbinot, D.; Guldi, D. M.; Paolucci, F.; Marcaccio, M.; Paolucci, D.; Melle-Franco, M.; Zerbetto, F., *Journal of the American Chemical Society* **2006,** *128* (34), 11222-11231.

53. Liu, L.; Wang, T.; Li, J.; Guo, Z.-X.; Dai, L.; Zhang, D.; Zhu, D., *Chemical physics letters* **2003,** *367* (5), 747-752.

54. Kim, S. W.; Kim, T.; Kim, Y. S.; Choi, H. S.; Lim, H. J.; Yang, S. J.; Park, C. R., *Carbon* **2012,** *50* (1), 3-33.

55. Kang, Y. K.; Lee, O.-S.; Deria, P.; Kim, S. H.; Park, T.-H.; Bonnell, D. A.; Saven, J. G.; Therien, M. J., *Nano letters* **2009,** *9* (4), 1414-1418.

56. Star, A.; Stoddart, J. F.; Steuerman, D.; Diehl, M.; Boukai, A.; Wong, E. W.; Yang, X.; Chung, S. W.; Choi, H.; Heath, J. R., *Angewandte Chemie International Edition* **2001,** *40* (9), 1721-1725.

57. Giulianini, M.; Waclawik, E. R.; Bell, J. M.; De Crescenzi, M.; Castrucci, P.; Scarselli, M.; Motta, N., *Applied Physics Letters* **2009,** *95* (1), 013304.

58. Kang, Y.; Taton, T. A., *Journal of the American Chemical Society* **2003,** *125* (19), 5650-5651.

59. Nativ-Roth, E.; Shvartzman-Cohen, R.; Bounioux, C.; Florent, M.; Zhang, D.; Szleifer, I.; Yerushalmi-Rozen, R., *Macromolecules* **2007,** *40* (10), 3676-3685.

60. Baskaran, D.; Mays, J. W.; Bratcher, M. S., *Chemistry of Materials* **2005,** *17* (13), 3389-3397.

61. Hirsch, A.; Vostrowsky, O., n *Functional molecular nanostructures*, Springer: 2005; pp 193-237.

62. O'Connell, M. J.; Boul, P.; Ericson, L. M.; Huffman, C.; Wang, Y.; Haroz, E.; Kuper, C.; Tour, J.; Ausman, K. D.; Smalley, R. E., *Chemical physics letters* **2001,** *342* (3), 265-271.

63. Goodwin, A. P.; Tabakman, S. M.; Welsher, K.; Sherlock, S. P.; Prencipe, G.; Dai, H., *Journal of the American Chemical Society* **2008,** *131* (1), 289-296.

64. Numata, M.; Sugikawa, K.; Kaneko, K.; Shinkai, S., *Chemistry–A European Journal* **2008,** *14* (8), 2398-2404.

65. Zheng, M.; Jagota, A.; Semke, E. D.; Diner, B. A.; McLean, R. S.; Lustig, S. R.; Richardson, R. E.; Tassi, N. G., *Nat Mater* **2003,** *2* (5), 338-342.

66. Zhang, L.; Li, T.; Li, B.; Li, J.; Wang, E., *Chemical Communications* **2010,** *46* (9), 1476-1478.

67. Park, H.; Zhao, J.; Lu, J. P., *Nano Letters* **2006,** *6* (5), 916-919.

68. Yu, H.; Jin, Y.; Peng, F.; Wang, H.; Yang, J., *The Journal of Physical Chemistry C* **2008,** *112* (17), 6758-6763.

69. Yang, S. J.; Park, C. R., *Nanotechnology* **2007,** *19* (3), 035609.

70. Yang, S. J.; Choi, J. Y.; Chae, H. K.; Cho, J. H.; Nahm, K. S.; Park, C. R., *Chemistry of Materials* **2009,** *21* (9), 1893-1897.

71. Banerjee, S.; Wong, S. S., *The journal of physical chemistry B* **2002,** *106* (47), 12144-12151.

72. Ziegler, K. J.; Gu, Z.; Peng, H.; Flor, E. L.; Hauge, R. H.; Smalley, R. E., *Journal of the American Chemical Society* **2005,** *127* (5), 1541-1547.

73. Liu, J.; Rinzler, A. G.; Dai, H.; Hafner, J. H.; Bradley, R. K.; Boul, P. J.; Lu, A.; Iverson, T.; Shelimov, K.; Huffman, C. B., *Science* **1998,** *280* (5367), 1253-1256.

74. Chen, J.; Hamon, M. A.; Hu, H.; Chen, Y.; Rao, A. M.; Eklund, P. C.; Haddon, R. C., *Science* **1998,** *282* (5386), 95-98.

75. Sun, Y.-P.; Huang, W.; Lin, Y.; Fu, K.; Kitaygorodskiy, A.; Riddle, L. A.; Yu, Y. J.; Carroll, D. L., *Chemistry of Materials* **2001,** *13* (9), 2864-2869.

76. Hamon, M.; Hui, H.; Bhowmik, P.; Itkis, H.; Haddon, R., *Applied Physics A* **2002,** *74* (3), 333-338.

77. Holzinger, M.; Vostrowsky, O.; Hirsch, A.; Hennrich, F.; Kappes, M.; Weiss, R.; Jellen, F., *Angewandte Chemie International Edition* **2001,** *40* (21), 4002-4005.

78. Holzinger, M.; Steinmetz, J.; Samaille, D.; Glerup, M.; Paillet, M.; Bernier, P.; Ley, L.; Graupner, R., *Carbon* **2004,** *42* (5–6), 941-947.

79. Holzinger, M.; Abraham, J.; Whelan, P.; Graupner, R.; Ley, L.; Hennrich, F.; Kappes, M.; Hirsch, A., *Journal of the American Chemical Society* **2003,** *125* (28), 8566-8580.

80. Dyke, C. A.; Tour, J. M., *Journal of the American Chemical Society* **2003,** *125* (5), 1156-1157.

81. Bahr, J. L.; Yang, J.; Kosynkin, D. V.; Bronikowski, M. J.; Smalley, R. E.; Tour, J. M., *Journal of the American Chemical Society* **2001,** *123* (27), 6536-6542.

82. Prato, M.; Maggini, M., *Accounts of Chemical Research* **1998,** *31* (9), 519-526.

83. Tagmatarchis, N.; Prato, M., *Journal of materials chemistry* **2004,** *14* (4), 437-439.

84. Sakellariou, G.; Ji, H.; Mays, J. W.; Hadjichristidis, N.; Baskaran, D., *Chemistry of Materials* **2007,** *19* (26), 6370-6372.

85. Brinkman, J. A., *Journal of Applied Physics* **1954,** *25* (8), 961-970.

86. Cook, I., *Nature materials* **2006,** *5* (2), 77-80.

87. Suenaga, K.; Wakabayashi, H.; Koshino, M.; Sato, Y.; Urita, K.; Iijima, S., *Nature Nanotechnology* **2007,** *2* (6), 358-360.

88. Moura, C. S.; Balzaretti, N. M.; Amaral, L.; Lacerda, R. G.; Pimenta, M. A., *AIP Advances* **2012,** *2* (1), 012174.

89. Hashimoto, A.; Suenaga, K.; Gloter, A.; Urita, K.; Iijima, S., *Nature* **2004,** *430* (7002), 870-873.

90. Gass, M. H.; Bangert, U.; Bleloch, A. L.; Wang, P.; Nair, R. R.; Geim, A. K., *Nat Nano* **2008,** *3* (11), 676-681.

91. Kis, A.; Csanyi, G.; Salvetat, J.-P.; Lee, T.-N.; Couteau, E.; Kulik, A.; Benoit, W.; Brugger, J.; Forro, L., *Nature materials* **2004,** *3* (3), 153-157.

92. Gómez-Navarro, C.; De Pablo, P.; Gómez-Herrero, J.; Biel, B.; Garcia-Vidal, F.; Rubio, A.; Flores, F., *Nature materials* **2005,** *4* (7), 534-539.

93. Wei, B.; D'Arcy-Gall, J.; Ajayan, P.; Ramanath, G., *Applied physics letters* **2003,** *83* (17), 3581-3583.

94. Esquinazi, P.; Spemann, D.; Höhne, R.; Setzer, A.; Han, K.-H.; Butz, T., *Physical Review Letters* **2003,** *91* (22), 227201.

95. Talapatra, S.; Ganesan, P.; Kim, T.; Vajtai, R.; Huang, M.; Shima, M.; Ramanath, G.; Srivastava, D.; Deevi, S.; Ajayan, P., *Physical review letters* **2005,** *95* (9), 097201.

96. Krasheninnikov, A.; Banhart, F., *Nature materials* **2007,** *6* (10), 723-733.

97. Banhart, F., *Reports on progress in physics* **1999,** *62* (8), 1181.

98. Krasheninnikov, A.; Nordlund, K., *Journal of applied physics* **2010,** *107* (7), 071301.

99. Cherns, D.; Minter, F.; Nelson, R., *Nuclear Instruments and Methods* **1976,** *132*, 369-376.

100. Seeger, A., *Radiation Effects and Defects in Solids* **1989,** *111* (1-2), 355-368.

101. Abromeit, C., *International Journal of Modern Physics B* **1989,** *3* (09), 1301-1342.

102. Crespi, V. H.; Chopra, N. G.; Cohen, M. L.; Zettl, A.; Louie, S. G., *Physical Review B* **1996,** *54* (8), 5927-5931.

103. Smith, B. W.; Luzzi, D. E., *Journal of Applied Physics* **2001,** *90* (7), 3509-3515.

104. Berber, S.; Oshiyama, A., *Physical Review B* **2008,** *77* (16), 165405.

105. Rossato, J.; Baierle, R.; Fazzio, A.; Mota, R., *Nano letters* **2005,** *5* (1), 197-200.

106. Lehtinen, P. O.; Foster, A. S.; Ma, Y.; Krasheninnikov, A. V.; Nieminen, R. M., *Physical Review Letters* **2004,** *93* (18), 187202.

107. Telling, R. H.; Ewels, C. P.; Ahlam, A.; Heggie, M. I., *Nature Materials* **2003,** *2* (5), 333-337.

108. Krasheninnikov, A. V.; Nordlund, K.; Lehtinen, P. O.; Foster, A. S.; Ayuela, A.; Nieminen, R. M., *Physical Review B* **2004,** *69* (7), 073402.

109. Krasheninnikov, A. V.; Nordlund, K.; Lehtinen, P. O.; Foster, A. S.; Ayuela, A.; Nieminen, R. M., *Carbon* **2004,** *42* (5–6), 1021-1025.

110. Urita, K.; Suenaga, K.; Sugai, T.; Shinohara, H.; Iijima, S., *Physical Review Letters* **2005,** *94* (15), 155502.

111. Huhtala, M.; Krasheninnikov, A. V.; Aittoniemi, J.; Stuart, S. J.; Nordlund, K.; Kaski, K., *Physical Review B* **2004,** *70* (4), 045404.

112. Berejka, A. J., *RadTech Report* **2002,** *16* (2), 33-39.

113. Berejka, A.; Cleland, M., *Int. At. Energy Agency* **2011**, 34-36.

114. Kovács, A.; Miller, A. In *Present status and expected progress in radiation processing dosimetry*, Technical meeting, IAEA, 2004; pp 85-93.

115. Regulla, D.; Deffner, U., *The International Journal of Applied Radiation and Isotopes* **1982,** *33* (11), 1101-1114.

116. Chapiro, A., Interscience New York: 1962; Vol. 22.

117. Rao, M.; Rao, K., *Radiation Physics and Chemistry (1977)* **1985,** *26* (6), 669-672.

118. Yang, D.-S.; Jung, D.-J.; Choi, S.-H., *Radiation Physics and Chemistry* **2010,** *79* (4), 434-440.

119. Zhang, B.; Xie, S.; Wei, R.; Ma, H.; Yu, M.; Li, L.; Li, J., *Science China Chemistry* **2016,** *59* (3), 303-309.

120. Nasef, M. M.; Hegazy, E.-S. A., *Progress in Polymer Science* **2004,** *29* (6), 499-561.

121. Guilmeau, I.; Esnouf, S.; Betz, N.; Le Moel, A., *Nuclear Instruments and Methods in Physics Research Section B: Beam Interactions with Materials and Atoms* **1997,** *131* (1), 270-275.

122. Stannett, V. T., *International Journal of Radiation Applications and Instrumentation. Part C. Radiation Physics and Chemistry* **1990,** *35* (1), 82-87.

123. Dargaville, T. R.; George, G. A.; Hill, D. J. T.; Whittaker, A. K., *Progress in Polymer Science* **2003,** *28* (9), 1355-1376.

124. Aydinli, B.; Tinçer, T., *Radiation Physics and Chemistry* **2001,** *60* (3), 237-243.

125. Chen, J.; Maekawa, Y.; Yoshida, M.; Tsubokawa, N., *Polymer journal* **2002,** *34* (1), 30-35.

126. Chen, S.; Wu, G.; Liu, Y.; Long, D., *Macromolecules* **2006,** *39* (1), 330-334.

127. Xu, H.; Wang, X.; Zhang, Y.; Liu, S., *Chemistry of materials* **2006,** *18* (13), 2929-2934.

128. Jung, C.-H.; Kim, D.-K.; Choi, J.-H., *Current Applied Physics* **2009,** *9* (1), S85-S87.

129. Yu, H.; Mo, X.; Peng, J.; Zhai, M.; Li, J.; Wei, G.; Zhang, X.; Qiao, J., *Radiation Physics and Chemistry* **2008,** *77* (5), 656-662.

130. Evora, M. C.; Klosterman, D.; Lafdi, K.; Li, L.; Abot, J. L., *Carbon* **2010,** *48* (7), 2037-2046.

131. Zou, H.; Yang, Y.; Li, Q.; Zhang, J.; Liu, Z.; Guo, X.; Du, Z., *Carbon* **2002,** *40* (12), 2282-2284.

132. Lu, W.; Zu, M.; Byun, J. H.; Kim, B. S.; Chou, T. W., *Advanced Materials* **2012,** *24* (14), 1805-1833.

133. Zhang, S.; Koziol, K. K.; Kinloch, I. A.; Windle, A. H., *Small* **2008,** *4* (8), 1217-1222.

134. Dalton, A. B.; Collins, S.; Razal, J.; Munoz, E.; Ebron, V. H.; Kim, B. G.; Coleman, J. N.; Ferraris, J. P.; Baughman, R. H., *Journal of Materials Chemistry* **2004,** *14* (1), 1-3.

135. Ericson, L. M.; Fan, H.; Peng, H.; Davis, V. A.; Zhou, W.; Sulpizio, J.; Wang, Y.; Booker, R.; Vavro, J.; Guthy, C., *Science* **2004,** *305* (5689), 1447-1450.

136. Kozlov, M. E.; Capps, R. C.; Sampson, W. M.; Ebron, V. H.; Ferraris, J. P.; Baughman, R. H., *Advanced Materials* **2005,** *17* (5), 614-617.

137. Jiang, K.; Li, Q.; Fan, S., *Nature* **2002,** *419* (6909), 801-801.

138. Zhang, M.; Atkinson, K. R.; Baughman, R. H., *Science* **2004,** *306* (5700), 1358-1361.

139. Zhang, Y.; Zou, G.; Doorn, S. K.; Htoon, H.; Stan, L.; Hawley, M. E.; Sheehan, C. J.; Zhu, Y.; Jia, Q., *ACS Nano* **2009,** *3* (8), 2157-2162.

140. Kuznetsov, A. A.; Fonseca, A. F.; Baughman, R. H.; Zakhidov, A. A., *ACS Nano* **2011,** *5* (2), 985-993.

141. Zhu, C.; Cheng, C.; He, Y. H.; Wang, L.; Wong, T. L.; Fung, K. K.; Wang, N., *Carbon* **2011,** *49* (15), 4996-5001.

142. Li, Y.-L.; Kinloch, I. A.; Windle, A. H., *Science* **2004,** *304* (5668), 276-278.

143. Motta, M.; Moisala, A.; Kinloch, I. A.; Windle, A. H., *Advanced Materials* **2007,** *19* (21), 3721-3726.

144. Koziol, K.; Vilatela, J.; Moisala, A.; Motta, M.; Cunniff, P.; Sennett, M.; Windle, A., *Science* **2007,** *318* (5858), 1892-1895.

145. Motta, M.; Li; Kinloch, I.; Windle, A., *Nano Letters* **2005,** *5* (8), 1529-1533.

146. Zu, M.; Li, Q.; Zhu, Y.; Dey, M.; Wang, G.; Lu, W.; Deitzel, J. M.; Gillespie Jr, J. W.; Byun, J.-H.; Chou, T.-W., *Carbon* **2012,** *50* (3), 1271-1279.

147. Miao, M., *Carbon* **2015,** *91*, 163-170.

148. Zhang, X.; Li, Q.; Holesinger, T. G.; Arendt, P. N.; Huang, J.; Kirven, P. D.; Clapp, T. G.; DePaula, R. F.; Liao, X.; Zhao, Y., *ADVANCED MATERIALS* **2007,** *19* (23), 4198.

149. Vilatela, J. J.; Elliott, J. A.; Windle, A. H., *ACS nano* **2011,** *5* (3), 1921-1927.

150. Beese, A. M.; Wei, X.; Sarkar, S.; Ramachandramoorthy, R.; Roenbeck, M. R.; Moravsky, A.; Ford, M.; Yavari, F.; Keane, D. T.; Loutfy, R. O.; Nguyen, S. T.; Espinosa, H. D., *ACS Nano* **2014,** *8* (11), 11454-11466.

151. Gspann, T. S.; Montinaro, N.; Pantano, A.; Elliott, J. A.; Windle, A. H., *Carbon* **2015,** *93*, 1021-1033.

152. Liu, K.; Sun, Y.; Zhou, R.; Zhu, H.; Wang, J.; Liu, L.; Fan, S.; Jiang, K., *Nanotechnology* **2010,** *21* (4), 045708.

153. Li, S.; Zhang, X.; Zhao, J.; Meng, F.; Xu, G.; Yong, Z.; Jia, J.; Zhang, Z.; Li, Q., *Composites Science and Technology* **2012,** *72* (12), 1402-1407.

154. Zhang, X.; Li, Q.; Tu, Y.; Li, Y.; Coulter, J. Y.; Zheng, L.; Zhao, Y.; Jia, Q.; Peterson, D. E.; Zhu, Y., *Small* **2007,** *3* (2), 244-248.

155. Zhao, J.; Zhang, X.; Di, J.; Xu, G.; Yang, X.; Liu, X.; Yong, Z.; Chen, M.; Li, Q., *Small* **2010,** *6* (22), 2612-2617.

156. Shaoli, F.; Mei, Z.; Anvar, A. Z.; Ray, H. B., *Journal of Physics: Condensed Matter* **2010,** *22* (33), 334221.

157. Liu, X.; Yang, Q.-S.; He, X.-Q.; Liew, K.-M., *Carbon* **2016,** *106*, 188-194.

158. Ma, W.; Liu, L.; Zhang, Z.; Yang, R.; Liu, G.; Zhang, T.; An, X.; Yi, X.; Ren, Y.; Niu, Z.; Li, J.; Dong, H.; Zhou, W.; Ajayan, P. M.; Xie, S., *Nano Letters* **2009,** *9* (8), 2855-2861.

159. Liu, K.; Sun, Y.; Lin, X.; Zhou, R.; Wang, J.; Fan, S.; Jiang, K., *ACS nano* **2010,** *4* (10), 5827-5834.

160. Jung, Y.; Kim, T.; Park, C. R., *Carbon* **2015,** *88* (0), 60-69.

161. Åström, J.; Krasheninnikov, A.; Nordlund, K., *Physical review letters* **2004,** *93* (21), 215503.

162. Cornwell, C. F.; Welch, C. R., *The Journal of Chemical Physics* **2011,** *134* (20), 204708.

163. Peng, B.; Locascio, M.; Zapol, P.; Li, S.; Mielke, S. L.; Schatz, G. C.; Espinosa, H. D., *Nature nanotechnology* **2008,** *3* (10), 626-631.

164. Boncel, S.; Sundaram, R. M.; Windle, A. H.; Koziol, K. K., *ACS nano* **2011,** *5* (12), 9339-9344.

165. Ryu, S.; Lee, Y.; Hwang, J. W.; Hong, S.; Kim, C.; Park, T. G.; Lee, H.; Hong, S. H., *Advanced Materials* **2011,** *23* (17), 1971-1975.

166. Cui, Y.; Zhang, M., *ACS applied materials & interfaces* **2013,** *5* (16), 8173-8178.

167. Tran, T. Q.; Fan, Z.; Liu, P.; Myint, S. M.; Duong, H. M., *Carbon* **2016,** *99*, 407-415.

168. Wang, Y.; Colas, G.; Filleter, T., *Carbon* **2016,** *98*, 291-299.

169. Choi, Y.-M.; Choo, H.; Yeo, H.; You, N.-H.; Lee, D. S.; Ku, B.-C.; Kim, H. C.; Bong, P.-H.; Jeong, Y.; Goh, M., *ACS Applied Materials & Interfaces* **2013,** *5* (16), 7726-7730.

170. Chen, I.-W. P.; Liang, R.; Zhao, H.; Wang, B.; Zhang, C., *Nanotechnology* **2011,** *22* (48), 485708.

171. Zhang, J.; Jiang, D.; Peng, H.-X.; Qin, F., *Carbon* **2013,** *63* (0), 125-132.

172. Baker, J. S.; Miller, S. G.; Williams, T. A.; Meador, M. A., **2013**.

173. Min, J.; Cai, J. Y.; Sridhar, M.; Easton, C. D.; R. Gengenbach, T.; McDonnell, J.; Humphries, W.; Lucas, S., *Carbon* **2013,** *52* (0), 520-527.

174. Miao, M.; Hawkins, S. C.; Cai, J. Y.; Gengenbach, T. R.; Knott, R.; Huynh, C. P., *Carbon* **2011,** *49* (14), 4940-4947.

175. Miller, S. G.; Williams, T. S.; Baker, J. S.; Solá, F.; Lebron-Colon, M.; McCorkle, L. S.; Wilmoth, N. G.; Gaier, J.; Chen, M.; Meador, M. A., *ACS Applied Materials & Interfaces* **2014,** *6* (9), 6120-6126.

176. Williams, T. S.; Orloff, N. D.; Baker, J. S.; Miller, S. G.; Natarajan, B.; Obrzut, J.; McCorkle, L. S.; Lebron-Colón, M.; Gaier, J.; Meador, M. A., *ACS Applied Materials & Interfaces* **2016**.

CHAPTER II

SIMULTANEOUS FUNCTIONALIZATION AND CROSSLINKING OF CARBON NANOTUBE FIBERS IN THE SOLID-STATE USING BENZOCYCLOBUTENE-BASED POLYMER

A version of this chapter was published by Lu, X et al *Nanotechnology* **2017,** *28* (14), 145603.[1]

The article was compiled and written by X. Lu. The reported synthesis and characterization was performed by X. Lu, except for XPS, and tensile tests.

Abstract

Individual carbon nanotubes (CNTs) exhibit exceptional mechanical properties. However, difficulties remain to fully realize these properties in CNT macro-assemblies, because of the sliding past one another resulting from the weak inter-tube forces. Herein, a simple solid-state reaction is presented that enhances the mechanical properties of carbon nanotube fibers (CNTFs) through simultaneous covalent functionalization and crosslinking. This is the first chemical crosslinking proposed without involvement of catalyst or byproducts. The specific tensile strength of CNTF obtained from the treatment employing a benzocyclobutene-based polymer is improved by 40%. Such improvement can be attributed to reduced voids, impregnation of polymer, and the formation of covalent crosslinks. This methodology is confirmed using both multiwalled nanotube (MWNT) powders and CNTF. Thermogravimetric analysis, differential scanning calorimetry, X-ray photoelectron spectroscopy, and transmission electron microscopy of the treated MWNT powders confirm the covalent functionalization and formation of inter-tube crosslinks. This simple one-step reaction can be applied to industrial-scale production of high-strength CNTFs.

2.1 Introduction

Carbon nanotube fibers (CNTFs) have received much attention for their promising applications in actuators, supercapacitors, and light-weight magnetic shields, but key challenges remain to realize their full potential in terms of mechanical properties.[2-4] The properties of the CNTF rely on the orientation of CNT building blocks in their macro-assembly[5] and the physical interactions between these building blocks. Thus, depending on the type of CNTs used, their packing, and associated processing the tensile strength of pristine CNTF reported thus far vary from 0.15-8.8 GPa.[6, 7] Even the highest reported strength (8.8GPa)[8] is only a fraction of that of the individual carbon nanotube (CNT) building blocks, on the order of 100 GPa.[9]

CNTFs are fabricated through various means resembling the traditional fiber spinning techniques, such as wet spinning from CNT solutions,[10, 11] dry spinning from vertically aligned CNT arrays,[6, 12] and direct spinning of aerogels from chemical vapor deposition(CVD) reactors.[13] The integrity and properties of as-spun CNTF rely on CNT bundle network, packing of the CNT bundles[14, 15] and weak Van der Waal's interactions and low friction forces present between components.[16] As a result, upon tensile loading of the fiber, the CNT building blocks and their bundles slide past one another causing inefficient load transfer from macroscopic CNTFs down to the individual tubes.[16] Numerous post treatment methods have been developed to enhance the load transfer and improve the

mechanical properties of CNTFs, such as solvent densification,[7] polymer infiltration,[17, 18] and crosslinking,[19-26] but each with its limitations.

There are two approaches reported in the literature which claimed to achieve "crosslinking" or CNTFs: (i) infiltration of functional monomer/polymer in CNTF followed by curing without involving reaction with CNTs (should be regarded as "consolidated"),[20-23] and (ii) covalent crosslinking between CNTs with or without chemical functionalization.[19, 24-28] In the first approach, curing of the infiltrated material such as catecholamine polymer,[20] photoreactive diene,[21] epoxy,[23] and polyacrylonitrile,[22] successfully trapped the CNTs in a rigid network and yielded mechanical interlocking. In the second approach, crosslinking shall be achieved by introducing covalent bonds within the CNTF. Simulations suggest that introducing covalent crosslinks to CNTF should improve their mechanical strength by 1-2 orders of magnitude,[29] However, only very few reports demonstrated the covalent crosslinking of CNTFs on the macroscopic scale, either through chemical functionalization,[25-27] or irradiation.[19, 24, 28] None of the reports have reached the predicted improvement, and most of them employed tedious process.

Covalent crosslinking of CNTFs using chemical functionalization is typically achieved through multiple steps in solution: a surface functionalization on CNT to introduce an active moiety followed by reaction with a multi-functional crosslinker or coupling of the functional groups.[25, 26] Despite the increase in mechanical strength observed in CNTFs treated by these chemically crosslinking methods, multiple steps of functionalization were required, which potentially means repetitive

reactions, rinsing and drying. Intramolecular cross-dehydrogenative coupling has been used as a single-step treatment for CNTFs,[27] but the reaction occurred in solution requiring catalysts, which may create obstacles to potential scale-up. Moreover, many of the results of these treatments were reported only in terms of traditional tensile strength, which is less comparable to other fibers than density normalized specific strength considering irregularity of the cross-sections.

Herein, we report a novel one-step solid-state chemical treatment using a benzocyclobutene (BCB) based polymer. This is a facile approach with BCB functional groups covalently attached onto CNT walls while these groups react with each other simultaneously to form stable covalent bonds. These chemical crosslinks between CNTs are visualized by transmission electron microscopy (TEM). Effect of the designed chemical crosslinking process on the tensile properties of CNTF is discussed both in terms of the traditional method and the density normalized method.

2.2 Experimental

2.2.1 Synthesis of Polymer Linker Poly(styrene-r-4-vinylbenzylcyclobutene) (PS-VBCB)

A series of PS-VBCB polymer linkers with varying monomer ratio were synthesized by anionic polymerization[30] with minor modificatons. In the preparation of a typical PS-VBCB, the monomers, 4-vinyl benzocyclobutene (4-VBCB, synthesized as previously reported[31]), and styrene (Fisher Scientific,>99%)

were purified by exposure to and distillation from calcium hydride (Acros Organics, 93%) and dibutylmagnesium (Sigma Aldrich, 1.0M in heptane), successively, then diluted in anhydrous THF (Fisher Scientific, ACS grade) to ~0.8M and sealed in glass ampules. A hand-crafted all-glass reactor was equipped with an ampule containing sec-butyl lithium (Acros Organics, 0.218 mmol, 1.3M in hexanes) as the initiator, an ampule containing a mixture of diluted monomers (26.9 mmol styrene and 6.9 mmol 4-VBCB) and an ampule of purified methanol (Fisher Scientific, 1mL, >99.5%). After the reactor was flame-sealed from the vacuum line, the initiator and the monomer ampules were cut open and allowed to polymerize for 30 minutes at -78°C before quenching with methanol. The mixture was released from the reactor and precipitated in methanol (500 mL) with vigorous stirring (3 times). Finally, the polymer was dried in a vacuum oven overnight at room temperature to afford a white powder.

2.2.2 Crosslinking MWNT powder

MWNT powder (>99%) was purchased from Cheap Tubes Inc., and used as received. In a small beaker, MWNT powder was immersed in PS-VBCB solution (5 mL, 90 wt.% in toluene) and the solvent was allowed to evaporate. The mixture was dried in vacuum for 2 hours to remove any residual solvent, which reduced the distance between the CNT bundles by the capillary effect. A sample at this point, denoted as PS-VBCB infiltrated MWNT, was then heated in N_2 for 24 hours to initiate the crosslinking reaction. The crosslinked MWNT appeared as sheering flakes due to rigid crosslinking between adjacent CNT bundles. Finally, the sample

was rinsed with copious THF and toluene to remove unreacted PS-VBCB. In order to prove that rinsing effectively removed most of the residual linker, a control sample was prepared by immersing MWNT powder into 90 wt.% PS-VBCB solution in toluene and washed by the same process without heat-induced crosslinking.

2.2.3 Crosslinking CNTF

CNTF was produced by University of Cincinnati through a proprietary process and were used as received. CNTF were treated with the solution of PS-VBCB in toluene at lower concentration (0.1 wt.%), because low linker content is desired to retain high purity in the resultant CNTF. The as-spun CNTFs, noted as pristine, was immersed in PS-VBCB solution (0.1 wt.% in toluene) for 1 hour to enable effective infiltration of the linker into the CNTF. This step is readily applicable in industry by simply adding a bath in the CNTF spinning process. The fiber was then removed from the solution and dried under vacuum at 60 °C for 2 hours. A sample at this stage was denoted as PS-VBCB infiltrated CNTF. A sample that was further heated at 250 °C in N_2 for 4 hours while being stretched to straight is named as PS-VBCB crosslinked CNTF. Both PS-VBCB infiltrated and crosslinked CNTF contained up to 7 wt.% of linker determined by gravimetric analysis.

2.2.4 Characterizations

Thermogravimetric analysis (TGA) (Q50, TA Instrument) was used to analyze the content of linker on treated CNT, at a ramp rate of 10 °C/min to 1000 °C in nitrogen. The thermal behavior of the crosslinking reaction was monitored by differential scanning calorimeter (DSC) (Q2000, TA Instrument) at 5 °C/min from 80 °C to 280 °C. The chemical characteristic of CNTs was evaluated using X-ray photoelectron spectroscopy (XPS) (K-Alpha, Thermo Scientific). Data were collected and analyzed using the Advantage data system (v.4.61). C 1s high resolution core level spectra were recorded at 50 eV pass energy. The atomic concentrations of the detected elements were calculated using integral peak intensities. Inter-tube crosslinking was visualized by transmission electron microscopy (TEM) (Libra 200 MC, Zeiss). The surface morphology and internal structure of CNTF were investigated by focused ion beam scanning electron microscope (FIB-SEM) (Auriga, Zeiss). Gallium ion was used as FIB source to mill the cross sections of the CNTFs inside the SEM chamber. The tensile properties of CNTFs were assessed on a MTS single filament tensile tester, with gauge length of 25mm and extension rate of 0.2mm/min. The diameters of the fibers were measured with $500\times$ optical microscope and used to calculate the ultimate strength (breaking force/ $(0.25\pi d^2)$). Eight specimens from each yarn sample were tested and the average of the results was reported. In addition, density-normalized tensile properties were derived from breaking force (N) and linear density (tex).

2.3 Results and discussion

2.3.1 Establishment of covalent functionalization and crosslinking

In this work, benzocyclobutene (BCB) chemistry was applied. Upon heating, the 4-membered ring of BCB transforms into reactive o-quinodimethane intermediate that can couple with sp^2 carbons of aromatic systems through [4+2] Diels-Alder (D-A) cycloaddition,[32, 33] as illustrated in **Figure 2.1**(a). BCB-containing materials can be widely used to covalently functionalize carbon nanomaterials for several advantages, such as 1) statistical distribution of functional groups on the CNT wall instead of favoring tube ends and defect sites, 2) no catalyst required, and 3) no release of any small molecules during the reaction. For our purpose, PS-VBCB random copolymer was prepared via anionic polymerization and characterized by size exclusion chromatography (SEC) and nuclear magnetic resonance (NMR) (see **Figure A1** and **A2** in the supporting information). The non-reactive styrene units were added to the copolymer to suppress the inevitable intramolecular reaction between BCB units, which leads to formation of collapsed polymer nano particles[31] that negatively affects mechanical properties of the fiber. However, polystyrene itself is a relatively rigid polymer, and the mechanical properties of CNTF can hardly reach the optimum if too much styrene is present. Therefore, a series of PS-VBCB with varying monomer ratio were synthesized and applied to CNTF to study the effect of monomer ratio on the mechanical properties of crosslinked CNTF, and the details will be discussed in Chapter III. The ratio of styrene to BCB leading to the best result is approximately 4:1 and an illustration of

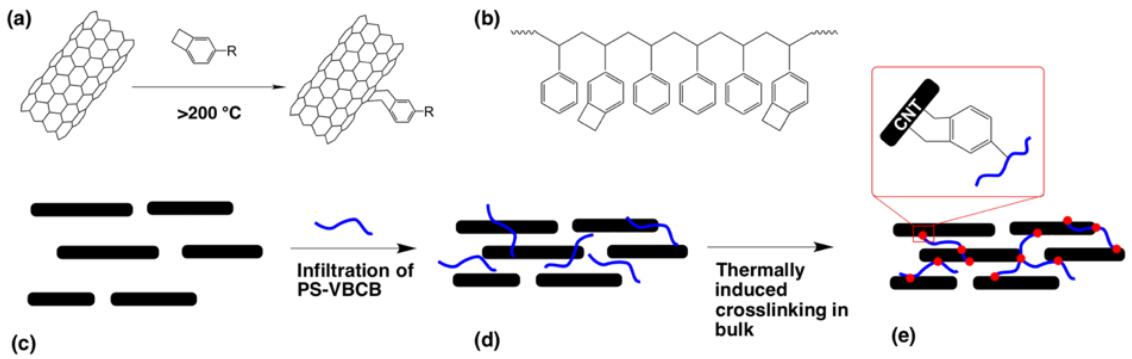

Figure 2.1 (a) D-A cycloaddition of BCB derivatives with CNT; (b) Chemical structure of PS-VBCB; (c-e) Preparation of PS-VBCB crosslinked CNTF by infiltration and thermally induced reaction, and the CNTFs at each stage during the crosslinking process denoted as (c) Pristine CNTF; (d) PS-VBCB infiltrated CNTF; (e) PS-VBCB crosslinked CNTF

the chemical structure is shown in **Figure 2.1** (b). As schematically shown in **Figure 2.1** (c-e), our approach involves infiltration of the polymer linker, PS-VBCB, into CNT materials followed by thermally induced reaction of BCB units with the sp^2 carbons on CNT walls. The polymer backbone acts as inter-tube crosslinks when BCB moieties on the same polymer chain grafts onto adjacent CNTs. In addition, the coupling of BCB with BCB generates a reticulate network that might also contribute to inter-tube crosslinks (**Figure 2.2**).

Given that a meter of the CNTF used in the study weighs only 0.7 mg, it is a big challenge to apply characterization methods that require milligrams of sample. In order to fully demonstrate the chemistry and support the proposed mechanism, bulk multi-walled nanotube (MWNT) powder samples were crosslinked and investigated for such characterizations, since CNT powder is very close to CNTFs in terms of chemical reactivity since they are both composed of MWNT bundles.

The thermogravimetric analysis (TGA) [**Figure 2.3**(a)] reveals a single-step 63% weight loss at around 400 °C for the crosslinked MWNT. This is attributed to the thermal decomposition of reticulate crosslinked PS-VBCB network. Uncured PS-VBCB infiltrated MWNT was rinsed with solvent to obtain physically adsorbed PS-VBCB on the MWNT (control MWNT). Such sample shows 3 wt.% PS-VBCB sorption on MWNT surface by TGA. The reacted portion of BCB linkers went through either cycloaddition with MWNT or with other BCB moieties to form crosslinks. In addition, the cycloaddition and crosslinking reaction of MWNT and

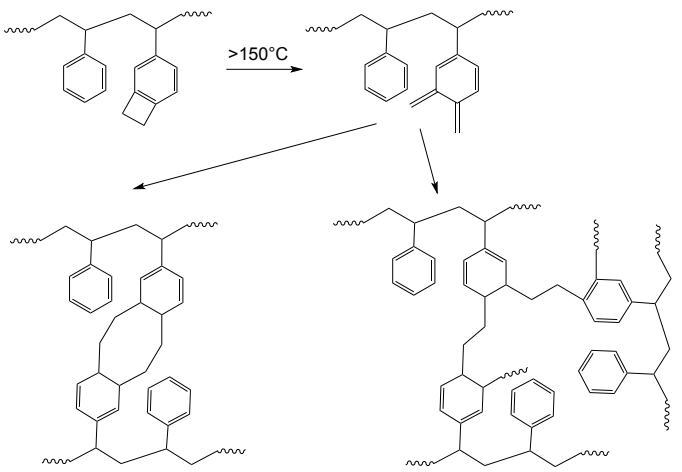

Figure 2.2 Reaction between BCB moieties to form cyclooctadiene (left) and crosslinked polymer (right)

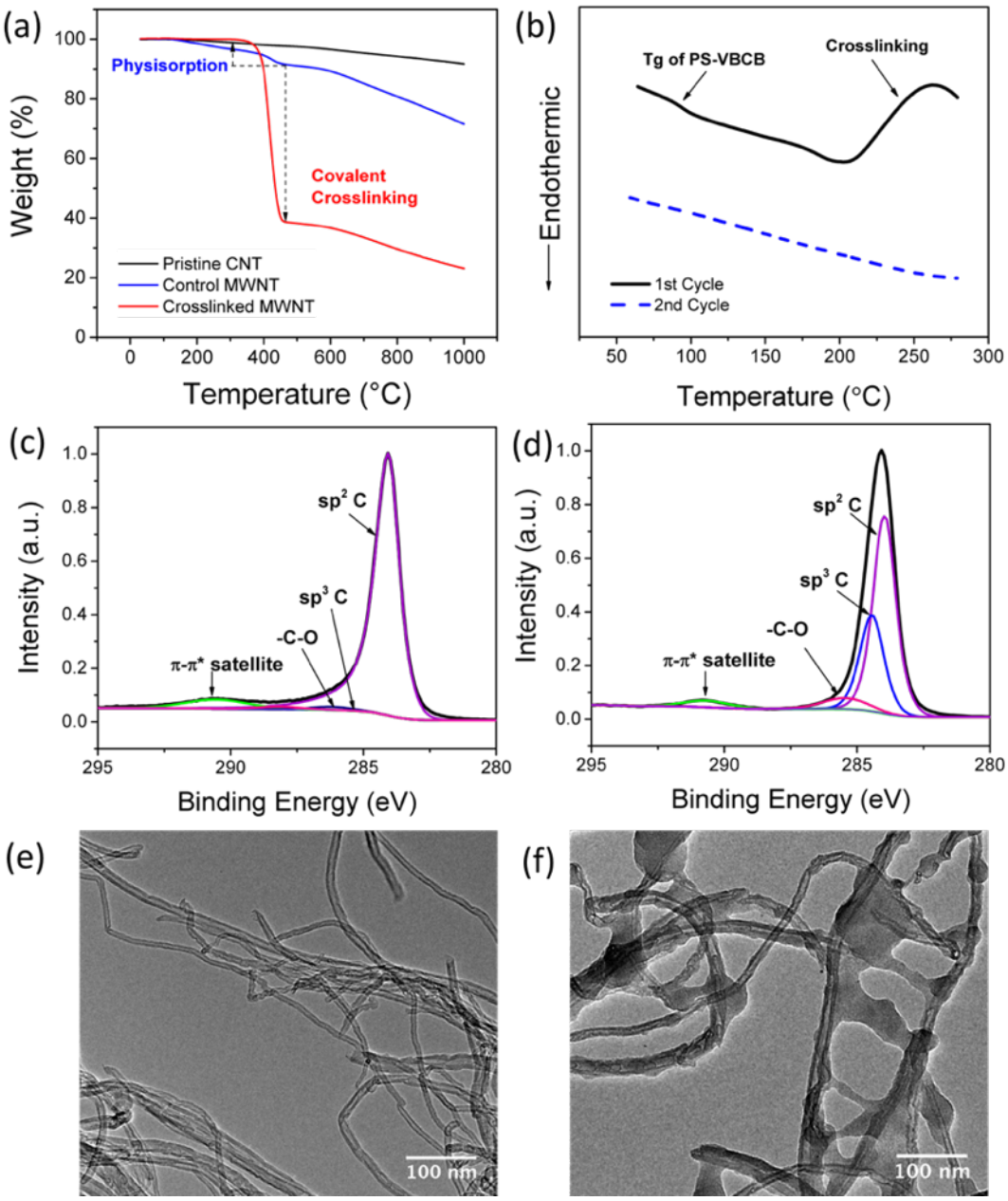

Figure 2.3 Thermal analyses of treated MWNT powder: (a) TGA overlay of PS-VBCB crosslinked MWNT with pristine and control MWNT; (b) DSC curve of PS-VBCB infiltrated MWNT. XPS of (c) control MWNT and (d) crosslinked MWNT. TEM image of (e) Pristine MWNT and (f) PS-VBCB crosslinked MWNT

PS-VBCB was verified through differential scanning calorimetry (DSC) by heating the PS-VBCB infiltrated MWNT *in-situ*, as shown in **Figure 2.3** (b). During the heating ramp in the first cycle, two signals were clearly observed at 100 °C and 200 °C. The endothermic step transition occurred near 100 °C is attributed to the glass transition of PS-VBCB where segmental movement of polymer chains is unlocked. The wide exothermic peak initiated at around 200 °C is associated with activation of BCB units for further cycloaddition and crosslinking with MWNT. As the sample was heated again, both of the signals disappeared. Absence of the glass transition confirms transformation of PS-VBCB to a crosslinked reticulate structure and loss of polymer segmental movement. Also, BCB has fully reacted prior to the second heat ramp due to the absence of an exothermic peak at 200 °C in the second cycle. These thermal characterizations by TGA and DSC provide solid evidence of BCB-induced crosslinking.

Covalent functionalization of BCB onto MWNTs through D-A cycloaddition is supported by X-ray photoelectric spectroscopy (XPS) results. Again, MWNT powder was used to demonstrate the reactivity of C=C on CNTs with PS-VBCB, and the result can be projected to the reaction with CNTs on CNTF. XPS results presented in **Figure 2.3**(c-d) show the high-resolution C 1s spectra of PS-VBCB infiltrated MWNTs and crosslinked MWNTs, respectively. In order to identify differences in the chemical states of carbon in these samples, deconvolution of the C 1s curve was performed and five characteristic peaks were revealed. Binding energy of 284.3, 284.8, 286.5 288.5, and 291.3 eV correspond to sp^2-hybridized

carbon, sp3-hybridized carbon, C-O, C=O, and π- π* satellite signals. These peaks were fitted with a combination of Gaussian-Lorentzian functions and integrated to quantify the contribution of each component. The relative intensity of sp^2 and sp^3 carbons is a good indication of covalent functionalization on MWNT. Since the reaction between BCB groups themselves (**Figure 2.2**) does not induce any changes in the chemical status of carbon on MWNT, lower sp^2 and higher sp^3 in the crosslinked MWNT suggests conversion of C=C unites on the CNT wall to C-C due to cycloaddition reaction with BCB. Negligible signals of C-O and C=O are attributed to defects on MWNT and adventitious carbon. The π- π* satellite signal is characteristic of aromatic structures which can be correlated to graphitic structure on MWNT.

The pristine MWNT and inter-tube crosslinking in the crosslinked samples were visualized via transmission electron microscopy (TEM), as shown in **Figure 2.3**(f). In contrast to the morphology of pristine MWNT in **Figure 2.3**(e), a near-homogeneous polymer layer was observed covering the MWNTs crosslinked with PS-VBCB [**Figure 2.3**(f)]. This suggests that the BCB functional groups were statistically distributed on the MWNTs, instead of being isolated at tube ends or defect sites. In addition to the layer covering the wall, polymeric material also formed inter-tube linkages, resembling the horizontal bars on a ladder.

2.3.2 Effect of the process on the morphology of CNTF

After validating our novel strategy using MWNT powder, we then studied the effect of the crosslinking process on the morphology and mechanical properties

of CNTFs. The surface structures of pristine CNTF with a diameter of 67.3±0.9 μm, PS-VBCB infiltrated CNTF with 37.1±1.1 μm, and PS-VBCB crosslinked CNTFs with 36.4±3.5 μm were observed under SEM at low magnification, as shown **Figure 2.4**(a-c). The CNTs were mostly aligned to the axis of the fiber at a twist angle. While the pristine CNTF exhibits loosely packed structure, PS-VBCB infiltrated and PS-VBCB crosslinked CNTF were condensed to smaller dimensions, primarily due to solvent evaporation after infiltration of linker. Intuitively, introducing crosslinks within the fibers can cause slight shrinkage in diameter, such as direct inter-tube linkages caused by irradiation.[19, 28] However, in many treatments crosslinking CNTF, especially chemical crosslinking methods that introduce functional groups as linkages, no obvious decrease in diameters have been reported due to crosslinking or curing.[19, 20, 25, 27] In this study, the average diameters of PS-VBCB infiltrated fiber before and after heating [**Figure 2.4** (b) and **Figure 2.4** (c), respectively] are very similar, but the error range of the diameters increased. This is due to low percentage of PS-VBCB infiltrated into the fiber (<7%), and the crosslinking reactions occur locally and irregularly, causing some area to shrink and others to swell. Furthermore, due to low void content in infiltrated CNTF, little space is left for crosslinking to further reduce the yarn diameter. In addition, the impregnated polymer in [**Figure 2.4**(b)] created a smooth layer on the surface of the fiber as compared with the less compact structure observed in the pristine sample [**Figure 2.4**(a)]. After thermally induced crosslinking, PS-VBCB collapsed into a reticulate structure, leading to an increase

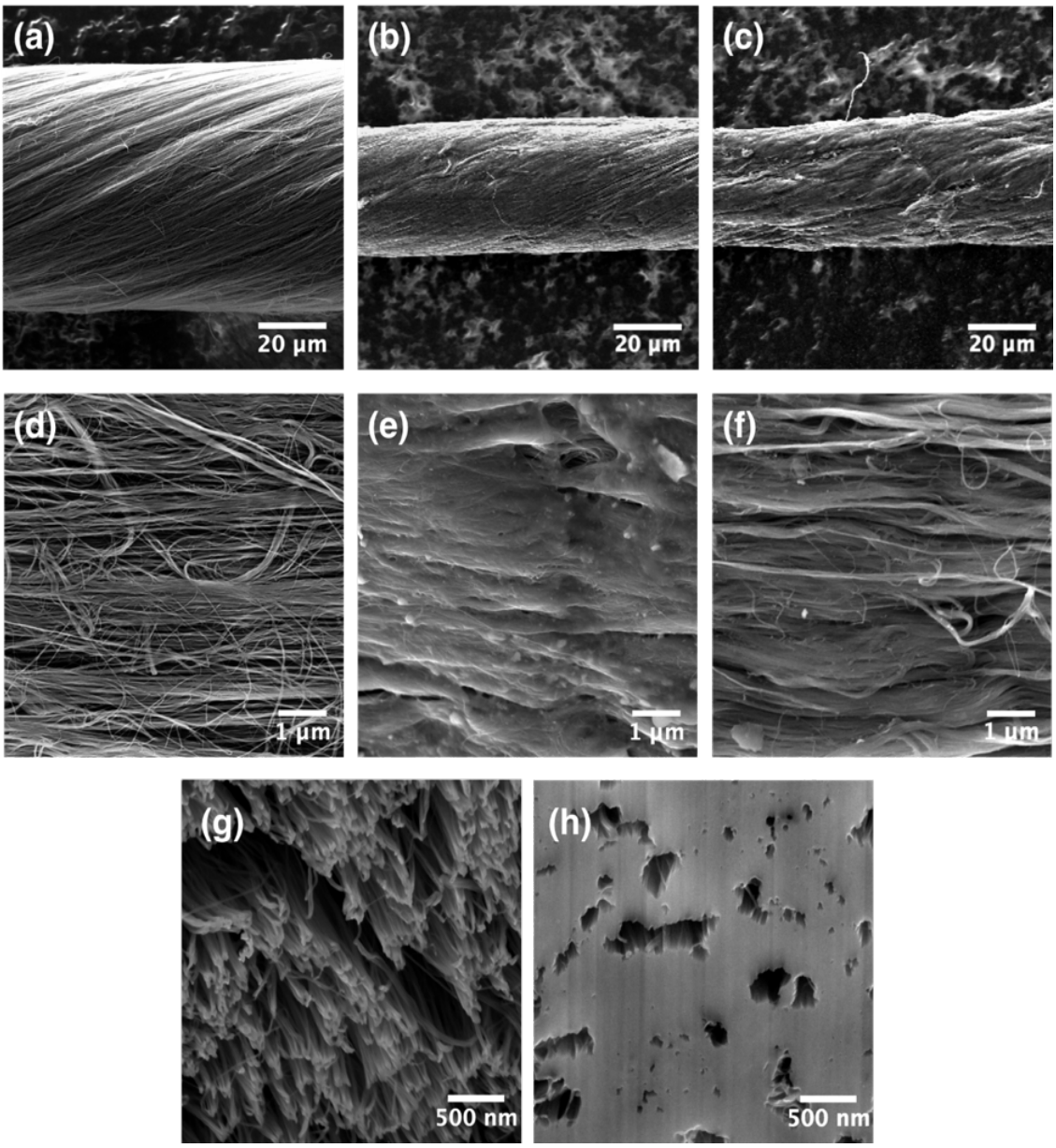

Figure 2.4 Low magnification SEM images of (a) Pristine, (b) PS-VBCB infiltrated, and (c) PS-VBCB crosslinked CNTF; high magnification SEM images of (d) Pristine, (e) PS-VBCB infiltrated, and (f) PS-VBCB crosslinked CNTF; FIB-milled cross-section of (g) Pristine, and (h) PS-VBCB infiltrated CNTF

in surface waviness of the fibers [**Figure 2.4**(c)]. Higher magnification images **Figure 2.4**(d-f) provided further details on the surface morphology. In contrast to pristine CNTF in **Figure 2.4**(d), lower void content was found in **Figure 2.4**(e-f), which is responsible for the difference in the diameters of these samples. Given their close proximity to each other, CNTs and CNT bundles in the densified fiber can easily get in contact with PS-VBCB to enable inter-tube/inter-bundle crosslinking. Consistent with observations from **Figure 2.4**(a-c), a continuous layer of polymer is shown on the CNTF in **Figure 2.4**(e) due to infiltration of PS-VBCB; subsequent heating has introduced irregularities to the surface by turning the continuous polymer cover on CNTs into rigid network that joins the CNTs into large bundles [**Figure 2.4**(f)].

The internal structure of the CNTFs was investigated by imaging at the focused ion beam (FIB)-milled cross-sections that are 10 μm deep [**Figure 2.4**(g-h)]. Again, the pristine fiber was composed of mostly empty spaces, as in **Figure 2.4**(g). After infiltration of the linker and evaporation of solvent, the CNTs were almost “welded” together, only exhibiting occasional vacancies [**Figure 2.4**(h)]. Note that the diameter of the PS-VBCB infiltrated CNTF was around 37 μm, thus the 10 μm-deep cut should fairly represent most of the cross-sectional area. This showed that our polymer was infused effectively towards the center of the fiber during infiltration for 1 hour.

2.3.3 Effect of the process on mechanical properties of CNTF

There are several methods to report the mechanical properties of CNTF,[34] and the two most commonly used ones were discussed below. The traditional tensile strength can be obtained from assuming cylindrical shape of the fiber, where the cross-sectional area $\mathrm{A} = 0.25\pi d^2$.[20, 22, 23, 25, 27]

$$\sigma = \frac{F}{A}$$

Another approach reports the specific strength in $GPa \cdot SG^{-1}$ (equivalent to N/tex) in terms of force (N) per the linear density of the fiber (g/km). The specific strength makes it easier to compare between different types of fibers.

$$\sigma^* = \frac{N}{tex}$$

Here we report the mechanical properties of the pristine and treated CNTF through both methods mentioned above, as shown in and **Table 2.1** and **Figure 2.5**. The overall crosslinking process improved the specific tensile strength by 40% from 0.33±0.04 N/tex to 0.46±0.04 N/tex. This does not appear as a remarkable improvement, but if traditional tensile strength is considered, as in many reports,[20, 22, 25, 27] the improvement becomes 230% from 70±20 MPa to 230±50 MPa, which is the highest among all reported chemical crosslinking processes. In this study, several factors present in the process can contribute to the improvement of mechanical properties: 1) solvent densification, 2) polymer infiltration, and 3) simultaneous covalent functionalization and crosslinking as discussed above. During solvent evaporation, a capillary force induced by surface tension of the

Table 2.1 Tensile properties of Pristine, Toluene densified, PS-VBCB infiltrated, and PS-VBCB crosslinked CNTF

	Strength (MPa)	Modulus (GPa)	Specific Strength (N/tex)	Specific Modulus (N/tex)
Pristine CNTF	70±20	3.5±2	0.33±0.04	17±4
Toluene Densified CNTF	170±30	6.6±2	0.42±0.05	17±3
PS-VBCB Infiltrated CNTF	190±40	11.8±3	0.43±0.05	26±3
PS-VBCB Crosslinked CNTF	230±50	15.6±3	0.46±0.04	28±4

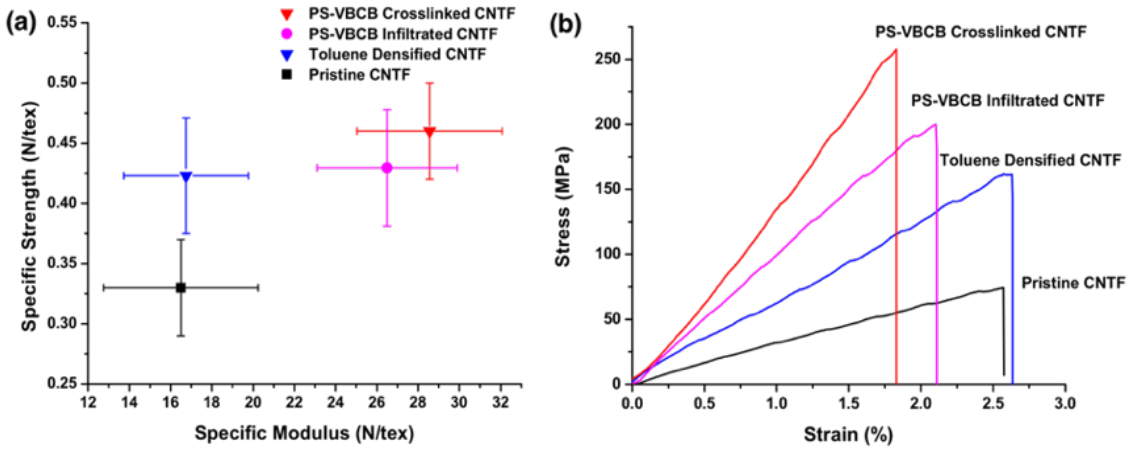

Figure 2.5 (a) Specific tensile properties of Pristine, Toluene densified, PS-VBCB infiltrated, and PS-VBCB crosslinked CNTFs with error bars; (b) Typical traditional stress-strain curve of Pristine, Toluene densified, PS-VBCB infiltrated, and PS-VBCB crosslinked CNTF

organic solvent brings the CNT bundles closer to each other, which causes the diameter of the fiber to decrease, and results in higher contact area for enhanced frictional forces.[35] Both **Figure 2.4**(a) and (b) show higher tensile strength of CNTF after being densified by toluene, but there was no significant change on modulus. Impregnation of polymer into the CNTF enhances the CNT junctions through molecular level coupling, which could benefit load transfer between the CNT bundles [17]. The forementioned two factors should be responsible for the improved tensile strength (from 70±20 MPa to 190±40 MPa or from 0.33±0.04 N/tex to 0.43±0.05 N/tex) shown for PS-VBCB infiltrated CNTF after it underwent PS-VBCB infiltration and drying. The infiltrated polymer results in higher stiffness of CNTF as compared to the solvent densified sample, possibly due to the inherent rigidity of polystyrene chains and its derivatives. Excluding this portion of improvement, the additional 93% increase in traditional tensile strength and 10% in specific strength should be attributed to PS-VBCB crosslinking with the CNTF. The covalent functionalization of BCBs onto CNT walls provides strong bondings, while concurrent BCB-BCB coupling results in a reticulate structure that filled the empty spaces between CNT bundles to achieve more effective load transfer.

2.4 Conclusion

A novel and simple one-step solid-state chemical crosslinking process was developed to improve stiffness and strength of CNTF using a BCB-based polymer. By infiltration of the polymer linker into CNTF followed by heating, covalent functionalization of CNTF with the polymer was achieved with simultaneous inter-

CNT crosslinking. Since the CNT bundles were covalently locked in a rigid network, an increase in mechanical properties is observed. The process remarkably improves the specific tensile strength by 40% and traditional tensile strength by 230%. These improvements are not only attributed to the process of polymer infiltration and solvent densification, but are also directly related to simultaneous functionalization and inter-tube linking. This reaction employed required no catalyst, and releases no byproducts. Considering the simplicity of the process with functionalization and covalent crosslinking achieved in a single step, BCB induced crosslinking appears promising for industrial post-treatment of CNTFs to greatly improve their mechanical performance.

References

1. Lu, X.; Hiremath, N.; Hong, K.; Evora, M. C.; Ranson, V. H.; Naskar, A. K.; Bhat, G. S.; Kang, N.-G.; Mays, J. W., *Nanotechnology* **2017,** *28* (14), 145603.

2. De Volder, M. F.; Tawfick, S. H.; Baughman, R. H.; Hart, A. J., *Science* **2013,** *339* (6119), 535-539.

3. Jiang, K.; Wang, J.; Li, Q.; Liu, L.; Liu, C.; Fan, S., *Advanced Materials* **2011,** *23* (9), 1154-1161.

4. Byrne, M. T.; Gun'ko, Y. K., *Advanced Materials* **2010,** *22* (15), 1672-1688.

5. Behabtu, N.; Green, M. J.; Pasquali, M., *Nano Today* **2008,** *3* (5), 24-34.

6. Zhang, M.; Atkinson, K. R.; Baughman, R. H., *Science* **2004,** *306* (5700), 1358-1361.

7. Koziol, K.; Vilatela, J.; Moisala, A.; Motta, M.; Cunniff, P.; Sennett, M.; Windle, A., *Science* **2007,** *318* (5858), 1892-1895.

8. Lu, W.; Zu, M.; Byun, J. H.; Kim, B. S.; Chou, T. W., *Advanced Materials* **2012,** *24* (14), 1805-1833.

9. Peng, B.; Locascio, M.; Zapol, P.; Li, S.; Mielke, S. L.; Schatz, G. C.; Espinosa, H. D., *Nat Nano* **2008,** *3* (10), 626-631.

10. Behabtu, N.; Young, C. C.; Tsentalovich, D. E.; Kleinerman, O.; Wang, X.; Ma, A. W.; Bengio, E. A.; ter Waarbeek, R. F.; de Jong, J. J.; Hoogerwerf, R. E., *Science* **2013,** *339* (6116), 182-186.

11. Kozlov, M. E.; Capps, R. C.; Sampson, W. M.; Ebron, V. H.; Ferraris, J. P.; Baughman, R. H., *Advanced Materials* **2005,** *17* (5), 614-617.

12. Zhang, X.; Jiang, K.; Feng, C.; Liu, P.; Zhang, L.; Kong, J.; Zhang, T.; Li, Q.; Fan, S., *Advanced Materials* **2006,** *18* (12), 1505-1510.

13. Li, Y.-L.; Kinloch, I. A.; Windle, A. H., *Science* **2004,** *304* (5668), 276-278.

14. Wang, Y.; Colas, G.; Filleter, T., *Carbon* **2016,** *98*, 291-299.

15. Beese, A. M.; Wei, X.; Sarkar, S.; Ramachandramoorthy, R.; Roenbeck, M. R.; Moravsky, A.; Ford, M.; Yavari, F.; Keane, D. T.; Loutfy, R. O.; Nguyen, S. T.; Espinosa, H. D., *ACS Nano* **2014,** *8* (11), 11454-11466.

16. Miao, M., *Carbon* **2015,** *91*, 163-170.

17. Sakellariou, G.; Avgeropoulos, A.; Hadjichristidis, N.; Mays, J. W.; Baskaran, D., *Polymer* **2009,** *50* (26), 6202-6211.

18. Jung, Y.; Kim, T.; Park, C. R., *Carbon* **2015,** *88* (0), 60-69.

19. Miller, S. G.; Williams, T. S.; Baker, J. S.; Solá, F.; Lebron-Colon, M.; McCorkle, L. S.; Wilmoth, N. G.; Gaier, J.; Chen, M.; Meador, M. A., *ACS Applied Materials & Interfaces* **2014,** *6* (9), 6120-6126.

20. Ryu, S.; Lee, Y.; Hwang, J. W.; Hong, S.; Kim, C.; Park, T. G.; Lee, H.; Hong, S. H., *Advanced Materials* **2011,** *23* (17), 1971-1975.

21. Boncel, S.; Sundaram, R. M.; Windle, A. H.; Koziol, K. K., *ACS nano* **2011,** *5* (12), 9339-9344.

22. Cui, Y.; Zhang, M., *ACS applied materials & interfaces* **2013,** *5* (16), 8173-8178.

23. Tran, T. Q.; Fan, Z.; Liu, P.; Myint, S. M.; Duong, H. M., *Carbon* **2016,** *99*, 407-415.

24. Williams, T. S.; Orloff, N. D.; Baker, J. S.; Miller, S. G.; Natarajan, B.; Obrzut, J.; McCorkle, L. S.; Lebron-Colón, M.; Gaier, J.; Meador, M. A., *ACS Applied Materials & Interfaces* **2016**.

25. Min, J.; Cai, J. Y.; Sridhar, M.; Easton, C. D.; R. Gengenbach, T.; McDonnell, J.; Humphries, W.; Lucas, S., *Carbon* **2013,** *52* (0), 520-527.

26. Zhang, J.; Jiang, D.; Peng, H.-X.; Qin, F., *Carbon* **2013,** *63* (0), 125-132.

27. Choi, Y.-M.; Choo, H.; Yeo, H.; You, N.-H.; Lee, D. S.; Ku, B.-C.; Kim, H. C.; Bong, P.-H.; Jeong, Y.; Goh, M., *ACS Applied Materials & Interfaces* **2013,** *5* (16), 7726-7730.

28. Miao, M.; Hawkins, S. C.; Cai, J. Y.; Gengenbach, T. R.; Knott, R.; Huynh, C. P., *Carbon* **2011,** *49* (14), 4940-4947.

29. Åström, J.; Krasheninnikov, A.; Nordlund, K., *Physical review letters* **2004,** *93* (21), 215503.

30. Sakellariou, G.; Baskaran, D.; Hadjichristidis, N.; Mays, J. W., *Macromolecules* **2006,** *39* (10), 3525-3530.

31. Harth, E.; Horn, B. V.; Lee, V. Y.; Germack, D. S.; Gonzales, C. P.; Miller, R. D.; Hawker, C. J., *Journal of the American Chemical Society* **2002,** *124* (29), 8653-8660.

32. Sakellariou, G.; Ji, H.; Mays, J. W.; Hadjichristidis, N.; Baskaran, D., *Chemistry of Materials* **2007,** *19* (26), 6370-6372.

33. Sakellariou, G.; Ji, H.; Mays, J. W.; Baskaran, D., *Chemistry of Materials* **2008,** *20* (19), 6217-6230.

34. Wu, A. S.; Chou, T.-W., *Materials Today* **2012,** *15* (7), 302-310.

35. Hiremath, N.; Lu, X.; Evora, M. C.; Naskar, A.; Mays, J.; Bhat, G., *Journal of Materials Science* **2016,** *51* (22), 10215-10228.

Appendix A

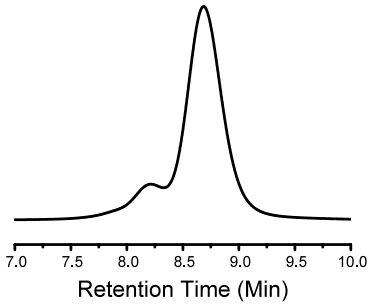

Figure A1 SEC curve of PS-VBCB

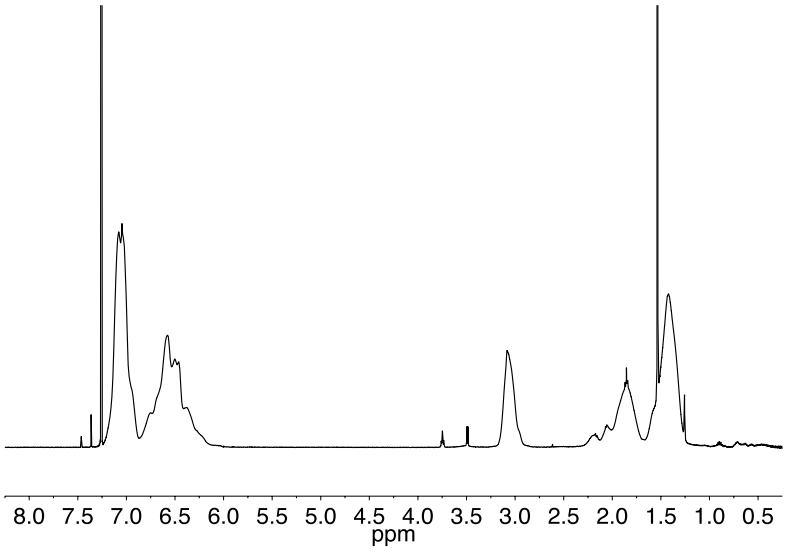

Figure A2 ^{1}H NMR of PS-VBCB

CHAPTER III

THE EFFECT OF POLYMER STRUCTURE AND TREATMENT PARAMETERS ON PROPERTIES OF CROSSLINKED CARBON NANOTUBE FIBERS

Abstract

In this chapter, the effects of several parameters on the process of benzocyclobutene (BCB)-based crosslinking with carbon nanotube fibers (CNTF) were assessed. The synthesis of poly(styrene-co-4-vinylbenzocyclobutene) random copolymer with various monomer ratio was accomplished. Their abilities to strengthen the mechanical properties of carbon nanotube fibers through covalent crosslinking were evaluated, and polymer with styrene percentage of 80% is found to yield the highest improvement. Various concentrations were used for the polymer solution during infiltration into CNTF. The mechanical testing of resulting crosslinked fibers confirmed the optimum concentration is around 0.05% or 0.1%. Thermal treatment on fibers without BCB impregnation lowered their tensile properties. The surface structure of thermally treated CNTF was examined by scanning electron microscope. The change in morphology of the fiber, such as lowered bundle size and formation of polymer agglomerates, should be responsible for the drop in tensile strength.

3.1 Introduction

Carbon nanotube fibers (CNTFs) are macroscopic assemblies of carbon nanotubes (CNTs), with the individual CNTs axially aligned to one another parallel to the axis of the fiber.[1, 2] These fibers containing only CNTs could lead to great applications in advanced technologies if they can translate a significant portion of the extraordinary properties of individual CNTs.[2] For this purpose, the CNTs in the fiber are required to be long, well-aligned, highly packed and arranged with minimum defects.[2]

In recent reports, CNTF are most often fabricated through dry-spinning methods, including direct spinning from aerogel out of chemical vapor deposition (CVD) furnace, and drawing from vertically grown CNT forests on a substrate. These solid-state spinning methods circumvents the dissolution difficulty of CNTs, however, the resulting fiber inherently suffer from porous morphology.[2] Post-treatments are necessary to reduce the void spaces in the fiber and enhance the load transfer between the CNT components, and important process parameters have been discussed in each case. For the CVD spinning process, higher winding rate has been observed to yield higher density and enhanced alignment.[3, 4] Twisting of the fiber is also beneficial for increasing fiber density, however there is an optimum twist angle above which the load is transferred to compress the tubes and strength of the fiber decreases.[5, 6] Solvent densification applied on dry-spun yarns lead to diameter shrinking by two to three orders of magnitude, driven by surface tension of the liquid.[3, 7, 8] The effect of solvent on the CNTF was correlated

to the affinity to graphitic carbons.[9, 10] Infiltration of a polymer solution such as PVA into the empty spaces in the fiber improves inter-tube load transfer without compromising the connectivity of the CNT.[11, 12] Differences in chemical structure and size of the polymers result in difference in bundle sizes, which can be correlated with the fiber strength.[13, 14] The concentration of the polymer solution has also been optimized for reinforcement of the CNTF.[13]

In more complicated chemical treatments, specific parameters are discussed with respect to each approach. For example, concentration of catalyst and reaction time for cross-dehydrogenative coupling of CNTF were varied to investigate their effect on the strength of the resulting fiber.[15] Cui et al. infiltrated polyacrylonitrile (PAN) polymer solution into CNTF and subsequently cured the composite to improve the tensile strength.[16] 1 % wt has been found to be the optimum concentration of PAN solution.

As a follow-up investigation for Chapter II, this part of the dissertation further discussed the possible parameters that affect the reinforcement of CNTF through crosslinking with benzocyclobutene (BCB) polymers. The chemical structure and concentration of BCB polymer were investigated. In addition, the effect of thermal treatment on the morphology was correlated to mechanical strength of CNTF.

3.2 Experimental

3.2.1 Materials

CNTF was produced by University of Cincinnati through a proprietary process and were used as received. The pristine fiber is a research grade material, with tensile strength of around 70 MPa, density of lower than 1g/m^3, and electrical resistivity of around $1\times10^{-5}\ \Omega\cdot$m.

The BCB-containing monomer, 4-vinyl benzocyclobutene (4-VBCB) was synthesized as reported by Hawker group with slight modification, as illustrated in **Scheme 3.1**.[17] The starting material 4-bromo benzocyclobutene (4-Br-BCB was purchased from Shanghai Medicilon Inc (>99.9%). To prepare for a typical Grignard reaction, 4-Br-BCB was stirred over CaH_2 (Fisher Scientific, >99%) overnight and distilled under vacuum. Magnesium turning (Sigma Aldrich, >99%) was dried overnight by heating at 60 °C under vacuum. Approximately 5g of Mg was transferred to the reactor with 75 mL of anhydrous tetrahydrofuran (THF). The reactor was purged with argon gas (Airgas, UHP Grade) for 10 mins, then 5 drops of 1,2-dibromoethane was added to the suspension to activate Mg. Approximately 40g of 4-Br-BCB was added to reaction via syringe pump at a rate of 50 mL/mL to generate dark brown colored Grignard reagent. The Grignard mixture is chilled to 0 °C, while 48.5 g dried 1,1-dimethylformamide (DMF, distilled over CaH_2, 3 times molar equivalence to 4-Br-BCB) was added dropwise at room temperature. The mixture was refluxed for 15 mins and acidified with saturated NH_4Cl solution with vigorous stirring. The product 4-aldehyde-benzocyclobutene (4-CHO-BCB) was

extracted with CH_2Cl_2, with excess solvent removed by rotorvap, 14 g crude product was obtained (yield ~50%). In the next step, the 4-CHO-BCB went through Wittig reaction to afford 4-VBCB. In detail, 42.4 g Methyltriphenylphosphonium bromide ($Br^-P^+Ph_2CH_3$, Sigma Aldrich, 99.9%) was mixed with 80 mL THF after purging with argon. 118 mL of 1M potassium tert-butoxide (KOBu, 1M solution in THF, TCI Chemicals) was introduced to the reactor making a yellow suspension and stirred for 2hrs. 13.1g 4-CHO-BCB was added slowly to the mixture to initiate the Wittig reaction. The reaction mixture was quenched with NH_4Cl saturated solution and the organic layer was purified by flash column chromatography with hexanes as eluent solvent. A total of 6.7 g 4-VBCB was obtained, with yield of 51.6%.

Scheme 3.1 Two-step synthesis of 4-VBCB monomer from 4-Br-BCB precursor including Grignard reaction and Wittig reaction

3.2.2 Synthesis of Polymer Linkers

The synthesis of PS-VBCB via anionic polymerization is presented in section 2.2.2, and **Figure 3.1** represents the apparatus for high-vacuum anionic polymerization.

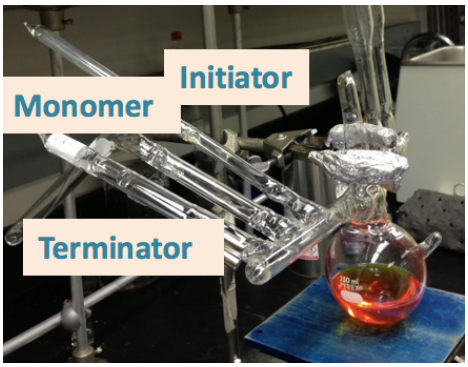

Figure 3.1 Representative apparatus for anionic copolymerization of styrene and PS-VBCB. s-BuLi is used as initiator while methanol is the terminator. The bright red color of the solution indicates the presence of active conjugate anion.

In addition, a series of polymer crosslinkers were prepared through conventional free radical copolymerization using 2,2'-Azobis(2-methylpropionitrile) (AIBN) as initiator, as described in **Scheme 3.2**. The molar ratio of monomers to initiator and molar ratio of the two monomers (styrene and 4-VBCB) varied to synthesize polymer with the desired structure. The monomer ratio in the starting feed is prepared the same as the desired copolymer content, because of similar reactivity ratio of two monomers in a radical polymerization (4-VBCB is slightly lower than styrene probably because of the more bulky structure).[18] Before a polymerization, the reagents are purified accordingly. Styrene (Fisher Scientific, 99.9% with stabilizer) was passed through a short basic alumina column. AIBN was recrystallized from saturated solution in methanol.

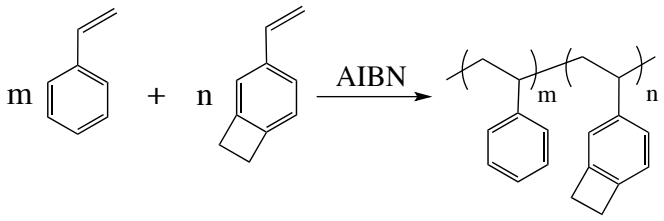

Scheme 3.2 Free radical copolymerization of styrene and 4-VBCB with AIBN as initiator

In a typical free radical copolymerization, where the target of Sty:4-VBCB is 3:1, 1.5g styrene (14.4 mmol), 0.75g 4-VBCB (5.76 mmol) as well as 0.022g purified AIBN (0.132 mmol) were mixed in a shlenk tube with 2 mL of toluene (Fisher Scientific, >99.5%). The mixture is degased three times through freeze-

pump-thaw cycles. After the shlenk tube was refilled with argon, it is transferred into 60 °C oil bath to allow for polymerization for 24 hrs. Finally, the reaction is quenched by inserting the tube into ice water. The solution was diluted by approximately 20mL toluene and dropped into 300 mL methanol with vigorous stirring. The white precipitate was filtered and dried to afford 1.12g copolymer powder. A list of copolymers synthesized to study their effect on the properties of CNTF is displayed in **Table 3.1**.

3.2.3 Crosslinking CNTF

The pristine CNTF is cut into 40cm-long pieces and wound onto a hand-crafted glass holder as shown in **Figure 3.2**(a). The setup is immersed into the solution of PS-VBCB in toluene at desired concentration (ranging from 0.05% wt. to 3% wt.) for 1 hour to enable effective infiltration of the linker into the CNTF. As demonstrated in **Figure 3.2**(b), t his step is readily applicable in industry by leading the as-spun CNTF into a bath. The fiber was then removed from the solution and dried under vacuum at 60 °C for 2 hours. A sample at this stage is denoted as PS-VBCB infiltrated CNTF. A sample that was further heated at 250 °C in N_2 for 4 hours while being stretched to straight is named as PS-VBCB crosslinked CNTF. For this step, an isotemp vacuum oven was used that is equipped with a gas inlet and an outlet. Both PS-VBCB infiltrated and crosslinked CNTF contains less than 7 wt.% of linker determined by gravimetric analysis. In order to study the effect of temperature on the fibers excluding the crosslinking factor, several control samples are prepared. A toluene densified CNTF and a PS infiltrated CNTF are further

Table 3.1 Molecular characteristics of PS-VBCB crosslinkers synthesized with different monomer ratio

Polymer ID	Mn (g·mol-1)	Styrene mol% in the polymer (%)	Poly-dispersity
S1B2	16,700	33	1.91
S1B1	17,800	50	1.75
S2B1	11,000	66	1.6
S3B1	16,500	75	1.6
S4B1	16,700	80	1.16
PS	17,900	100	1.09

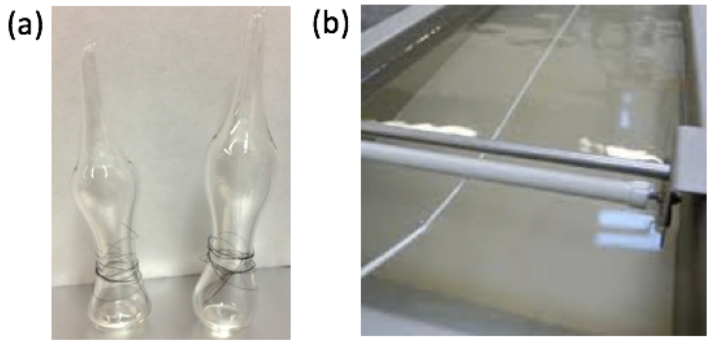

Figure 3.2 (a) Facilities for infiltration of a polymer into the inter-tube spaces of CNTF on a laboratory scale. (b) Illustration of a solution bath that can be utilized for impregnation of polymer into CNTF on the industry scale.

allowed through thermal treatment along with the samples to be crosslinked.

3.2.4 Characterizations

All ^{1}H NMR analyses were performed on a Varian VNMR 500 MHz spectrometer using deuterated chloroform (CDCl3) as the solvent. Molecular weights and their distributions were determined by size exclusion chromatography (SEC) measurements performed using a Tosoh EcoSEC System equipped with two Tosoh TSKgel SuperMultiporeHZ-M and one TSKgel SuperMultipore HZ-M guard column. The polymers samples were made into solution in THF at approximately 0.1 g/mL. Analytes are eluted with THF at 40 °C with a flow rate of 0.35 mL/min and a run time of 15 mins. The results were acquired from an RI detector based on calibration with polystyrene standards (6000-7500000 Da). The tensile properties of CNTFs were assessed on a MTS single filament tensile tester, with gauge length of 25mm and extension rate of 0.2mm/min. The diameters of the fibers were measured with 500× optical microscope and used to calculate the ultimate strength (breaking force/ ($0.25\pi d^2$)). Eight to ten specimens from each yarn sample were tested and the average of the results was reported. The surface morphology and of CNTF were investigated by scanning electron microscope (SEM) (Auriga, Zeiss) at a voltage of 5 keV.

3.3 Results and discussion

3.3.1 Characterization of PS-VBCB poly crosslinkers

As displayed in **Table 3.1**, a series of PS-VBCB copolymers with similar molecular weight and varying BCB content have been synthesized. SEC was used to determine their molecular weight and distribution. For the purpose of comparison, an overlay of the chromatograms of related polymers is displayed in **Figure 3.3**. The retention time of all the polymers fall between 7 to 10 minutes, with slight shifts between one another. The PS-VBCB crosslinkers synthesized through radical polymerization exhibit broader peak in the chromatogram because of their polydispersity of around 1.5. The S4B1 sample synthesized through anionic polymerization exhibits a small shoulder at the low retention time side of the chromatogram. Analysis of the integrated shoulder shows doubled molecular weight of the main peak, indicating small portion of bi-coupling during the synthesis.

The chemical structure of the PS-VBCB linkers are examined by NMR spectroscopy. ^{1}H NMR of the copolymers shows the prominent resonance for the methylene protons of the cyclobutene group at 3.10 ppm. The integrated area of aromatic protons and the aliphatic BCB protons are used to determine the molar ratio of styrene to BCB (m:n) in the final polymer, through the equation

$$\begin{cases} aromatic\ H = 5m + 3n \\ BCB\ methylene\ H = 4n \end{cases}$$

The ^{1}H NMR spectrum of S1B1 PS-VBCB copolymer is displayed in **Figure 3.4**.

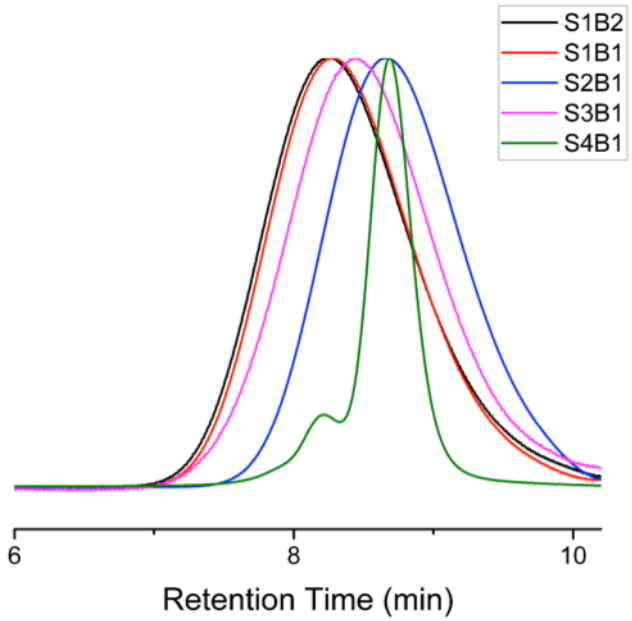

Figure 3.3 SEC overlay of PS-VBCB corsslinkers with similar Mn

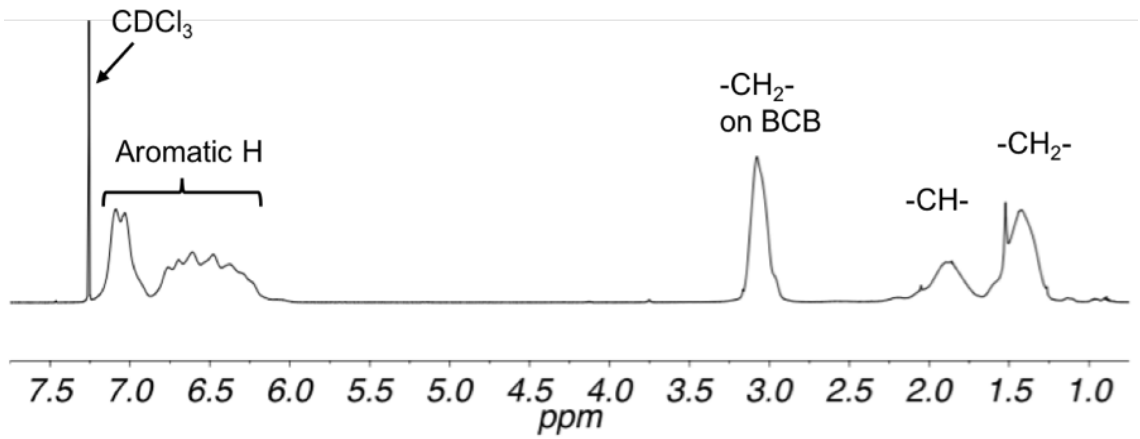

Figure 3.4 ^{1}H NMR spectra of PS-VBCB copolymers with varying BCB content

3.3.2 Effect of monomer ratio in the copolymer on the mechanical properties of resulting crosslinked CNTF

The proposed post-treatment takes advantage of BCB chemistry for covalent crosslinking of CNTF in order to enhance their mechanical properties. As elaborated in section 2.3.1, BCB groups are incorporated into polymers at the pendent group position. When BCB crosslinkers are thermally treated at the presence of CNT materials, the cyclobutene rings are opened and covalent bonds are formed with the carbons on the surface of the tube, turning these graphitic carbons into their sp^3 hybridized alternatives.[19, 20] In the meantime, activated BCB groups also react with each other to form dimers and oligomers through coupling of radicals, which has been applied to crosslinking of different needs.[17, 18, 21] As such, the BCB moieties not only contribute to covalent crosslinks in CNT materials, also to formation of unfavored collapsed polymer nanoparticles.[17] These reticulate aggregates of crosslinked BCB in the treated fiber could be considered as defect sites as they force the nearby CNT fiber elements to kink and reduce the efficiency of load transfer. Such concern drives our motive to impart non-reactive styrene units in the BCB polycrosslinker and control the crosslink density of the polymer. Since all polystyrene will not have a crosslinking effect, we investigated the optimized styrene content on the mechanical properties of the resulting CNTF.

As displayed in **Table 3.1** and **Figure 3.3**, the polymer crosslinkers have similar number average molecular weight of 17 kDa, with sample S2B1 as an exception (Mn= 11 kDa). Presumably, the polycrosslinkers should demonstrate

similar kinetics during the infiltration into internal structure of CNTF, and as expected, the impregnated amount of crosslinker is stable at 3~7 %wt, acquired from mass difference of the same fiber before and after infiltration.

The effect of styrene content in the PS-CBCB crosslinker on the tensile strength and modulus of CNTF crosslinked (or thermally treated in the case of PS-infiltrated CNTF) with these polymers are displayed in **Figure 3.5** and **Figure 3.6**, respectively. The elastic strengths of all treated fibers are higher than that of the pristine fiber, which is at 70±18 MPa. The fiber that was impregnated with PS (denoted as 100% styrene content in the polymer in both **Figure 3.5** and **3.6**) exhibits 167±27 MPa of strength, 140% higher than the pristine CNTF. The improvement is attributed to two aspects: (i) solvent densification of the fiber induced by the evaporation of the liquid after the polymer was infiltrated; (ii)intermolecular coupling of polymer chains with CNT bundles that enhanced the load transfer between CNT elements in the fiber. Surprisingly, this improvement is even higher than those shown for fibers crosslinked with S1B2, S1B1, and S2B1, with corresponding styrene content of 33%, 50%, and 66%. These three polymers have relatively low styrene content compared to other crosslinkers. Even though we expect the crosslinking of BCB moieties on S1B2, S1B1, and S2B1 to lead to higher improvement in the tensile strength of the resulting fiber since covalent bonds are stronger than non-covalent intermolecular coupling between PS and CNTs, the observation was opposite. This phenomenon may be due to the high density of BCB and lack of enough styrene units to prevent over-crosslinking and

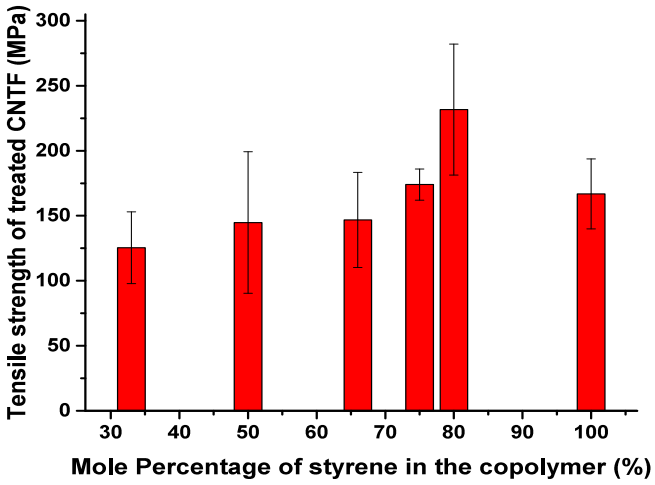

Figure 3.5 Effect of styrene content in the copolymer on the tensile strength of resulting crosslinked CNTF

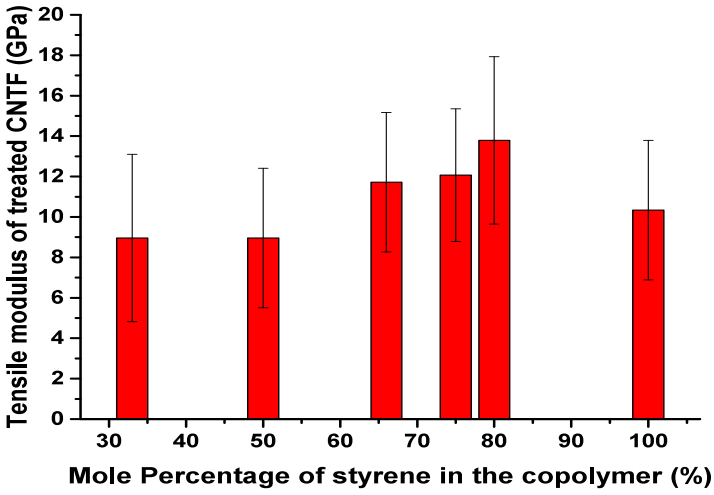

Figure 3.6 Effect of styrene content in the copolymer on the tensile modulus of resulting crosslinked CNTF

formation of local reticulate BCB network. Under such conditions, the negative effect of BCB units on the mechanical properties of CNTF overrides their potential of strengthening the fibers through formation of inter-tube bonding. As styrene content increases to 75% (in polymer S3B1), the improvement caused to the resulting CNTF compared to the pristine yarns becomes 149%, slightly higher than the PS treated sample. For polymer S4B1, where styrene percentage in the polymer is increased to 80%, the highest positive effect was observed.

As displayed in **Figure 3.6**, the stiffness of CNTF crosslinked with polymers with varying BCB/styrene content exhibit the same trend as their tensile strengths. The modulus of treated fiber increase slowly as there is more nonreactive styrene in the polymer chain (from 33%-80%) and drops again when BCB is no longer present (styrene content of 100%). However, the magnitude of difference in percentage improvement caused on modulus by different polymers is smaller than that caused on strength. This can be possibly attributed to the nature of modulus, where formation of reticulate 3D network can be beneficial since the individual tubes and CNT bundles are more difficult to displace. Part of the unfavorable effect of high BCB density to the mechanical performance of the fibers (collaped BCB particles may force damage on CNTs, making them less load bearing) is counterbalanced by the suggested positive effect.

3.3.3 Effect of infiltrated polymer solution on the mechanical properties of crosslinked CNTF

Another parameter to be controlled in the designed crosslinking process is the amount of polymer linker impregnated into the void spaces of CNTF. This can be tuned by two methods: (i) controlling the duration of the infiltration step, and (ii) controlling the concentration of the polymer solution in the bath. Cui and coworkers reported that dipping CNTF into 1% wt PAN solution for 5 mins leads to insufficient impregnation, where the polymers only ingressed 2 μm deep into a fiber with diameter of 25 μm.[16] On the other hand, Ryu et al. claimed that immersion of CNTF into catecholamine polymer solution for 30mins is sufficient for the polymers to diffuse to the center of the fiber with final diameter of 17.1 μm (which was the result of shringking from 91.8 μm).[22] The kinetics of the infiltration into the inner structure of CNTF should vary with many factors, such as affinity of the polymer to graphitic carbon, size of the polymer, and compactness of the fiber structure. Therefore, the infiltration time is not absolutely comparable from study to study. In this work, we let the fiber immerse in the solution for 1h to ensure effective diffusion of polymer into the center of the fiber.

Keeping the infiltration time constant at 1h, the concentration of the polymer solution was varied from 0.05% wt to 1% wt in toluene. The polymer content (% wt) in the impregnated fiber was measured and compared between different concentrations. As shown in **Figure 3.7**(a), the general trend is that the longer the infiltration time, the more polymer in the impregnated fiber. Note that the linear

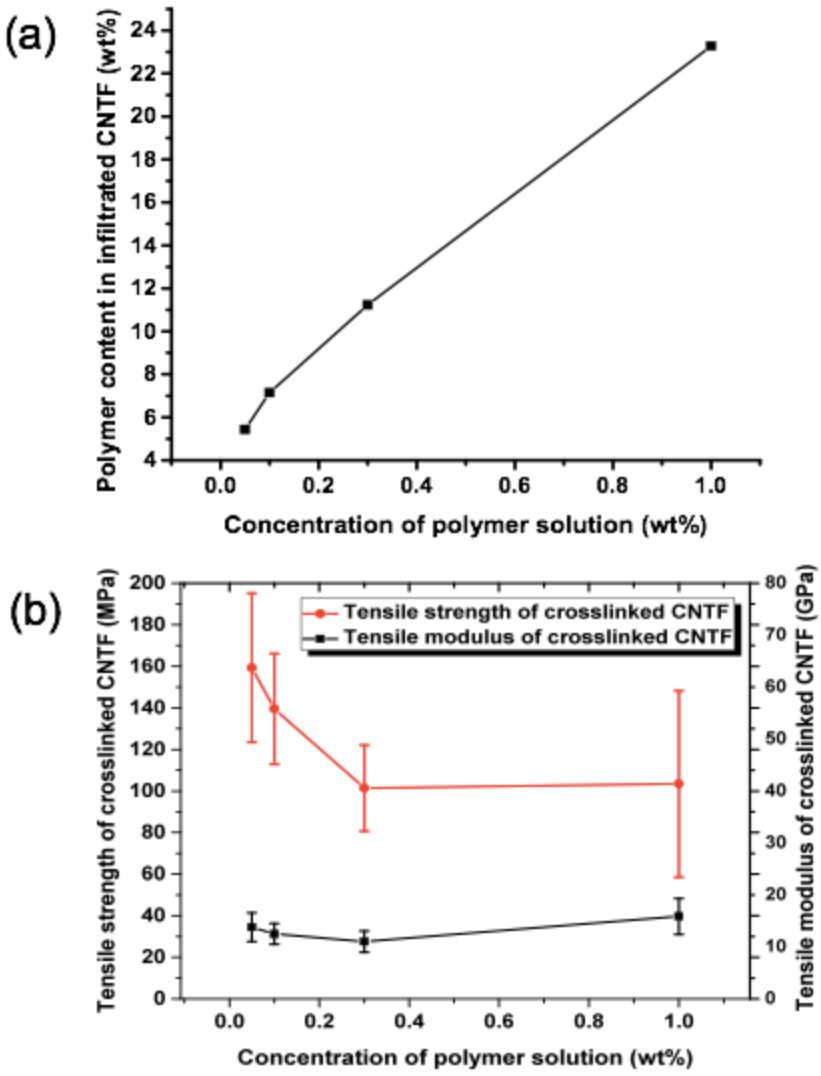

Figure 3.7 Effect of concentration of polymer solution on (a) fraction of polymer in the impregnated fiber, and (b) the tensile properties of subsequently crossllinked CNTF

densities of the fiber sections are very statistical, thus the increase in weight after infiltration of polymer is measured as an average of 3 samples. The correlation between the solution concentration and the polymer content in the fiber is almost consistent with previous reports on infiltration of differet polymers with various molecular weight (PVA, PS and PAN).[13] Subsequently, the batch of CNTF was allowed for thermal treatment and the tensile properties are compared in **Figure 3.7**(b). Generally, the tensile strength is lowered as the fraction of crosslinking agent increases in the final fiber. This is logical, because as more BCB polymer network is present in the material, there is lower percentage of load-bearing CNT. In addition, as discussed earlier in this chapter, the alignment of CNTs can be interfered and even the structure of CNT can be damaged by the excessive formation of BCB collapsed network. There is subtle difference between the strength of CNTF that was initially treated with 0.3% wt solution and with 1% wt one. Therefore, we assume that the breaking strength of crosslinked CNTF would not further decrease at a large magnitude as the concentration is greater than 1% wt. Though modulus follows the similar trend, the value is higher for the fiber treated with 1% wt solution than 0.3% wt. This is similar to the report by Ma et al.,[23] which suggested formation of cured 3D network makes it difficult for the orientation or rotation of CNTs, thus making the modulus higher. Considering the effect of both strength and modulus, the polymer concentrations of 0.05% wt and 0.1% wt are most favorable for the BCB crosslinking post-treatment.

3.3.4 Effect of thermal treatment on the noncrosslinked CNTF

In the proposed post-treatment for CNTF, heating at 250 °C is a critical step as it initiates thermal crosslinking for BCB functional groups. We have proved in previous section that crosslinking BCB can effectively improve the mechanical performances of CNTF given the right conditions. In order to make a thorough comparison, toluene densified CNTF and PS infiltrated CNTF (no BCB available for covalent crosslinking) are thermally treated in the same fashion as the crosslinking. Interestingly, both of the fibers exhibited smaller maximum strength after thermal treatment, as shown in the stress-strain curve in **Figure 3.8**. On the other hand, this result is further supporting the effectiveness of crosslinking on improving the mechanical properties of PS-VBCB treated CNTF, since the strength should be even lower if there was no active BCB moieties.

Though it is still not well understood in the literature, the negative effect of high temperature on the strengths of CNTFs could be due to changes in the morphology. The surface structures of CNTF before and after heat treatment are revealed by SEM images in **Figure 3.9**. The CNTF that only went through solvent densification exhibits relatively large bundle size, as in **Figure 3.9**(a). After 4hrs of heating, as in **Figure 3.9**(b), the bundle size significantly decreased. This might be attributed to weakened Van der Waal's forces between the tubes at high temperature, which resulted in original bundles to break apart to smaller ones. The smaller bundle size within CNTF has been correlated with lower tensile strength by Jung et al in their polymer infiltrated CNTF.[13] Our observation is in agreement

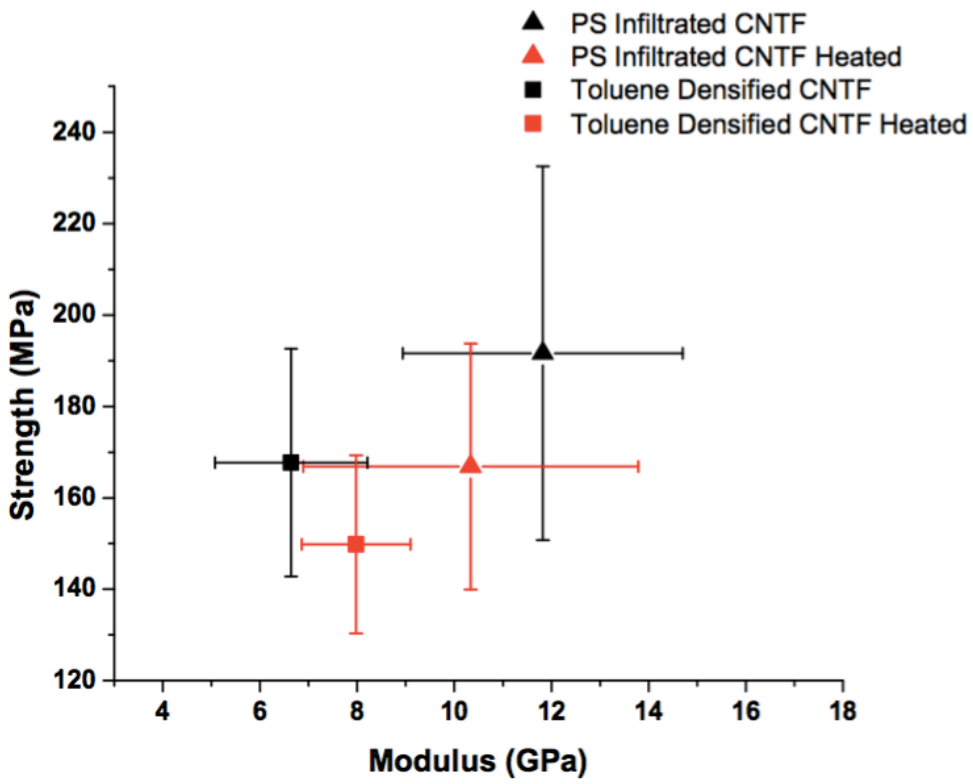

Figure 3.8 Typical stress strain curve of CNTFs: (a) toluene densified CNTF before and after heating, and (b) PS infiltrated CNTF before and after heating

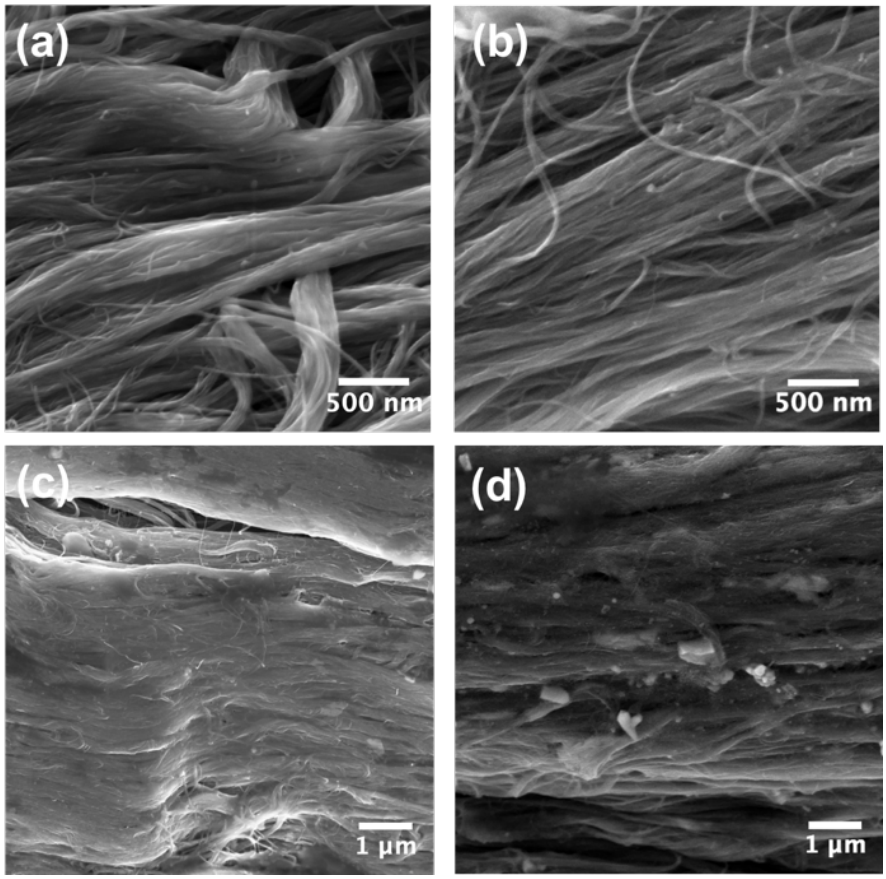

Figure 3.9 Effect of thermal treatment on the morphology of CNTF revealed by SEM images: (a) toluene densified CNTF, (b) toluene densified CNTF after heating @ 250 °C for 4hrs, (c) PS infiltrated CNTF, and (d) PS infiltrated CNTF after heating @ 250 °C for 4hrs.

with the reference, and the lowered strength could also be explained by weakened inter-tube forces. Furthermore, the alignment of the bundles was improved [**Figure 3.9**(b)] because of the load applied to the ends of the fiber during the thermal treatment. For the CNTF infiltrated with PS, a decrease in bundle size was also observed. In addition, the smooth layer of polymer observed in the fiber before heating [**Figure 3.9**(c)] turned into agglomerates in **Figure 3.9**(d). This is because the temperature used for heat treatment (250 °C) is above the Tg of PS, which caused the segment movement of the polymer chain and separation of PS from CNT to form aggregates. The PS particles are less effective than PS homogeneous layer in transferring tensile loads from bundles to bundles, therefore the strength of PS infiltrated CNTF decreased after thermal treatment.

3.4 Conclusion

This investigation into the process of BCB-based crosslinking of CNTF demonstrated that the effectiveness of the process in reinforcing the fiber depend on multiple factors, including chemical structure of BCB poly crosslinker, concentration of polymer solution during infiltration, and thermal treatment. PS-VBCB random copolymers with various monomer ratios were synthesized by anionic polymerization and free radical polymerization. The mechanical properties of the CNTF crosslinked with these polymer linkers indicated that the polymer with 80 mol% of styrene and 20 mol% of 4-VBCB leads to the highest improvement. The concentration of the polymer solution used for infiltration of CNTF was optimized to 0.05% wt or 0.1% wt, based on the mechanical testing of the final

crosslinked fibers. It was also observed that thermal treatment on fibers without BCB impregnation lowered their tensile properties. SEM imaging of the surface structure of thermally treated CNTF revealed lower bundle size than the sample prior to heating. For the PS infiltrated CNTF, the smooth layer of polymer covering the CNT bundles turned into agglomerates after heating, because of the segment movement of the polymer. The lowered bundle size and formation of polymer agglomerates could be possible causes for the drop in tensile strength. The results obtained in this chapter provide guidlines for designing post-treatments for reinforced CNTFs.

References

1. Lu, W.; Zu, M.; Byun, J. H.; Kim, B. S.; Chou, T. W., *Advanced Materials* **2012,** *24* (14), 1805-1833.

2. Behabtu, N.; Green, M. J.; Pasquali, M., *Nano Today* **2008,** *3* (5), 24-34.

3. Koziol, K.; Vilatela, J.; Moisala, A.; Motta, M.; Cunniff, P.; Sennett, M.; Windle, A., *Science* **2007,** *318* (5858), 1892-1895.

4. Motta, M.; Moisala, A.; Kinloch, I. A.; Windle, A. H., *Advanced Materials* **2007,** *19* (21), 3721-3726.

5. Zhang, X.; Li, Q.; Tu, Y.; Li, Y.; Coulter, J. Y.; Zheng, L.; Zhao, Y.; Jia, Q.; Peterson, D. E.; Zhu, Y., *Small* **2007,** *3* (2), 244-248.

6. Zhao, J.; Zhang, X.; Di, J.; Xu, G.; Yang, X.; Liu, X.; Yong, Z.; Chen, M.; Li, Q., *Small* **2010,** *6* (22), 2612-2617.

7. Zhang, X.; Jiang, K.; Feng, C.; Liu, P.; Zhang, L.; Kong, J.; Zhang, T.; Li, Q.; Fan, S., *ADVANCED MATERIALS-DEERFIELD BEACH THEN WEINHEIM-* **2006,** *18* (12), 1505.

8. Liu, K.; Sun, Y.; Zhou, R.; Zhu, H.; Wang, J.; Liu, L.; Fan, S.; Jiang, K., *Nanotechnology* **2010,** *21* (4), 045708.

9. Qiu, J.; Terrones, J.; Vilatela, J. J.; Vickers, M. E.; Elliott, J. A.; Windle, A. H., *ACS nano* **2013,** *7* (10), 8412-8422.

10. Li, S.; Zhang, X.; Zhao, J.; Meng, F.; Xu, G.; Yong, Z.; Jia, J.; Zhang, Z.; Li, Q., *Composites Science and Technology* **2012,** *72* (12), 1402-1407.

11. Liu, K.; Sun, Y.; Lin, X.; Zhou, R.; Wang, J.; Fan, S.; Jiang, K., *ACS nano* **2010,** *4* (10), 5827-5834.

12. Fang, C.; Zhao, J.; Jia, J.; Zhang, Z.; Zhang, X.; Li, Q., *Applied Physics Letters* **2010,** *97* (18), 181906.

13. Jung, Y.; Kim, T.; Park, C. R., *Carbon* **2015,** *88* (0), 60-69.

14. Ye, Y.; Zhang, X.; Meng, F.; Zhao, J.; Li, Q., *Journal of Materials Chemistry C* **2013,** *1* (10), 2009-2013.

15. Choi, Y.-M.; Choo, H.; Yeo, H.; You, N.-H.; Lee, D. S.; Ku, B.-C.; Kim, H. C.; Bong, P.-H.; Jeong, Y.; Goh, M., *ACS Applied Materials & Interfaces* **2013,** *5* (16), 7726-7730.

16. Cui, Y.; Zhang, M., *ACS applied materials & interfaces* **2013,** *5* (16), 8173-8178.

17. Harth, E.; Horn, B. V.; Lee, V. Y.; Germack, D. S.; Gonzales, C. P.; Miller, R. D.; Hawker, C. J., *Journal of the American Chemical Society* **2002,** *124* (29), 8653-8660.

18. So, Y. H.; Hahn, S. F.; Li, Y.; Reinhard, M. T., *Journal of Polymer Science Part A: Polymer Chemistry* **2008,** *46* (8), 2799-2806.

19. Sakellariou, G.; Ji, H.; Mays, J. W.; Hadjichristidis, N.; Baskaran, D., *Chemistry of Materials* **2007,** *19* (26), 6370-6372.

20. Sakellariou, G.; Ji, H.; Mays, J. W.; Baskaran, D., *Chemistry of Materials* **2008,** *20* (19), 6217-6230.

21. Alley, O. J.; Plunkett, E.; Kale, T. S.; Guo, X.; McClintock, G.; Bhupathiraju, M.; Kirby, B.; Reich, D. H.; Katz, H. E., *Macromolecules* **2016**.

22. Ryu, S.; Lee, Y.; Hwang, J. W.; Hong, S.; Kim, C.; Park, T. G.; Lee, H.; Hong, S. H., *Advanced Materials* **2011,** *23* (17), 1971-1975.

23. Ma, W.; Liu, L.; Zhang, Z.; Yang, R.; Liu, G.; Zhang, T.; An, X.; Yi, X.; Ren, Y.; Niu, Z.; Li, J.; Dong, H.; Zhou, W.; Ajayan, P. M.; Xie, S., *Nano Letters* **2009,** *9* (8), 2855-2861.

CHAPTER IV

EFFECT OF ELECTRON BEAM RADIATION INDUCED FUNCTIONALIZATION ON PROPERTIES OF CARBON NANO STRUCTURES

An excerpt of this chapter was published by Hiremath, N. and Lu, X. et al. *Journal of Materials Science* **2016,** *51* (22), 10215[1]

An excerpt of this chapter is submitted by Evora, MC and Lu, X et al.

The articles were partially written by X. Lu. The reported synthesis was partially conducted by X. Lu. Some SEM characterization was performed by X. Lu.

Abstract

Electron beam (e-beam) radiation has been widely applied in industry for sterilizing, functionalization, and strengthening of materials. In this work, two aspects of e-beam effects on carbon nano-materials were investigated: altering the carbon arrangement, and grafting functionalization. Carbon nanotube (CNT) yarns as macro-assembly of CNTs were irradiated by e-beam at various doses and both surface damage and bridging were observed under scanning electron microscope (SEM). Increased tensile modulus yet lowered strength were observed as a result of the balancing effect. Furthermore, the radiation graft polymerization of acrylonitrile (AN) and acrylic acid (AA) were studied both on carbon nanofiber (CNF) and carbon nanotube yarns. From thermogravimetric analysis (TGA) and X-ray photoelectron spectroscopy (XPS) results of functionalized CNF powders, the optimum concentration of monomer solution (40% v/v) was derived which lead to highest amount of polymer grafting. In addition, e-beam induced functionalization of AN and AA on CNT yarns were performed, and significant improvements in tensile properties were observed, especially for yarns functionalized with AA that showed 77% higher strength. The reinforcement is correlated with increased friction from functional groups, tighter packing of CNTs,

and presence of polymer, indicated by Raman spectra, XPS, and SEM. All of these factors lead to improved stress transfer within the CNT yarn.

4.1 Introduction

Electron beam (e-beam) radiation has wide commercial applications such as sterilizing, functionalization, and reinforcement of plastic materials due to its undemanding process and versatile ability. As the family of graphitic carbon materials emerged, the exploding interest in manipulating their structures drew wide attention on the effect of e-beam irradiation on carbon nanomaterials.[2]

The early researches mainly focused on the the damaging effect of nano-carbons under transmission electron microscope (TEM), where the samples are subject to electron beam of 100-300 keV energy. [3-6] More recently, the focus is turned to deliberately engineering of carbon nanostructures using e-beam, such as formation of interlinks, merging, and welding.[7] Given the inherent weak interaction between graphitic lattices,[8] e-beam induced rearrangement of carbons could be beneficial for the properties of the resulting material. For example, e-beam crosslinking of concentric shells of multiwalled nanotubes (MWNTs) have been reported to improve the maximum load of the MWNT by a factor of 11.6.[9] On the bundle scale, e-beam induced crosslinking between single walled nanotubes (SWNTs) yielded bending modulus up to 750 GPa.[10] On the macroscopic scale, only one group have observed improvement in mechanical performance of CNT fibers and mats by solely e-beam irradiation.[11, 12] There is a need for more thorough studies on the counter-balancing effects of e-beam on CNT macro assemblies.

In addition to altering the atomic arrangements of solid materials, e-beam can also initiate various radical-based functionalizations. Carbon nanomaterials can be grafted with polymer when irradiated at the presence of the corresponding monomer, which would lead to enhanced dispersion of the carbon.[13] To the best of our knowledge, e-beam induced polymerization on CNT macro-assemblies have not been reported.

In this chapter, the effect of e-beam irradiation on carbon nano-materials were investigated from two aspects: altering the carbon arrangement, and grafting functionalization. Different types of structural defects were observed on irradiated CNT yarns, and correlated to their mechanical properties. E-beam initiated polymerization was performed both on carbon nanofiber (CNF) and CNT yarns. The changes in chemical and morphological structures were carefully characterized to explain the improved mechanical properties of the functionalized yarn.

4.2 Experimental

4.2.1 Materials

Carbon nano fiber powder was purchased from Applied Sciences Inc. Carbon nanotube fiber (CNTF) was produced through a proprietary process by the University of Cincinnati. All chemicals, including acrylic acid (AA, Acros Organics, 98%, stabilized with 200 ppm quinone), acrylonitrile (AN, Acros Organics, 99%, stabilized with 200 ppm quinone), methanol (Fisher Chemicals, 99.8%),

tetrahydrofuran (THF, Fisher Chemical, ACS reagent, 0.025% butylated hydroxytoluene), Ammonium iron(II) sulfate hexahydrate [$(NH_4)_2Fe(SO_4)_2$• $6H_2O$, ACROS Organics, 99%] were used as received.

4.2.2 E-beam irradiation of CNTF

CNTFs were irradiated with electron beam generated from an industrial accelerator operated by NEO Beam Mercury Plastics, Inc (Middlefield,OH) with beam energy of 3.8 MeV, and pulse current of 38.3 mA. The facility was operated based on a continuous production line at 27 kGy/pass with dose rate of 5 kGy/s. The CNTYs were irradiated in air with the fiber ends fixed on a cardboard covered by a layer of aluminum foil. Doses of approximately 100, 200, 300 and 400 kGy were acquired by allowing the sample to pass through the beam chamber multiple times.

4.2.3 E-beam functionalization of CNF using various monomers

CNF as a loose powder was irradiated through direct radiation grafting technique. The CNF was immersed in a solution of acrylonitrile (AN), acrylic acid (Ac), or methyl methacrylate (MMA) at various concentrations and subsequently exposed to electron beam for different doses. Take GAN as an example, the CNF powder was immersed in acrylonitrile solution at 20 % (*v/v)* in MeOH/H_2O (50/50) mixture with 4 % of inhibitor Mohr's salt $(NH_4)_2Fe(SO_4)_2$• $6H_2O$ added. The mixture was placed in a plastic bag and forwarded to the electron accelerator to be irradiated. A blank sample was prepared using the same procedure without

exposure to irradiation. The irradiated MWNTs were washed with copious amount of THF and vacuum dried at room temperature.

4.2.4 E-beam functionalization of CNTF using various monomers

Two CNTF were functionalized with acrylic acid and acrylonitrile, respectively. For the first set of experiment, as-received CNTF was immersed in solutions of 40 % and 80 % (*v/v*) of acrylic acid in mixture of MeOH/H_2O (30/70) and the second set of CNT fiber was functionalized with acrylonitrile 80 % (*v/v*) in MeOH/water (30/70). In order to suppress the homo-polymerization process, 4% of inhibitor Mohr's salt $(NH_4)_2Fe(SO_4)_2 \bullet 6H_2O$ was added to all the solutions prepared.

After the fibers were removed from the solution, they were stretched on a cardboard with a light tension applied on the ends to maintain straight during irradiation, and covered with aluminum foil for protection. The CNTF were irradiated up to 108 kGy and rinsed with copious amount of THF. The grafted CNTF were vacuum dried at room temperature.

4.2.5 Characterization

Surface chemical composition and bonding were analyzed by X-ray photoelectron spectroscopy (XPS) using a Thermo Scientific K-Alpha instrument. The K-Alpha uses Al-Ka X-rays focused to a spot 400 microns in diameter. Energy of emitted photoelectrons were analyzed using a 180° double focusing hemispherical analyzer with a 128-channel detector. Survey data was collected at

200 eV pass energy and an energy resolution of 1 eV/step, while core level data were collected at 50 eV pass energy and energy resolution of 0.1 eV/step. Sample charging was eliminated by using the K-Alpha's dual-beam charge compensation source which uses both low energy Ar-ion and low energy electrons. Data were collected and analyzed using the Advantage data system (v.4.61).

Raman analyses were carried out in a Horiba Jobin-Yvon T64000 Raman spectrometer equipped with a peltier cooled CCD with excellent sensitivity from 200-1000 nm and using a 600 gr/mm grating. The samples were deposited onto a glass slide, and the spectra were collected using a 50 × objective in a backscattering configuration. The excitation energy was 2.33 eV from the 532.1 nm line of an Argon laser. For each sample, a set of 5 spectra were collected at different points in the interval of 300 cm^{-1} to 3000 cm^{-1}. All spectra were treated to subtract the background and the peaks were fitted using Lorentzian curves.

The tensile properties of CNT fibers were assessed on a MTS single filament tensile tester, with 25 mm gauge length and at a 0.2 mm/min extension rate. Ten specimens from each yarn sample were tested, and the average of the test results is reported. The yarn diameter (d) was measured using 500 × optical microscope and was used to calculate the yarn specific strength.

The morphology of the CNT fibers was investigated using a Zeiss Auriga dual beam focus ion beam and scanning electron microscope (SEM) equipped with electron and ion beam in the same facility. The focused ion beam (FIB) is generated from gallium liquid metal ion source with resolution of 7 nm at 30 kV

acceleration voltages. The electron beam is generated from FEG electron source with high resolution SEM 1nm at 15 kV and 1.9 nm at 1kV.

4.3 Results and discussion

4.3.1 Formation of Defect on CNTF induced by e-beam irradiation

The purpose of radiation was to investigate its effect on improving internanotube adhesion by introducing crosslinks. There is no doubt about the high strength that these yarns can reach yet still a subject of investigation lies in the understanding of their internal structure and how the radiation treatment changes the morphology as well as the strength of the fiber. In general, materials treated with radiation are amenable to crosslinking and scissioning processes simultaneously. These two are competing processes. In **Figure 4.1**, the effect of radiation exposure on CNTY surface with the increase in dose is visible. The pristine yarn in **Figure 4.1**(a) shows a regular surface with the fibers aligned in longitudinal direction with no sign of residue deposited on the surface. The presence of defects on the irradiated fibers surface can be easily noticed. Redeposition of the vaporized carbonaceous material over the yarn surface could be due to reaction with oxygen—resulting in chemical damage. The chemical damage on the nanotube structure will always happen when nanocarbon structures react with heteroatoms under radiation processes and the expected reactions could be

$$C + 2H_2O \longrightarrow CO_2 + 2H_2$$

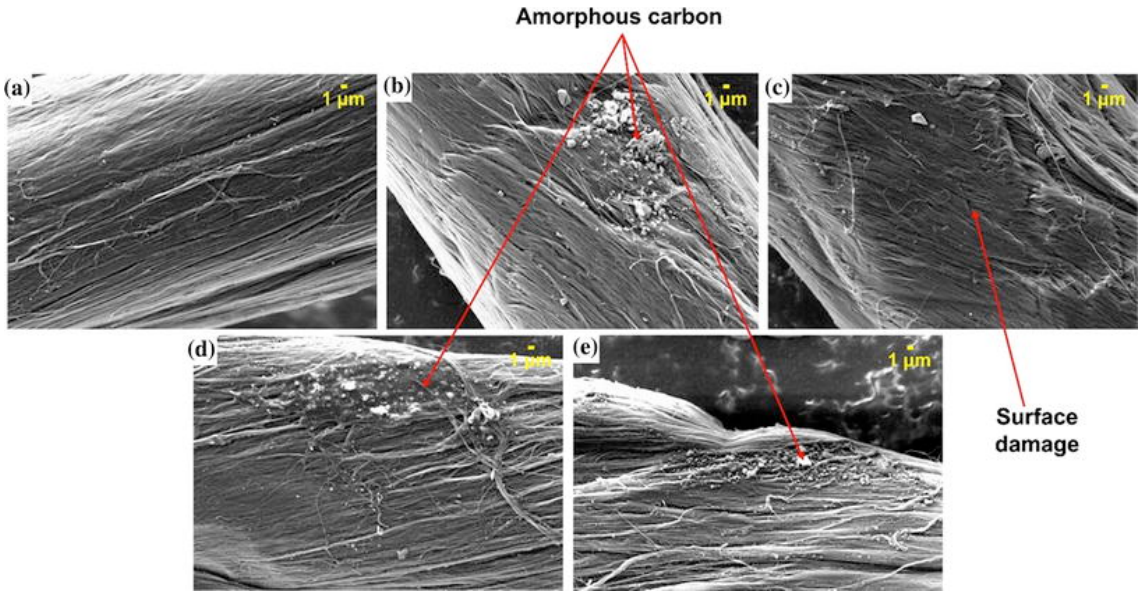

Figure 4.1 SEM images of CNT yarns (a) pristine, (b) irradiated up to 100 kGy, (c) irradiated up to 200 kGy, (d) irradiated up to 300 kGy, (e) irradiated up to 400 kGy

or

$$C + O_2 \longrightarrow CO_2$$

or

$$C + \tfrac{1}{2} H_2 \longrightarrow CH$$

and will lead to a deposition of a carbonaceous layer or etching of holes on the yarn surface.[13] The oxidation process should be considered because this radiation process was carried out in the presence of air, and ozone is generated by the dissociation of air under the electron beam.[14] Besides chemical damage, there is also physical damages. Depending depending on the amount of energy involved in the process (considering primary and secondary electrons from the cascade effect), defects (dangling bonds, vacancies, interstitial, pentagon–heptagon pair defects) are created in the graphene structure, resulting in high strain at these sites. With defects expanding, the increased tensile load leads to a less stable structure as compared with a perfect hexagonal carbon network. The continuous electron beam heating may easily break C–C bonds from defects, causing carbon atom sublimation and further evaporation of graphene fragments.[4] Clusters of atoms may be detached from the surface and attach back, and carbonaceous debris generated from the oxidation of the graphite shells may strongly adhere to the surface of grapheme via π–π stacking and hydrogen bonds.[15-17]

The knock-off process induced by electron beam is the most important event that is responsible to initiate the modifications on carbon nano structure. Dislocations of carbon atoms, dangling bonds and electronic excitations should be

expected as a consequence of this knock-off process. All these effects are related to the capacity of carbon nano structures to react with heteroatoms, self heal and rearrange themselves by going through a recombination process. The recombination of interstitials and vacancies is expected to be the primary step in Wigner energy release which is stored in the interstitial when the atom is dislocated at this position and is liberated posterior recombination process.[18] The damage on the CNT structure will totally depend on the energy of the beam. Besides the carbonaceous debris and possible oxidation residue, we can notice peelings in **Figure 4.1** (c), probably from poorly bonded basic structural units.

Higher magnification SEM images of the yarns are shown in **Figure 4.2** (a-d). After the fibers were irradiated, part of the yarn became disorganized and new connections between the fibers are noticeable [**Figure 4.2** (c)], with simultaneous increase in surface roughness. Some of the disordering of the fibers may be attributed to the change from sp^2 to sp^3 hybridization leading to possible crosslinking between some adjacent planes of the nanotubes, but not enough to improve the mechanical properties and avoid the predominant damage. The irradiation with electron beam also promoted breakage of same fibers [**Figure 4.2** (d)].

Besides some breakage at 400 kGy dose showed in **Figure 4.2** (d)., separation of the bundles, random welding [**Figure 4.3** (a-b)], oxidation and deposition of carbonaceous debris were also observed that affects the load

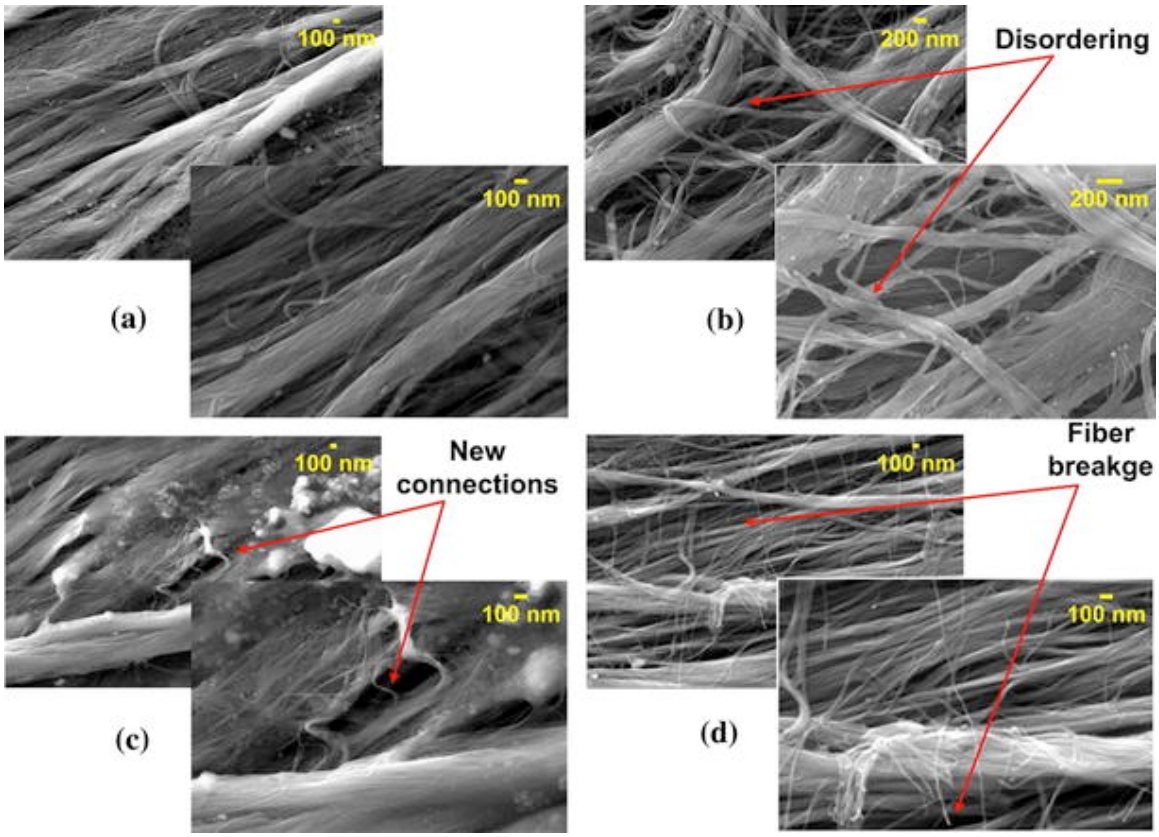

Figure 4.2: SEM images high magnifications of CNT yarns (a) pristine, (b) irradiated up to 200 kGy, (b) irradiated up to 300 kGy, (d) yarn irradiated up to 400 kGy

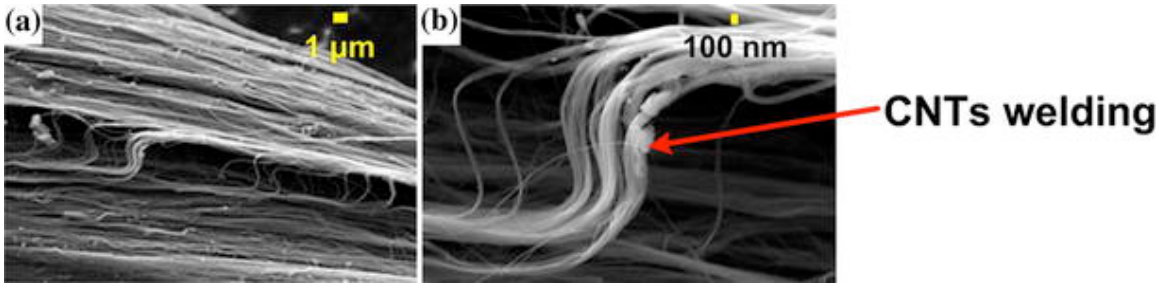

Figure 4.3 SEM images at (a) low and (b) high magnification of CNTY irradiated up to 400 kGy

transfer between the fibers.

The tensile test results show that the yarns irradiated with e-beam experienced damage and the scission process was predominant. The mechanical properties of the irradiated yarns are lower than that of the pristine (**Figure 4.4**). From SEM images, effect of crosslinking was observed on the samples irradiated up to 200 and 300 kGy. Filleter et al. reviewed crosslinking due to irradiation with high-energy particles of CNT-based materials and the radiation-induced crosslinking between CNT shells and tubes.[19] The high concentration of energy over a small volume of material results in e-beam heating. This may anneal defects, and promote crosslinking and welding between the tubes. The yarns irradiated at 300 kGy had higher elastic modulus and became more rigid and stiff due to the crosslinking process. However, the deposition of amorphous carbon and damages on the surface of CNT yarns induced by irradiation contribute to the stress concentration for initiation of failure. This could be the reason for decrease in yarn strength.

Figure 4.5 shows the Raman spectra of the pristine and irradiated yarns at 200 and 400 kGy. Raman spectroscopy uses a monochromatic laser to interact with molecular vibrational modes and phonons in a sample, shifting the laser energy down (stokes) or up (anti-stokes) through inelastic scattering. It is a powerful, noninvasive method to characterize graphene and related materials and it is capable of detecting small changes in the crystal structure. Generally, the Raman spectra of carbon materials are simple, with two most intense bands

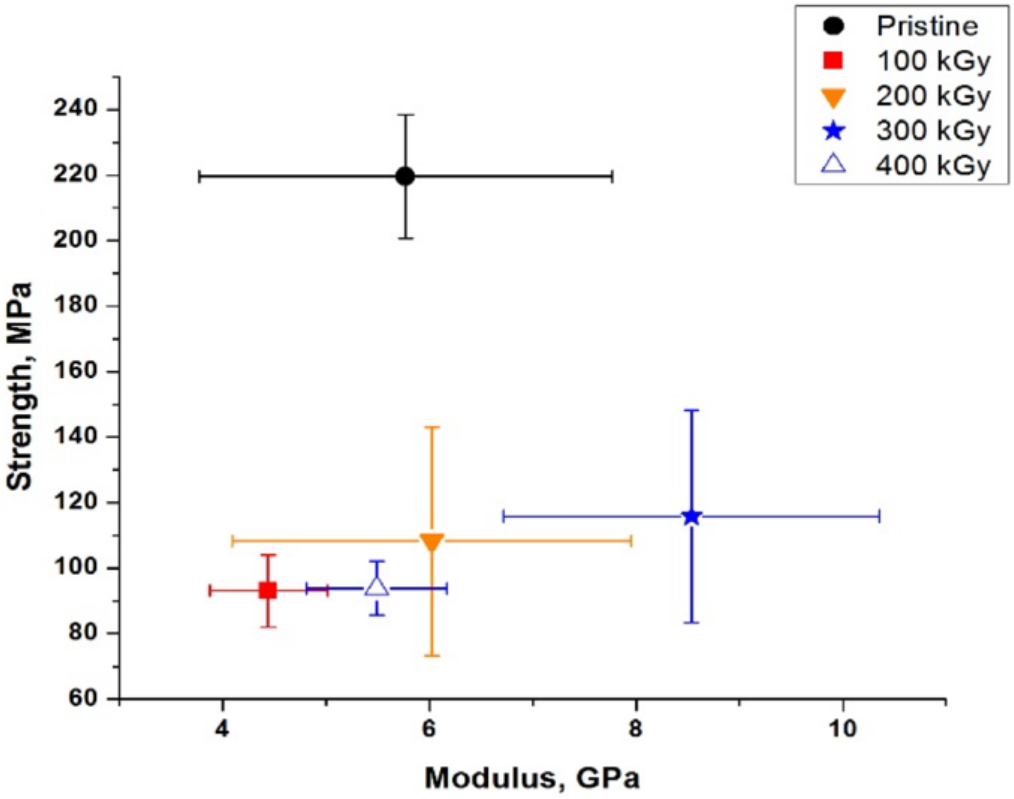

Figure 4.4 Tensile strength versus modulus of 100 kGy, 200 kGy, 300 kGy, and 400 kGy e-beam irradiated CNTY samples

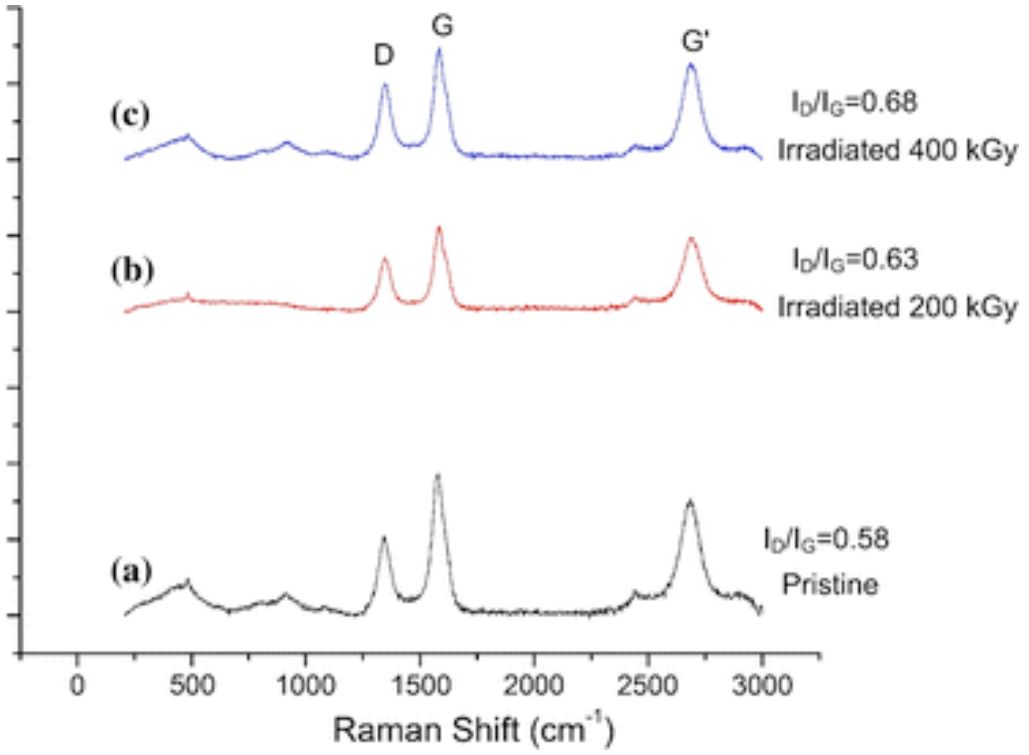

Figure 4.5 Raman spectra of: pristine yarn (a), yarn irradiated at 200 kGy dose (b) and yarn irradiated 400 kGy.

between 1000 and 2000 cm^{-1}. The peaks near 1595 and 1370 cm^{-1} correspond to the G band due to stretching vibrations of the sp^2-hybridized carbon and the disorder induced D band, respectively. The intensity ratio of D band to G band in the Raman spectra has been widely used to evaluate the degree of disorder in sp^2 hybridized carbon systems. Although D intensity is proportional to the amount of disorder (crystallite boundary) in the sample, the ratio between the intensities of the disorder D band and the first-order graphite G band (I_D/I_G) provides a parameter that can be used for quantifying degree of disorder.[20] There is an increase from 0.58 to 0.63 and 0.68 in I_D/I_G ratio when the pristine samples were irradiated at 200 and 400 kGy of e-beam dose, respectively, indicating increase in defects due to radiation process. These defects could be crossliking, scission, reactions with heteroatoms, turbostratic carbon, and transition from sp^2 to sp^3, while the G peak is due to the bond stretching of all pairs of sp^2 atoms in both rings and chains.[21] The Raman spectra of the CNTY also showed a second order of the *D* peak called *G'* around 2685 cm^{-1}. In graphene structures, G' is a single peak in a single-layer graphene, while it splits into four in bilayer graphene, reflecting the evolution of the electron band structure.[22, 23] It is an important peak as it provides information for level of graphitization of a material at full-width half-maximum position. G´ has a close correlation with the electronic band structure of the graphitic material. It is not only present in Raman spectra of monolayer graphene but also in turbostratic graphite. Both structures present a Lorentzian peak; however, turbostratic graphite has larger line width. The results showed that the

decrease of G´peak FWHM from 107.25 cm^{-1}(pristine) to 91.56 cm^{-1} (sample irradiated at 400 kGy) confirms the presence of damage in the graphitic structure. Adding to that, the samples irradiated had the G´ intensity decreased confirming that the sample structure became less ordered, in agreement with observations from the SEM images.

Although the strength decreased drastically (**Figure 4.4**) for the sample irradiated at 100 kGy compared with pristine, the samples irradiated up to 200 and 300 kGy showed improvement on strength compared with 100 kGy irradiated sample. Nevertheless, there is a drastic decrease in strength resulting defect formation, vacancies, reactions with heteroatom from the environment, direct interwall sp^3 bonding atoms and interstitial carbon that also form sp^3 bonding with adjacent, also called crosslinking.[18] The crosslinking could be the reason for improvement in the modulus of the 300 kGy irradiated sample. On the other hand, the structure modification at those doses were not substantial on strength due to other defects. In general, in graphite planes there are C double bonds around the defects on graphite structure which is very easy to be broken by radiation process and produce free radical. This new free radical combines randomly and quickly and it aim to reduce the amount of defects in carbon structure and this change the orientation of some carbon nanotube that used to be (pristine) highly oriented. The prolonged irradiation may decrease the inter-wall distance leading to the improvement of the graphitization and grow the crystal size. The tensile strength is governed; in part by the crystallite size and the increment of voids in the fiber

structure. Larger crystallite tends to decrease the tensile strength[24] but increases the modulus.

4.3.2 Effect of E-beam functionalization on carbon nanofibers using various monomers

The effect of e-beam irradiation on functionalization of carbon nanofiber functionalization has been studied with vinyl monomers AN and AA. CNF-1 was used for functionalization with AN and lower purity CNF-2 was used for functionalization with AA.

XPS provided useful information towards the changes in chemical composition of the samples. The XPS survey spectra were collected from 0 to 1350 eV for the CNF samples through different treatments to afford qualitative and semi-quantitative surface elemental analysis. The surface atomic percentage of the CNF related to functionalization of AN is shown in **Table 4.1**. The surface composition (atomic %) clearly showed an increase of N content for the samples irradiation grafted with AN. Non-irradiated blank sample that went through thorough rinsing revealed no residue of AN, thus indicating the increased N content in the irradiation grafted samples were as a result of covalent functionalization of PAN oligomers onto the CNF wall. As the concentration of AN increases in the aqueous solution, the N content in the surface composition dropped accordingly, suggesting fewer AN radicals grafted onto the walls of CNF. This phenomenon might be attributed to the tendency of monomers to homo-polymerize at higher concentrations. As the solution approaches a bulk system, there is higher probability of auto-acceleration

Table 4.1 Surface compositions (atomic %) calculated from XPS survey spectra for blank CNF treated with AN (nonirradiated), CNF irradiated in aqueous solution of AN at 40%, 60%, and 80% in concentration with 100 kGy dose of electron beam.

	C	O	N	Fe
Blank CNF/AN	97.1	2.4	0.0	0.0
CNF 40% AN	79.0	4.7	14.0	0.0
CNF 60% AN	86.1	3.4	8.7	0.0
CNF 80% AN	89.7	3.4	6.0	0.2

(Trommsdorff's Effect). The higher viscosity of the mixture limited the termination of the radicals, which led to a rapid increase in the rate of polymerization and consumption of monomer. This could have reduced the concentration of activated AN radical that could attack the aromatic structure on CNF to form covalent functionalization.

The high resolution C 1s core level spectra of AN functionalized CNF were presented in **Figure 4.6**. In order to identify differences in the chemical states of carbon in these samples, deconvolution of the C 1s curve was performed and five characteristic peaks were revealed. Binding energy of 284.3, 284.8, 286.9, and 288.8 correspond to sp^2-hybridized carbon, sp^3-hybridized carbon (including C-C and C-N), C ≡ N, and O=C-O, respectively. These peaks were fitted with a combination of Gaussian-Lorentzian function and integrated to quantify the contribution of each component. The binding energy of 284.1 eV essentially corresponds to non-functionalized sp^2 carbons which would be expected for CNT materials. The lower relative intensity of this peak along with increase of sp^3 C, C-N and C≡N peaks indicate successful covalent grafting of AN species onto the CNF. In addition, the binding energy position and width of these peaks were similar and consistent with those of polyacrylonitrile (PAN) from the literature[25]. This suggests possible existence of PAN polymeric clusters on the surface of the material, induced by electron beam activation.

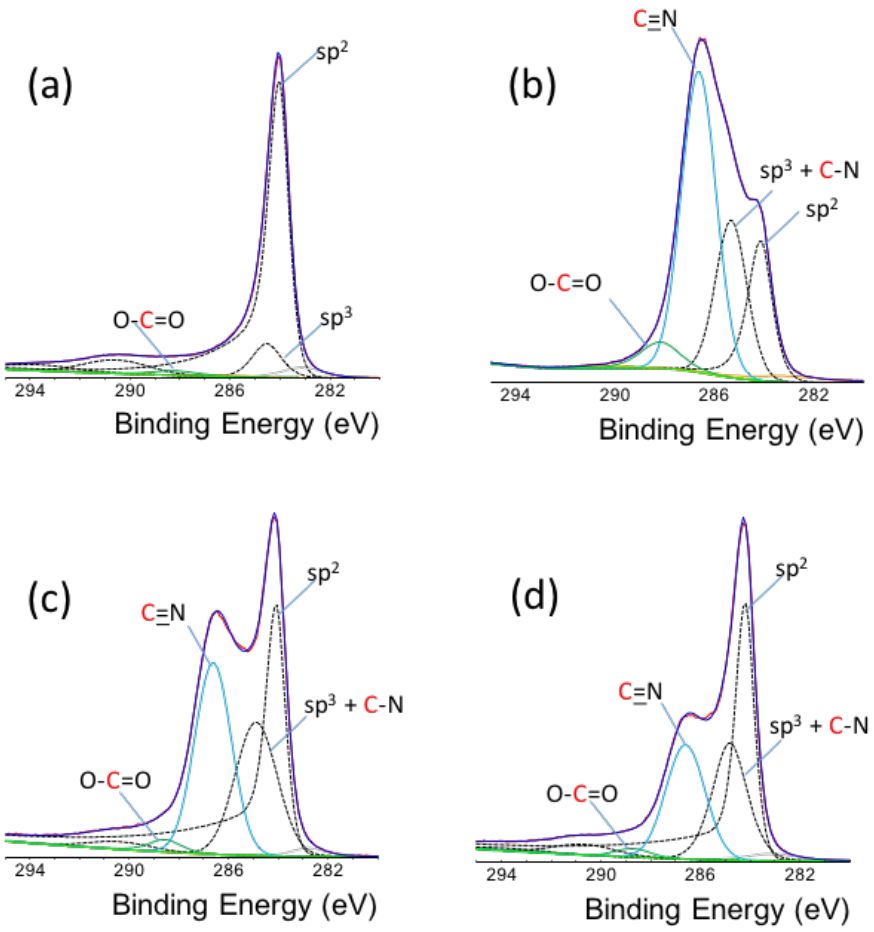

Figure 4.6 High resolution C 1s core level spectra of CNF with different treatments: (a) non-irradiated control, and (b-c) irradiated with electron beam at 100 kGy in aqueous solution of AN at various concentration (b) 40%, (c) 60%, and (d) 80%

The TGA overlay is presented in **Figure 4.7**. The non-irradiated and rinsed CNF control sample exhibited no weight loss, indicating similar structure of the control to the pristine CNF. The irradiated samples **Figure 4.7** (a-c) all showed two-step weight loss at 250 ˚C and 350˚C, respectively. These thermal degradations could potentially be attributed to grafted PAN oligomers and polymer clusters. In agreement with the conclusions drawn from the XPS surface composition as well as the C 1s core level spectra, the highest grafting level was found for the CNF sample irradiated with 40% (*v/v*) AN aqueous solution, while lowest grafting percentage was observed for the 80% (*v/v*) AN alternative.

Similarly, the effect of electron beam induced functionalization of CNF was also studied with another monomer, AA. The carbon material utilized for this part of the experiment was CNF-2, as mentioned in the experimental section. The chemical compositions were first evaluated using the XPS. The surface elemental composition calculated from XPS survey spectra as listed in **Table 4.2**. The results indicate small monomer residue on the blank CNF sample (non-irradiated) comparing its C and O content with the pristine CNF. There was a slight increase in O content for the irradiated samples (from 9.9 to 12.1 and from 9.9 to 13.7), but the concentration of the AA solution did not make a significant difference. The O content of CNF irradiated with 60% AA was slightly higher than the 40% AA sample, while the C content showed a reverse trend. Traces of N and Na content was similar with all samples within statistical range, which indicates that this is a result of contamination.

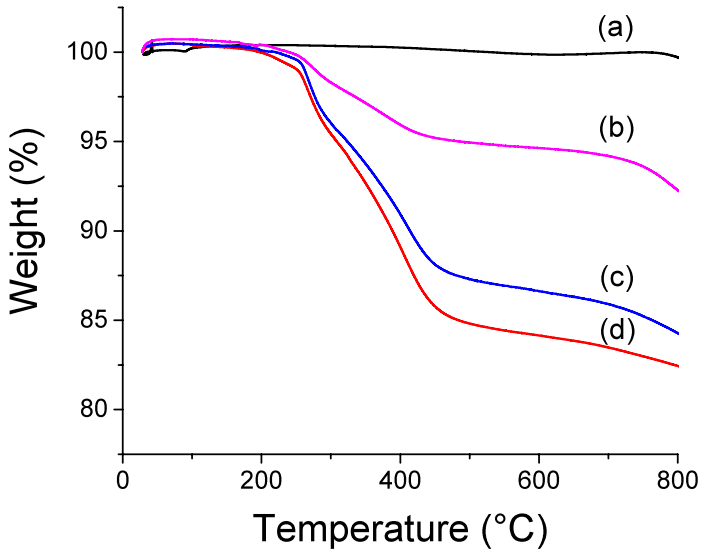

Figure 4.7 TGA overlay of CNF with different treatments: (a) non-irradiated control, and (b-c) irradiated with electron beam at 100 kGy in aqueous solution of AN at various concentration (b) 80%, (c) 60%, and (d) 40%

Table 4.2 Surface compositions (atomic %) calculated from XPS survey spectra for pristine CNF, blank CNF treated with AA (nonirradiated), CNF irradiated in aqueous solution of AA at 40% and 60% in concentration with 100 kGy dose of electron beam.

	C	O	N	Na
Pristine CNF	96.5	2.4	0.4	0.3
Blank CNF/ AA	85.7	9.9	0.6	1.5
CNF 40% AA	86.1	12.1	0.3	0.8
CNF 60% AA	84.3	13.7	0.3	1.0

The chemical states of the carbon atoms were further investigated by high resolution C 1s core level spectra. As illustrated in **Figure 4.8**, C 1s curves were deconvoluted into four characteristic components, sp^2-hybridized carbon, sp^3-hybridized carbon, C-O, and O=C-O, respectively. These peaks were fitted with a combination of Gaussian-Lorentzian functions and integrated to quantify the percentage of each component. The ratio of sp^2 to sp^3 hybridized carbon was slightly lower in the blank sample compared to the pristine CNF, indicating small amount of AA residue present in the non-irradiated CNF even after rinsing. This was also confirmed by increased intensity of the C-O peak in the blank sample. The sp^2/sp^3 decreased further in the irradiated samples, due to the effective covalent functionalization of poly acrylic acid (PAA) oligomers onto the CNF walls. Meanwhile, as another evidence, the C-O peaks in the irradiated samples were more intense than the blank sample.

The TGA overlay of the AA treated samples is presented in **Figure 4.9**. Corresponding to the results in XPS data, TGA shows that the irradiated CNF with AA displays a small portion of grafting which is almost irrelevant to the concentration of the monomer solution. The non-irradiated and rinsed CNF control sample exhibited a single step weight loss at around 100 ˚C, which could be attributed to remaining moisture. The TGA curve of the control did not show other obvious weight losses. On the other hand, the irradiated samples (b-c) both exhibited two step weight losses, at around 200 ˚C and 380 ˚C. This weight loss refers to the portion of AA monomer that underwent covalent functionalization and

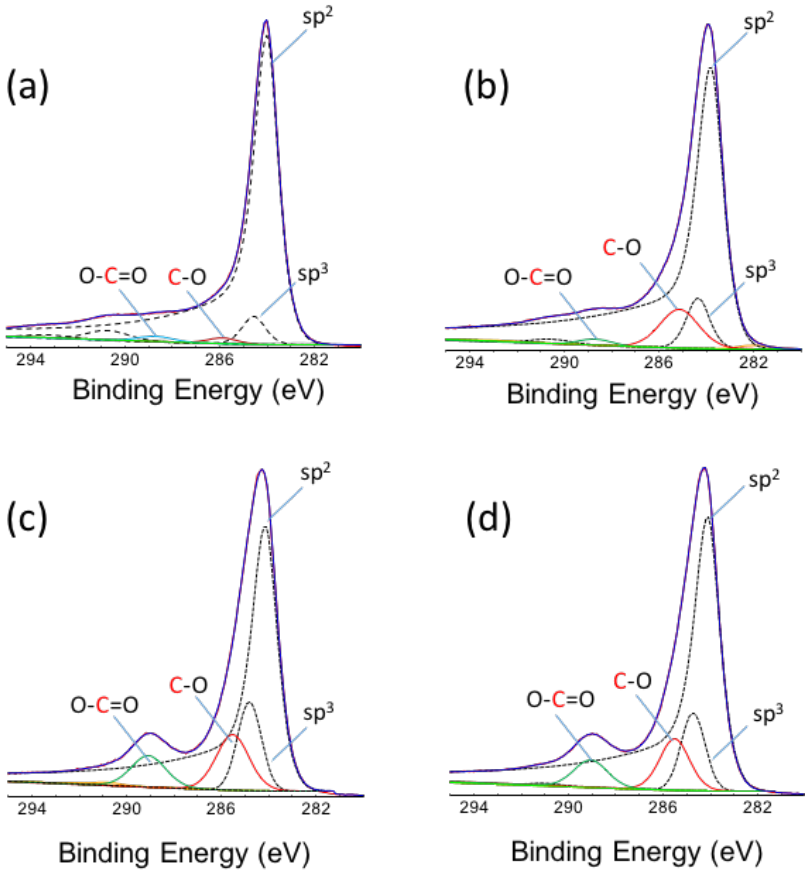

Figure 4.8 High resolution C 1s core level spectra of CNF with different treatments: (a) Pristine, (b) non-irradiated control (c-d) irradiated with electron beam at 100 kGy in aqueous solution of AA at different concentrations (c) 40%, and (d) 60%

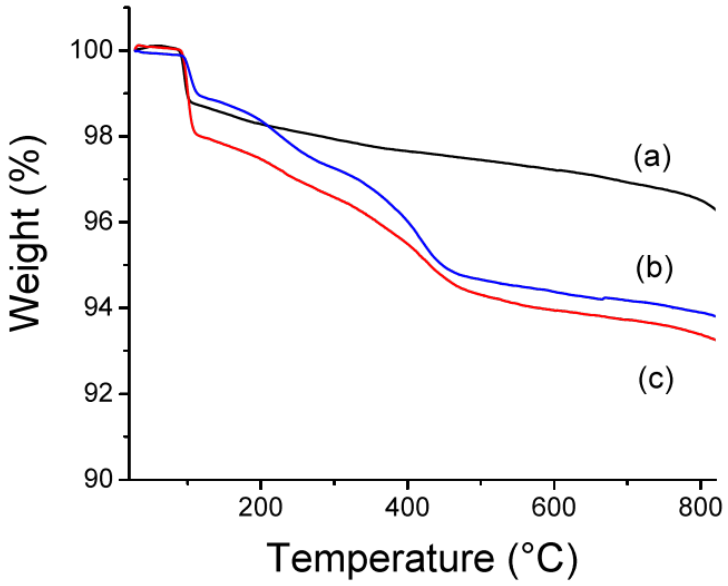

Figure 4.9 TGA overlay of CNF with different treatments: (a) non-irradiated control, and (b-c) irradiated with electron beam at 100 kGy in aqueous solution of AA at different concentrations (b) 40% and (c) 60%

surface graft polymerization. The **Figure 4.9**(b) and (c) were very similar to each other in terms of shape and weight loss percentage. This leads to the conclusion that concentration of AA monomer in the solution during irradiation does not play an important role, which agrees to the result from XPS surface composition (**Table 4.2**) as well as the C 1s core level spectra (**Figure 4.8**).

4.3.3 Modification of carbon nanotube fibers by electron beam using different monomers and improvement of the mechanical properties

The CNTFs were functionalized using AN and AA with 108kGy of electron beam. Raman spectroscopy results for these fibers are shown in **Figure 4.10**. As discussed earlier, the peaks near 1580 cm^{-1} and 1350 cm^{-1} that correspond to the C=C in-plane stretching mode (G band) and the disorder peak (D band), respectively. The intensity ratio of D band to G band (I_D/I_G) is indicative of the disorder in sp^2 hybridized carbon system, and it increases with the number of defects on the sidewall. Chemical functionalization introduces sp^3 defects and the disruption of π-π conjugation of the graphitic structure, therefore I_D/I_G would be useful for the investigation of functionalization on carbon nano structures. All Raman results were fitted with Lorentzian distribution and the I_D/I_G ratio was calculated for each sample. As is shown in **Figure 4.10**, the I_D/I_G ratio increased from 0.54 for non-functionalized CNT fiber up to 0.74 for the sample functionalized with AA and AN, showing successful chemical functionalization of these groups on the side wall of CNT. Additionally, to support this conclusion, a shoulder known as

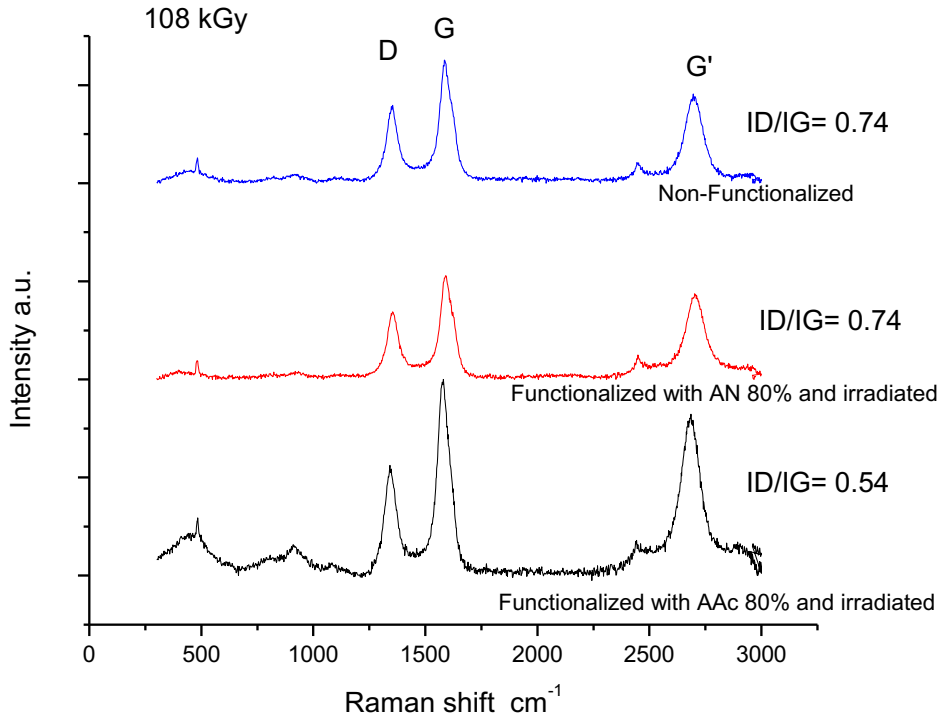

Figure 4.10 Raman spectroscopy results for CNT yarns: pristine, irradiated with aqueous solution of AN 80% at 108 kGy, and irradiated with aqueous solution of AA 80% at 108 kGy

D’ peak was observed around 1613 cm^{-1}. For the samples functionalized, this peak became more prominent than the D’ found for the non-treated one (**Figure 4.11**). Shi et al. also observed this in their investigation of successfully grafting poly(styrene-co-acrylonitrile) onto MWCNTs. The presence of the shoulder is an indication of an increase in the number of defects.[26] These results are in agreement with the I_D/I_G ratio and it is probably related to the e-beam irradiation breakage of the C=C bonds in the graphitic wall where the growth of polymer chains is initiated.[27]Another information from the Raman spectra is the G’ peak at a shift of close to 2700 cm^{-1}. The full width at half maximum (FWHM) of G’ peak gives information on the level of graphitization of the material since G’ is correlated with the electronic band structure of graphitic material. There was a decrease of the G´ peak FWHM from 117.51 cm^{-1} (non-functionalized sample) to 109.51 cm^{-1} (irradiated at 108 kGy at the presence of 80% AN solution) and 105cm^{-1} (irradiated at 108 kGy at the presence of 80% AA solution) (**Figure 4.10**). This is because of damage onto graphitic structure through covalent bond formation with functional groups originated from the vinyl monomers as well as crosslinking.

Figure 4.12 illustrate the morphology of CNT yarns before and after e-beam irradiation with vinyl monomers through SEM imaging. **Figure 4.12** (a, c, e) indicate the surface structure of the CNT yarns all at magnification of 5k, while **Figure 4.12** (b, d, f) show the internal morphology by imaging at the yarn cross-section milled by Gallium(III) ion beam, all at magnification of 50k. Images of both yarns functionalized with AN and AA showed a considerable amount of polymer

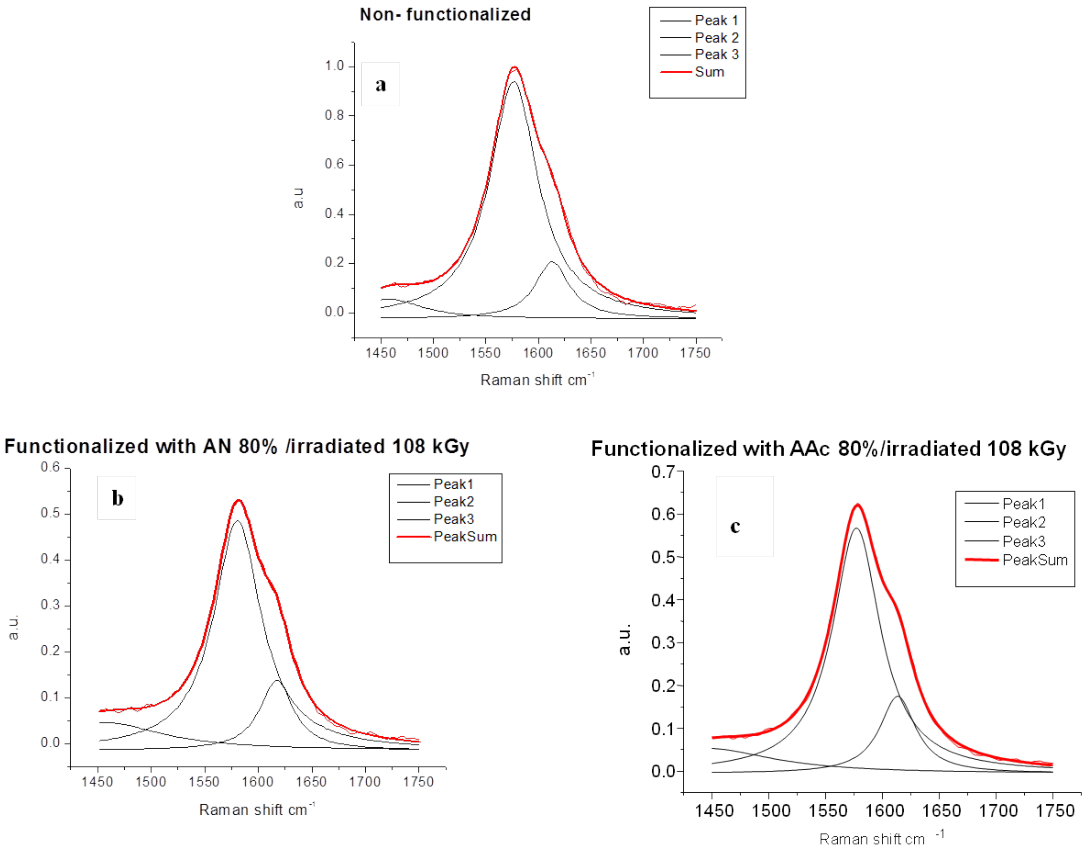

Figure 4.11 G peak of CNT yarns: (a) non functionalized, (b) irradiated at 108 kGy with aqueous solution of AN 80%, and (c) irradiated at 108 kGy with aqueous solution of AA 80%

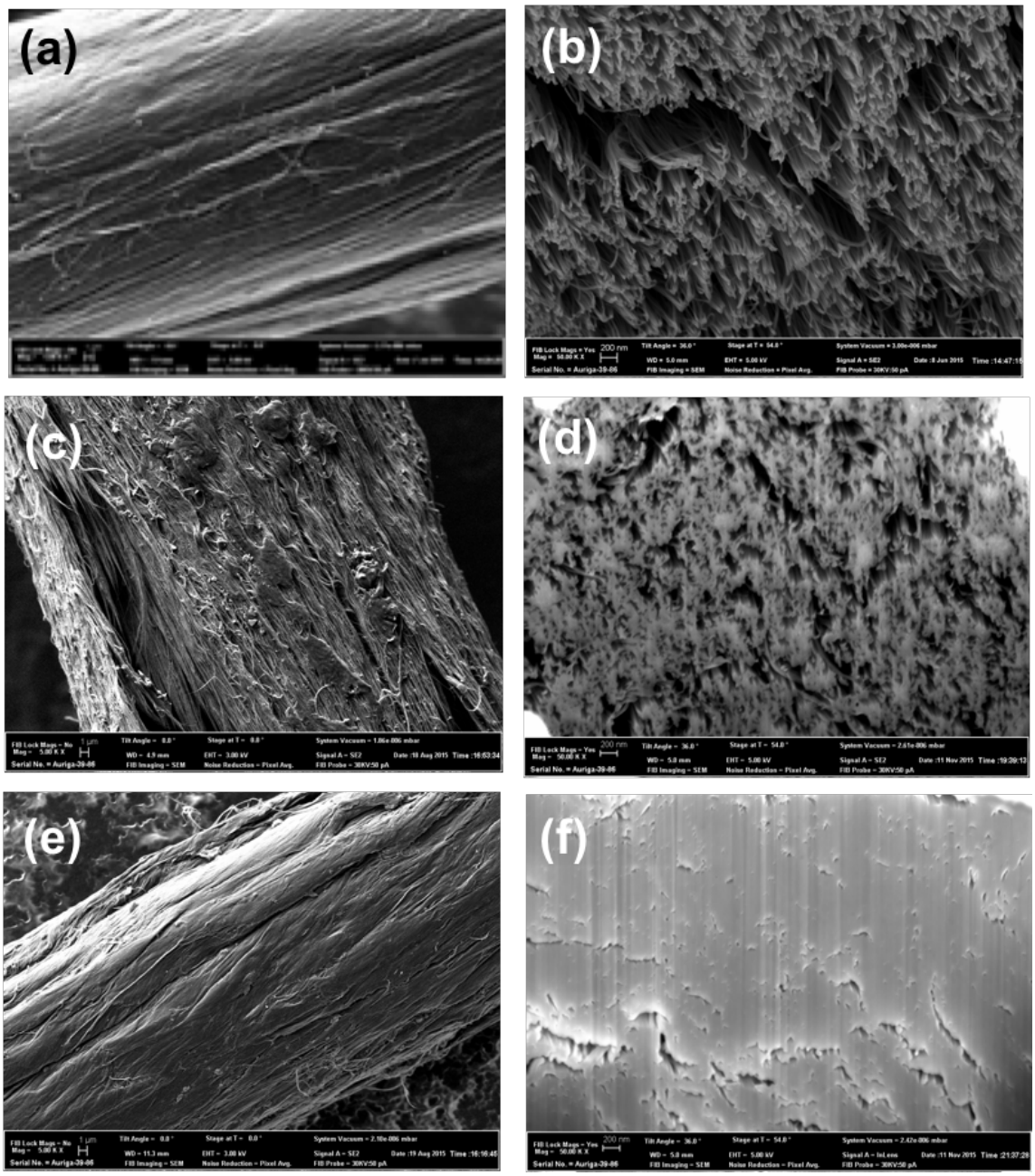

Figure 4.12 SEM images of surface morphology (left column a,c,e) and cross-sections (right column b,d,f) of CNT yarns at the same magnification (5k). (a,b) Pristine CNT yarn; (c,d) irradiated at 108 kGy with aqueous solution of AN 80%; and (e,f) irradiated at 108 kGy with aqueous solution of AA 80%

deposition on the fiber surface in **Figure 4.12** (c and e). The CNT fiber functionalized with AN showed more roughness on the surface in **Figure 4.12** (c), while the CNT fiber functionalized with AA exhibited a smoother appearance in **Figure 4.12** (e). This morphology change can be related to surface damage caused by e-beam irradiation and functional groups repulsion. On the FIB images, it is evident that the grafting polymerization occurred on the internal bundles in the fiber structure **Figure 4.12** (d,f) compared with that of the non-functionalized in **Figure 4.12** (b). In detail, the cross-section of non-functionalized CNT yarn showed high percentage of void content between the aligned CNTs and their bundles. On the other hand, the fiber irradiated and grafted with PAN in **Figure 4.12** (d) exhibited slightly more compact structure, with some bundles visibly joinedtogether. The surface of the larger bundles formed after irradiation showed a fuzzy network structure absent in the pristine sample, which was attributed to polymers and oligomers. Therefore, the modification happens not only on the surface but also inside the structure of the fiber. Similar phenomenon is observed in the FIB images of the samples modified with AA, as presented in **Figure 4.12** (f). The grafted PAA oligomers lead to such a good adhesion that there is left with almost no empty spaces between the CNT bundles and the PAA phase.

The tensile strength and modulus of the e-beam functionalized CNT yarns are presented in **Figure 4.13**. There was an increase in strength from 250 ±27 MPa for the non treated to 350±67 MPa after the modification of the yarn structure with PAN and the modulus from 8.8±1.2 GPa to 15.4±1.2 GPa, respectively, mainly

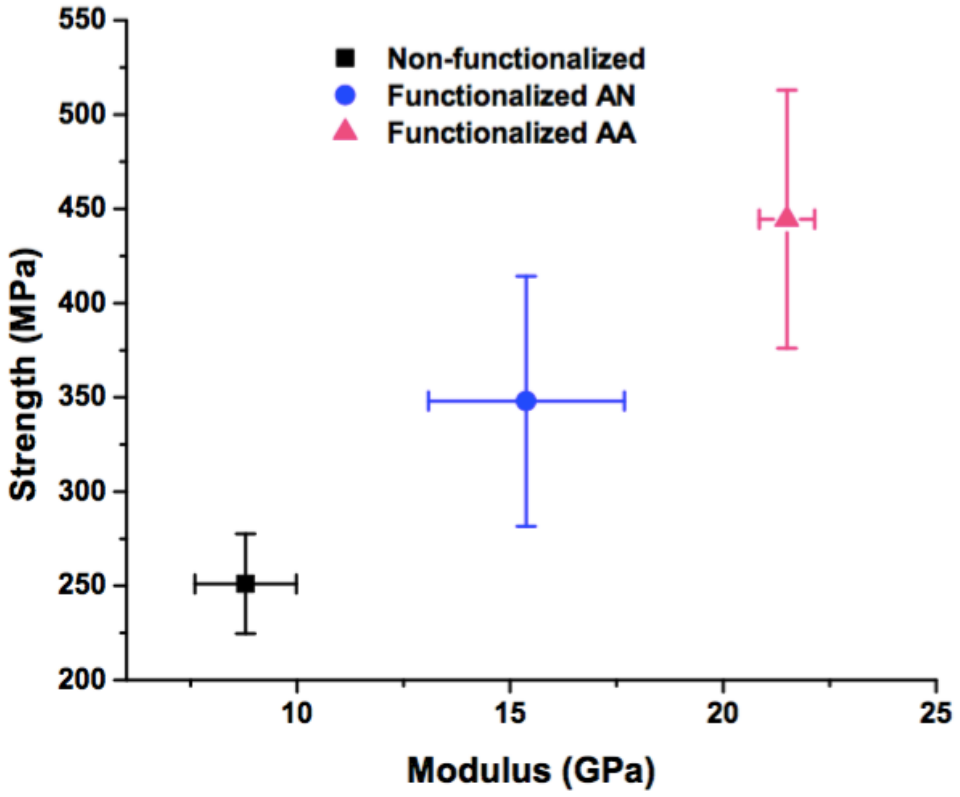

Figure 4.13 Tensile properties of CNT yarns: pristine, irradiated at the presence of AN, and irradiated at the presence of AA

due to the decreased empty spaces and enhanced friction between the CNT bundles. The cross linking that might occur at nitrogen the =C=N- functionality could also contribute to the improvement.[28]

A better result was achieved with radiation grafting polymerization using aqueous solution of AA 80%. These samples showed an increase in the strength from 250 ±27 MPa for the pristine to 440±70 MPa and the modulus from 8.8±1.1 to 21.5±0.7, respectively. The advantageus result over PAN grafted CNT yarns can be correlated to the morphology observed in **Figure 4.12** (f), where the Poly (AA) species grafted onto the CNT visibly filled in the empty spaces in the CNT fiber. The high compactness of the fiber structure along with enhanced adhesion due to the nature of PAA lead to more effective inter-bundle and inter-tube stress transfer. In addition to radiation graft polymerization, possible crosslinks could form between PAA on the basis of anhydride formation.[27]

4.4 Conclusion

The effect of e-beam irradiation and associated functionalization was investigated on CNF and CNT yarns. Irradiation of CNT fiber in air lead to changes in morphology of the fiber, such as disordering, scissions, welding, and crosslinking. Stiffness of the fiber was enhanced yet the strength was lowered after irradiating at 300 kGy. Adjustment on the irradiation process and the counter balancing effects could potentially lead to increased strength of CNT yarns. A preliminary study on e-beam induced functionalization of PAN/PAA polymers on CNF powders concluded that intermediate concentration (40 % v/v) of monomer

solution is most desired for effective functionalization, supported by TGA and XPS. Finally, similar e-beam functionalization was applied on CNT yarns. The covalent functionalization on the CNT surface was confirmed by Raman spectra, and formation of PAN/PAA polymer on CNT was suggested by XPS and visualized by SEM. The presence of grafted polymer in the CNT fiber effectively filled the void spcaces and enhanced load transfer. Especially for the PAA grafted CNTF, 445 MPa of tensile strength was achieved that is 77% higher than the pristine fiber. This chapter demonstrated the potential of e-beam in versatile manipulation of carbon nano-materials to obtain desired functional groups or enhanced mechanical performance.

References

1. Hiremath, N.; Lu, X.; Evora, M. C.; Naskar, A.; Mays, J.; Bhat, G., *Journal of Materials Science* **2016,** *51* (22), 10215-10228.

2. Banhart, F., *Nano Letters* **2001,** *1* (6), 329-332.

3. Suenaga, K.; Wakabayashi, H.; Koshino, M.; Sato, Y.; Urita, K.; Iijima, S., *Nature Nanotechnology* **2007,** *2* (6), 358-360.

4. Moura, C. S.; Balzaretti, N. M.; Amaral, L.; Lacerda, R. G.; Pimenta, M. A., *AIP Advances* **2012,** *2* (1), 012174.

5. Hashimoto, A.; Suenaga, K.; Gloter, A.; Urita, K.; Iijima, S., *Nature* **2004,** *430* (7002), 870-873.

6. Gass, M. H.; Bangert, U.; Bleloch, A. L.; Wang, P.; Nair, R. R.; Geim, A. K., *Nat Nano* **2008,** *3* (11), 676-681.

7. Krasheninnikov, A.; Banhart, F., *Nature materials* **2007,** *6* (10), 723-733.

8. Boncel, S.; Sundaram, R. M.; Windle, A. H.; Koziol, K. K., *ACS nano* **2011,** *5* (12), 9339-9344.

9. Peng, B.; Locascio, M.; Zapol, P.; Li, S.; Mielke, S. L.; Schatz, G. C.; Espinosa, H. D., *Nature nanotechnology* **2008,** *3* (10), 626-631.

10. Kis, A.; Csanyi, G.; Salvetat, J.-P.; Lee, T.-N.; Couteau, E.; Kulik, A.; Benoit, W.; Brugger, J.; Forro, L., *Nature materials* **2004,** *3* (3), 153-157.

11. Miller, S. G.; Williams, T. S.; Baker, J. S.; Solá, F.; Lebron-Colon, M.; McCorkle, L. S.; Wilmoth, N. G.; Gaier, J.; Chen, M.; Meador, M. A., *ACS Applied Materials & Interfaces* **2014,** *6* (9), 6120-6126.

12. Williams, T. S.; Orloff, N. D.; Baker, J. S.; Miller, S. G.; Natarajan, B.; Obrzut, J.; McCorkle, L. S.; Lebron-Colón, M.; Gaier, J.; Meador, M. A., *ACS Applied Materials & Interfaces* **2016**.

13. Evora, M. C.; Klosterman, D.; Lafdi, K.; Li, L.; Abot, J. L., *Carbon* **2010,** *48* (7), 2037-2046.

14. Zou, H.; Yang, Y.; Li, Q.; Zhang, J.; Liu, Z.; Guo, X.; Du, Z., *Carbon* **2002,** *40* (12), 2282-2284.

15. Li, X.; Yang, X.; Jia, L.; Ma, X.; Zhu, L., *Electrochemistry Communications* **2012,** *23*, 94-97.

16. Telling, R. H.; Ewels, C. P.; Ahlam, A.; Heggie, M. I., *Nature Materials* **2003,** *2* (5), 333-337.

17. Zhang, X.; Cao, A.; Sun, Q.; Xu, C.; Wu, D., *Materials Transactions* **2002,** *43* (7), 1707-1710.

18. Fonseca, A. F.; Borders, T.; Baughman, R. H.; Cho, K., *Physical Review B* **2010,** *81* (4), 045429.

19. Filleter, T.; Espinosa, H. D., *Carbon* **2013,** *56* (0), 1-11.

20. Dresselhaus, M. S.; Jorio, A.; Souza Filho, A. G.; Saito, R., *Philosophical Transactions of the Royal Society of London A: Mathematical, Physical and Engineering Sciences* **2010,** *368* (1932), 5355-5377.

21. Ferrari, A. C., *Solid state communications* **2007,** *143* (1), 47-57.

22. Cançado, L. G.; Jorio, A.; Ferreira, E. M.; Stavale, F.; Achete, C.; Capaz, R.; Moutinho, M.; Lombardo, A.; Kulmala, T.; Ferrari, A., *Nano letters* **2011,** *11* (8), 3190-3196.

23. Malard, L.; Pimenta, M.; Dresselhaus, G.; Dresselhaus, M., *Physics Reports* **2009,** *473* (5), 51-87.

24. Xu, Z.; Huang, Y.; Min, C.; Chen, L.; Chen, L., *Radiation Physics and Chemistry* **2010,** *79* (8), 839-843.

25. Beamson, G.; Briggs, D., Wiley: 1992.

26. Shi, J.-H.; Yang, B.-X.; Goh, S. H., *European polymer journal* **2009,** *45* (4), 1002-1008.

27. Zhang, B.; Xie, S.; Wei, R.; Ma, H.; Yu, M.; Li, L.; Li, J., *Science China Chemistry* **2016,** *59* (3), 303-309.

28. Rao, M.; Rao, K., *Radiation Physics and Chemistry (1977)* **1985,** *26* (6), 669-672.

CHAPTER V

PRELIMINARY INVESTIGATION INTO ELECTRON BEAM RADIATION INDUCED CROSSLINKING OF CARBON NANOTUBE FIBER WITH BENZOCYCLOBUTENE-BASED BI- AND POLY-LINKERS

Abstract

Di-functional and multi-functional crosslinkers based on benzocyclobutene were synthesized. Preliminary study on combined effect of e-beam irradiation and BCB crosslinking on CNT materials were performed. Functionalization of MWNT with di-functional crosslinker at e-beam irradiation of 100, 200, and 300 kGy under N_2 was unsuccessful shown by TGA, presumably because of the limited penetration deapth of the beam. Crosslinking of CNTF under e-beam with infiltrated BCB containing polymer at 50, 75 and 105 kGy in air was attempted. The mechanical properties of the resulting fiber were over 100% higher than irradiated CNTF without polymer pretreatment, indicating more effective inter-tube crosslinking and stress transfer caused by polymer infiltration. At higher e-beam dose, the modulus of the fiber increased, while the strengths dropped slightly. This might be attributed to a trade-off between more effective formation of crosslinks and more irradiation damage at high dose. Formation of BCB crosslinked network is also suspected to contribute to improved modulus. More in-depth investigation is required to support the proposed explanations.

5.1 Introduction

Currently, the strengths of carbon nanotube (CNT) macro-assemblies are several magnitudes lower than that of individual CNTs, and challenges remain to realize the true potential of CNTs in useful materials.[1] It is believed that the sliding of the CNTs past one another caused by insufficient inter-tube/inter-bundle interactions is the major limiting factor to effective load transfer in a carbon nanotube fiber (CNTF).[2, 3]

Several strategies have been developed to improve the load transfer between CNTs in a fiber. Solvent densification or physical twisting improves the tensile strength of CNTF by reducing void spaces in a fiber and increasing the contact area between the tubes.[4-7] Collapsing the CNT bundles above a critical pressure improves the interfacial friction, thus show a promising way to reinforce CNTF.[2] Infiltration of polymer into the macro-assembly improves inter-tube load transfer through molecular-level coupling of polymer chains with the tubes.[8, 9] Curing the infiltrated precursors may result in even higher improvement in the strength of CNTF because of the 3D-network generated to lock the CNTs in place.[1, 10, 11] Despite a typical 100% improvement achieved by these strategies, it is still far from unlocking the full potential of CNTs.

Apart from the methods mentioned above, theoretical predictions show that introducing covalent cross-links may improve the strength of CNT fibers and mats by 1-2 orders of magnitude.[12] In practice, such high improvement has only been demonstrated on a bundle scale, within the electron microscope.[13, 14] Several

groups have reported the electron-beam (e-beam) induced crosslinking of CNT macro-assemblies to limit shear-failure of the material.[15-17] The researchers at NASA Glenn Research Center observed 140% improvement in strength of CNTF induced by solely e-beam irradiation in ambient environment, and combining chemical functionalization of hydroxyl groups with e-beam irradiation showed an 200% increase in strength compared to the pristine yarn.[15] Given the fact that e-beam facilities are already widely applied in industry, crosslinking through e-beam irradiation could be a easy and promising method to reinforce the CNTF.

In this chapter, we attempted to utilize commercial e-beam facility to crosslink CNTF at the presence of benzocyclobutene (BCB) di-functional and poly-functional crosslinkers. We searched for crosslinking effects resulted from both the formation of interstitial carbons and irradiation-induced activation of BCB groups. Analyzing mechanical properties of the resulting CNTF provide a preliminary perception on the role of BCB in the process, and evaluated the effectiveness of the proposed method in reinforcement of CNTF.

5.2 Experimental

5.2.1 Materials

MWNT (>99%) powder is manufactured by Cheaptubes Inc. through catalytic chemical vapor deposition (CCVD). CNTF was produced by University of Cincinnati through a proprietary process and were used as received. The pristine

fiber is a research grade material, with tensile strength of around 70 MPa, density of lower than 1g/m^3, and electrical resistivity of around $1\times10^{-5}\ \Omega\cdot$m.

4-Bromo-benzocyclobutene (4-Br-BCB) (>99.5%) was purchased from Shanghai Medicilon Inc. 1,4-Benzenediboronic Acid (96%) was provided by Alfa Aesar. Tetrakis(triphenylphosphine) Palladium (0) (99%) was acquired from Acros Organics. Potassium Carbonate (ACS reagent) was purchased from Acros Organics.

5.2.2 Synthesis of bi-crosslinker 1,4-dibenzocycobutenyl-benzene (diBCB)

The bi-functional crosslinker was synthesized through Suzuki coupling reaction, as demonstrated by **Scheme 5.1**. In a typical reaction, 26.5 g 4-Br-BCB (144.8 mmol), 4.8 g diboronic acid (28.96 mmol), and 2.0g [Pd (0)] catalyst (1.448 mmol) were introduced to the reactor with 100 mL of THF. 12.0 g (86.88 mmol) K2CO3 was dissolved to 55 mL deionized water and the solution was transferred to the reactor. The bi-phase mixture was stirred vigorously and allowed to reflux at 80 °C for 24 hrs. After terminating the reaction, the organic layer was separated and extracted with saturated $NaHCO_3$ solution, subsequently dried by $MgSO_4$ overnight. The solution was slightly increased in concentration using rotorvap, and allowed to rest for 1h until light yellow crystals formed. The light-yellow crystals were vacuum-filtered from the mixture and dried in the vacuum oven to remove excess solvent residue. 3.8 g diBCB was acquired with a yield of 46%.

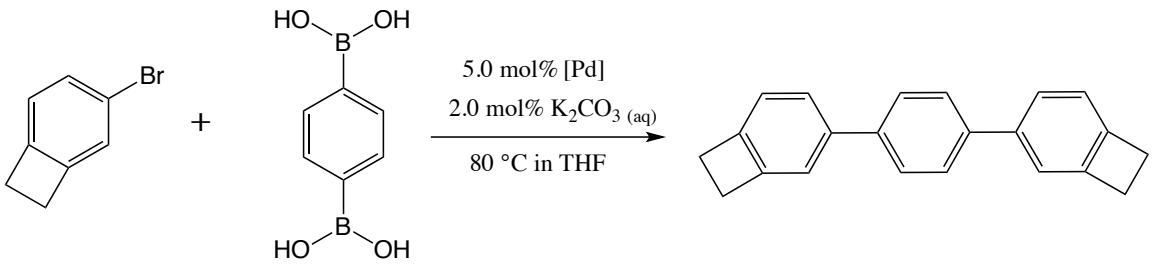

Scheme 5.1 Suzuki coupling to synthesize diBCB

The chemical structure of diBCB was confirmed by ^{1}H and ^{13}C NMR, as shown in **Figure 5.1**. ^{1}H NMR (500 MHz, $CDCl_3$, δ): 7.11-7.48 (Ar H of BCB), 7.60 (Ar H of phenyl in the middle), 2.85-3.20 (CH_2 of BCB). ^{13}C NMR (500 MHz, $CDCl_3$, δ): 146.27, 144.95, 140.87, 139.89, 127.51 (4C), 125.99, 122.75, 121.41. The exact molar mass ($[M+H]^+$ m/z=283.11 Da) was examined by DART-MS.

5.2.3 Synthesis of poly-crosslinker poly (4-vinyl benzocyclobutene) (PVBCB) and poly(styrene-r-4-vinylbenzylcyclobutene) (PS-VBCB)

The polymer crosslinkers were synthesized by anionic polymerization as reported with minor modification.[18] The detail was discussed in section 2.2.2. The molecular weight of PVBCB is 50kDa, and that of PS-VBCB is 16.7 kDa determined by size exclusion chromatography. In the copolymer PS-VBCB, a styrene: BCB ratio of 1:4 in the polymer was confirmed using integrated peaks of ^{1}H NMR. The styrene units are incorporated into the polymer to suppress intramolecular crosslinking of BCB polymer and formation of collapsed polymer nanoparticles.

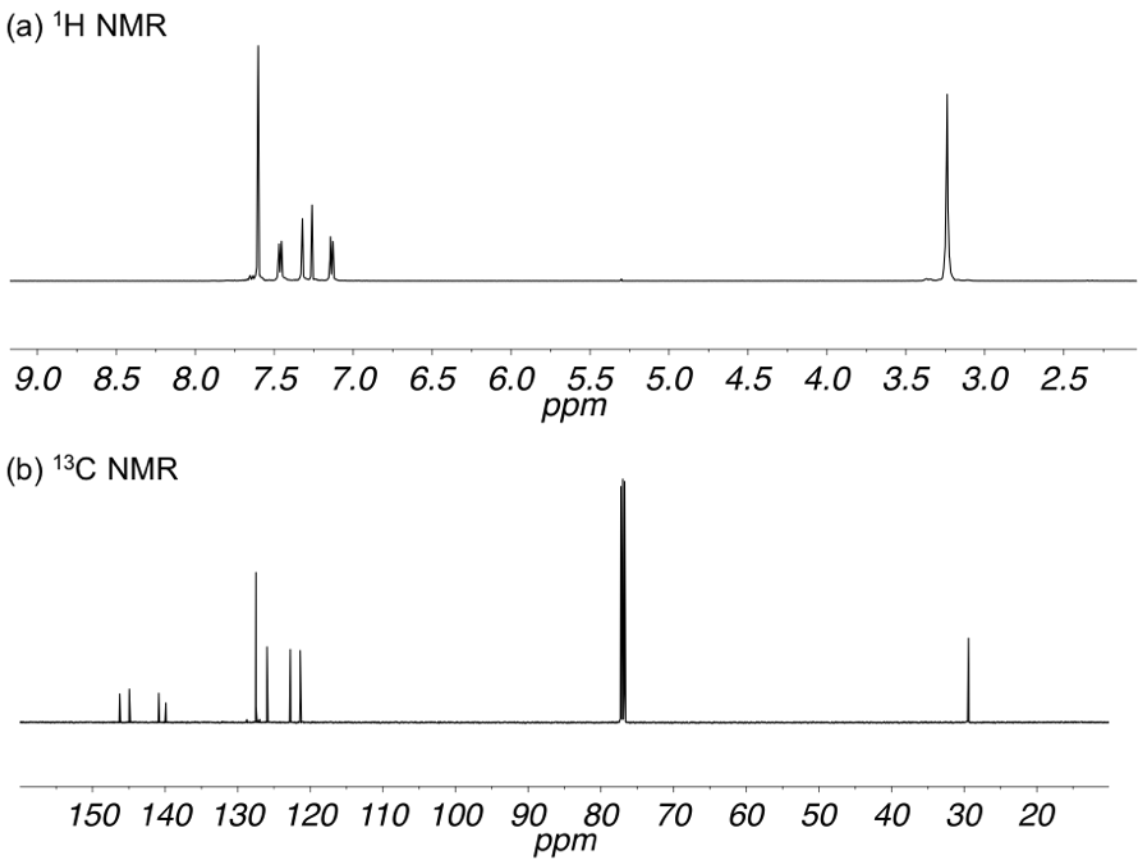

Figure 5.1 NMR spectra of diBCB, (a) ^{1}H NMR, and (b) ^{13}C NMR

5.2.4 E-beam irradiation of MWNT powder with the presence of BCB

To prepare a mixture of MWNT and diBCB as homogeneous as possible, MWNT powder and diBCB of the same weight (80mg) were mixed in a beaker with $CHCl_3$ just covering the solid to assist dispersion. The suspension was sonicated by Fisher Scientific ultrasonic cleaner for 10 mins, and subsequently allowed the solvent to evaporate in air. The mixture was further dried in vacuum oven overnight. The e-beam irradiation of MWNT powder was performed using EBLab (EBEAM, Comet Group) under nitrogen gas protection. The mixture of MWNT and diBCB was tapped flat in a small aluminum cup and placed on the sample tray. As shown in **Figure 5.2**, the sample tray is inserted into the chamber from the right and it was transferred to the center of the beam automatically. The desired dose of 100, 200, and 300 kGy was put into the system, and the process parameters such as tray speed and beam current were calculated automatically by the EBEAM facility, with beam energy held constant at 200 keV. After irradiation, the powder was rinsed with copious amount of THF to remove unreacted diBCB.

5.2.4 E-beam irradiation of CNTF with the presence of poly-crosslinkers

A 40 cm long CNTF was first infiltrated with 0.1% wt solution of PCBCB (50k) or PS-VBCB (16.7k) in toluene for 1 hr. Subsequently, the fiber was taken out of the solution and dried in vacuum oven to remove excess solvent. The polymer infiltrated CNTFs were irradiated with electron beam generated from an industrial accelerator operated by NEO Beam Mercury Plastics Inc. (Middlefield,OH). The ends of the polymer impregnated fibers were taped on a

Figure 5.2 EBEAM facility by the Comet Group for laboratory scale e-beam applications.

cardboard while stress was applied to keep the fiber straight with a layer of aluminum foil for protection. The cardboard was allowed to be placed in the continuous production line (moving at a rate of 48 feet/min) and exposed to electron beam in air at 27 kGy/pass. with dose rate of 5 kGy/s. The beam energy was 3.8 MeV, and the pulse current was 38.3 mA. The samples were irradiated at approximately 50, 75, and 100 kGy by passing through the beam chamber multiple times.

5.2.5 Characterization

Thermogravimetric analysis (TGA) (Discovery TGA-MS, TA Instrument) was used to analyze the content of linker on treated CNT, at a ramp rate of 10 °C/min to 1000 °C in nitrogen.

The tensile properties of CNTFs were assessed on a MTS single filament tensile tester, with gauge length of 25mm and extension rate of 0.2mm/min. The diameters of the fibers were measured with 500× optical microscope and used to calculate the ultimate strength (breaking force/ ($0.25\pi d^2$)). Eight specimens from each yarn sample were tested and the average of the results was reported.

5.3 Results and discussion

5.3.1 Failure of functionalization and crosslinking of BCB on MWNT using e-beam

The MWNT irradiated with diBCB at 100, 200, and 300 kGy were examined by TGA-MS. Surprisingly, none of these three samples showed any weight loss

that should correspond to covalently grafted diBCB molecules and crosslinked oligomers, as in **Figure 5.3**. A possible explanation is the low penetration depth limited by beam energy of 200 MeV. According to the calculations, for a material with a density of 1 g/cm^3, the dose magnitude is decreased by 60% at 250 μm, and becomes completely zero at 380 μm. The mixture of MWNT and diBCB was in clumps and agglomerates instead of fine powder. Even after tapping with spatula, the thickness of the sample that went through irradiation was several millimeters, indicating only a layer of material on the surface received enough dose.

5.3.2 Effect of e-beam initiated BCB functionalization and crosslinking on CNTF

The mechanical properties of CNTF irradiated with PS-VBCB copolymer at different doses in air were compared with pristine CNTF, PS-VBCB infiltrated CNTF, and simply irradiated CNTF, as illustrated in **Figure 5.4**. Generally, irradiation of CNTFs in air weakens their tensile strength, but could possibly have a positive effect on elastic modulus. Specifically, e-beam irradiation of 100 kGy cased both strength and stiffness of pristine CNTF to decrease, by 58% and 23%, respectively. The decrease in properties is likely due to overwhelming oxidative damages introduced onto the structure with respect to desired inter-tube crosslinkings, and these damages become failure sites upon tensile loading. Infiltration of PS-VBCB polymer into the fiber slightly enhances both the stiffness (from 5.8$\pm$2.0 to 7.8$\pm$4.9 GPa) and strength (from 220$\pm$19 to 260$\pm$35 MPa)

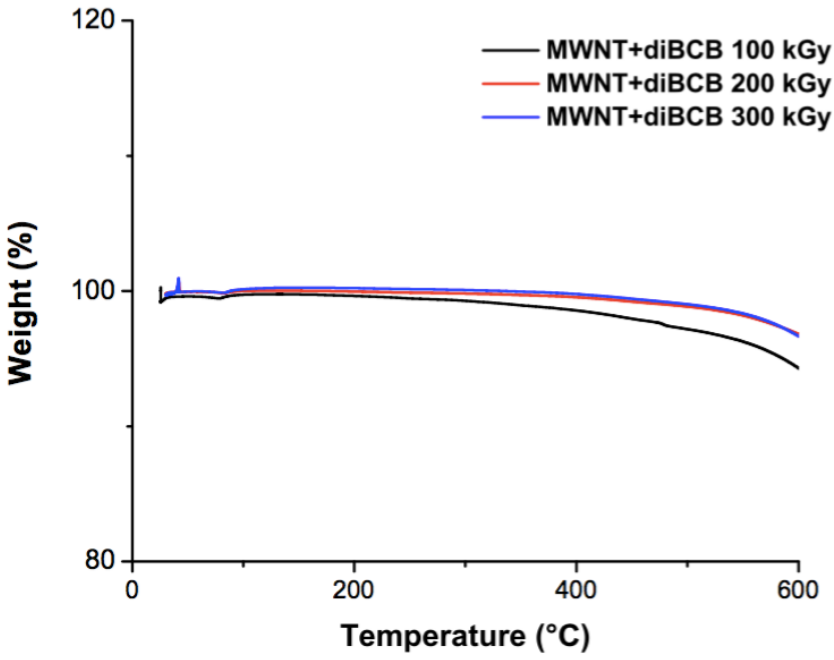

Figure 5.3 TGA curve of MWNT powder irradiated with diBCB at 100, 200, and 300 kGy

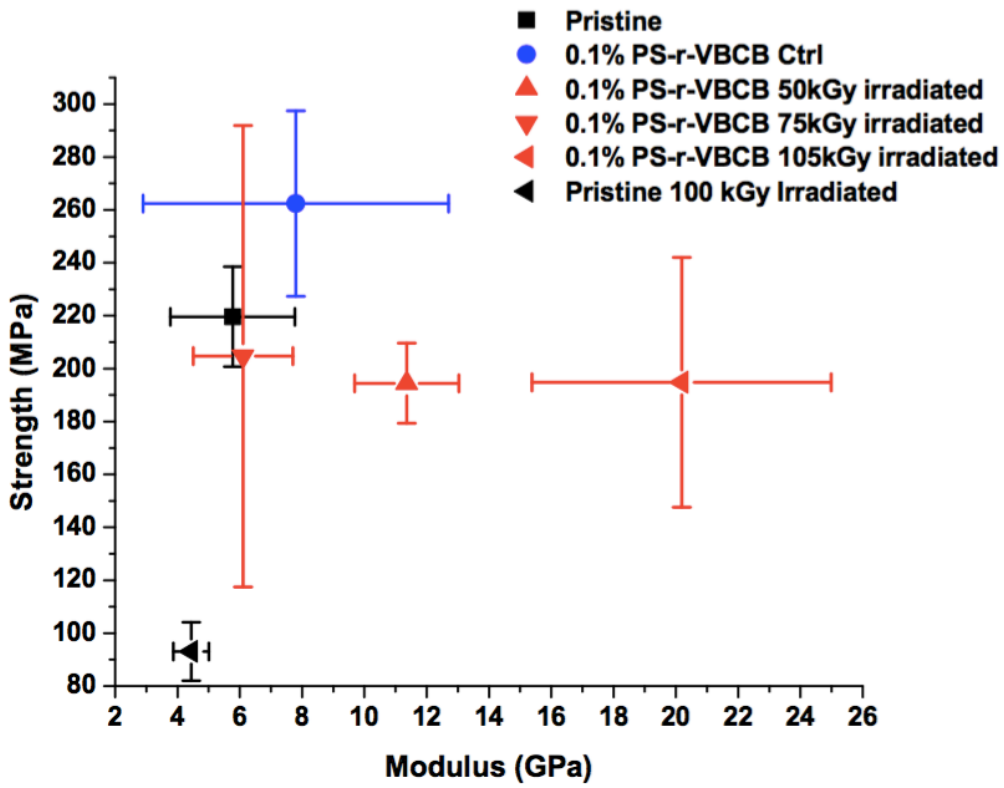

Figure 5.4 Tensile strengths and moduli of CNTF irradiated at the presence of infiltrated PS-VBCB poly-crosslinker at 50, 75 and 105 kGy dose of e-beam compared to pristine CNTF, non-irradiated control, and non-treated CNTF irradiated at 100 kGy

However, after irradiation with e-beam at 50 kGy, the average mechanical performance decrease again. The CNTF with PS-VBCB irradiated at 50 kGy has similar elastic modulus to Pristine CNTF without any treatment, and the tensile strength is slightly lower than the pristine. Further increasing the irradiation dose (to 75 and 105 kGy) does not show significant effect on the strength of the fiber, yet the stiffness is greatly enhanced, by 250% in the 105 kGy irradiated CNTF/PS-VBCB sample compared to the pristine. This could be partially due to more formation of BCB crosslinked network as the irradiation dose increases, which prevents the bundles from shifting in position. In order to discuss the role of polymer in this process, we may compare the fibers with and without the presence of PS-VBCB irradiated at similar dose (approximately 100 kGy). Though both of them exhibit lower strength than the non-treated pristine CNTF, the irradiated fiber without polymer decreased by 58% while the alternative showed a minor decrease of 11%. A major reason for this difference could be the higher level of compactness in the structure of the polymer infiltrated CNTF, allowing more formation of inter-tube linking to balance out the irradiation induced defects. The positive effect of polymer also suggests that the BCB units in the polymer might have gone through crosslinking with the CNTs.

Similar experiments were carried out for PVBCB homo polymer crosslinkers with a molecular weight of 50 kDa, with the results shown in **Figure 5.5**. In general, the ability of “protection” against irradiation damage of PVBCB is lower than PS-VBCB. Unlike PS-VBCB infiltrated CNTF, as the dose increases for irradiation of

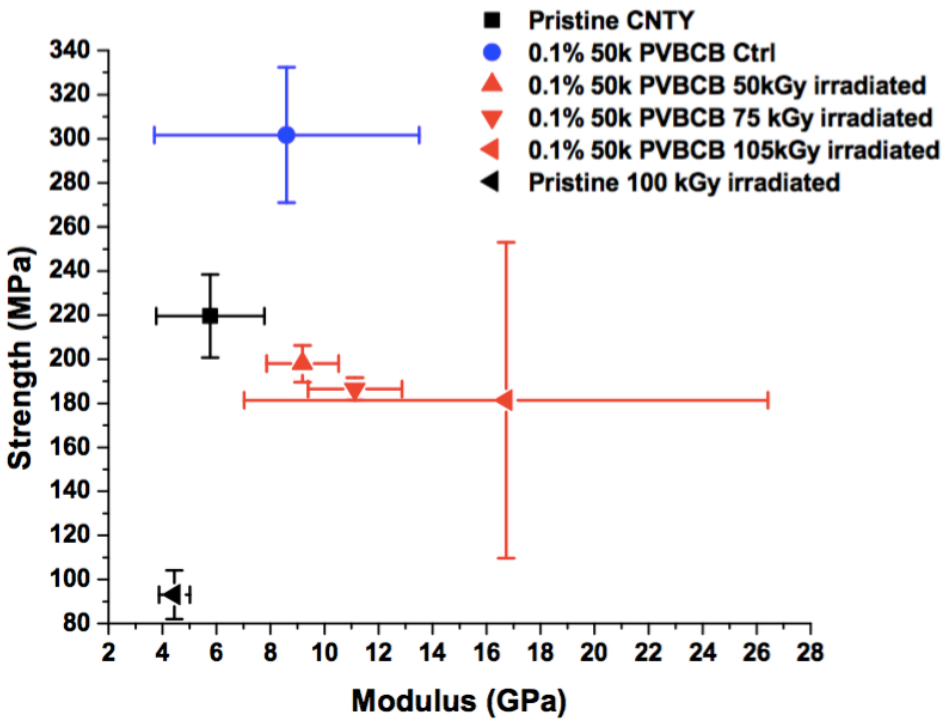

Figure 5.5 Tensile strengths and moduli of CNTF irradiated at the presence of infiltrated PVBCB poly-crosslinker at 50, 75 and 105 kGy dose of e-beam compared to pristine CNTF, non-irradiated control, and non-treated CNTF irradiated at 100 kGy

PVBCB-infiltrated CNTF, the average increase in stiffness is not as significant (190% for sample irradiated at 105 kGy compared to the pristine) with a high standard variation. Though it is natural that the rigid materials exhibit statistical mechanical performance,[19] the randomness in this specific sample is still unusual. One possible factor is the higher molecular weight and higher BCB crosslinking density in the PVBCB polymer than PS-VBCB. Assuming that the BCB crosslinking did occur, the probability of forming highly crosslinked polymer nanoparticles is greater for homopolymer, which contributes negatively to the mechanical properties of the resulting CNTF. Further investigation is required to support this proposed explanation.

5.4 Conclusion

In summary, this chapter presented preliminary results on e-beam irradiation of CNT materials in the presence of BCB crosslinkers. MWNT was mixed with di-functional crosslinker and exposed to e-beam irradiation at 100, 200, and 300 kGy under N_2, yet no significant grafting was observed from TGA data. The failure of the grafting may be attributed to limited penetration of the beam. CNTF was infiltrated with BCB containing poly-crosslinkers and irradiated at 50, 75 and 105 kGy in air. The infiltration step lead to more compact structure of CNTF, resulting in more effective crosslinking in the structure and caused less damage, as compared to irradiated CNTF without polymer pretreatment. As dose increased, the modulus of the fiber also increased, while the strengths dropped slightly. This was attributed to a trade-off between formation of crosslinks and irradiation

damage. In addition, formation of BCB crosslinked network could contribute to higher modulus as well. Further characterization is awaiting to support the proposed explanations.

References

1. Boncel, S.; Sundaram, R. M.; Windle, A. H.; Koziol, K. K., *ACS nano* **2011,** *5* (12), 9339-9344.

2. Zhang, X.; Li, Q., *Acs Nano* **2009,** *4* (1), 312-316.

3. Salvetat, J.-P.; Briggs, G. A. D.; Bonard, J.-M.; Bacsa, R. R.; Kulik, A. J.; Stöckli, T.; Burnham, N. A.; Forró, L., *Physical Review Letters* **1999,** *82* (5), 944.

4. Li, S.; Zhang, X.; Zhao, J.; Meng, F.; Xu, G.; Yong, Z.; Jia, J.; Zhang, Z.; Li, Q., *Composites Science and Technology* **2012,** *72* (12), 1402-1407.

5. Liu, K.; Sun, Y.; Zhou, R.; Zhu, H.; Wang, J.; Liu, L.; Fan, S.; Jiang, K., *Nanotechnology* **2010,** *21* (4), 045708.

6. Koziol, K.; Vilatela, J.; Moisala, A.; Motta, M.; Cunniff, P.; Sennett, M.; Windle, A., *Science* **2007,** *318* (5858), 1892-1895.

7. Zhang, M.; Atkinson, K. R.; Baughman, R. H., *Science* **2004,** *306* (5700), 1358-1361.

8. Jung, Y.; Kim, T.; Park, C. R., *Carbon* **2015,** *88* (0), 60-69.

9. Liu, K.; Sun, Y.; Lin, X.; Zhou, R.; Wang, J.; Fan, S.; Jiang, K., *ACS nano* **2010,** *4* (10), 5827-5834.

10. Ryu, S.; Lee, Y.; Hwang, J. W.; Hong, S.; Kim, C.; Park, T. G.; Lee, H.; Hong, S. H., *Advanced Materials* **2011,** *23* (17), 1971-1975.

11. Cui, Y.; Zhang, M., *ACS applied materials & interfaces* **2013,** *5* (16), 8173-8178.

12. Åström, J.; Krasheninnikov, A.; Nordlund, K., *Physical review letters* **2004,** *93* (21), 215503.

13. Peng, B.; Locascio, M.; Zapol, P.; Li, S.; Mielke, S. L.; Schatz, G. C.; Espinosa, H. D., *Nature nanotechnology* **2008,** *3* (10), 626-631.

14. Kis, A.; Csanyi, G.; Salvetat, J.-P.; Lee, T.-N.; Couteau, E.; Kulik, A.; Benoit, W.; Brugger, J.; Forro, L., *Nature materials* **2004,** *3* (3), 153-157.

15. Miller, S. G.; Williams, T. S.; Baker, J. S.; Solá, F.; Lebron-Colon, M.; McCorkle, L. S.; Wilmoth, N. G.; Gaier, J.; Chen, M.; Meador, M. A., *ACS Applied Materials & Interfaces* **2014,** *6* (9), 6120-6126.

16. Williams, T. S.; Orloff, N. D.; Baker, J. S.; Miller, S. G.; Natarajan, B.; Obrzut, J.; McCorkle, L. S.; Lebron-Colón, M.; Gaier, J.; Meador, M. A., *ACS Applied Materials & Interfaces* **2016**.

17. Wang, S., 2006.

18. Sakellariou, G.; Baskaran, D.; Hadjichristidis, N.; Mays, J. W., *Macromolecules* **2006,** *39* (10), 3525-3530.

19. Lu, W.; Zu, M.; Byun, J. H.; Kim, B. S.; Chou, T. W., *Advanced Materials* **2012,** *24* (14), 1805-1833.

CHAPTER VI

CONCLUSION

In summary, this dissertation is focused on enhancing the interaction between the CNTs and their bundles in a macro-assembly (e.g. fibers, mats) through chemical methods and irradiation, with the goal of improving the tensile properties of the material.

First, a novel and simple one-step solid-state chemical crosslinking process was developed to improve stiffness and strength of CNTF using a BCB-based polymer. By infiltration of the polymer linker into CNTF followed by heating, covalent functionalization of CNTF with the BCB moiety was achieved with simultaneous inter-CNT crosslinking, confirmed by TGA, DSC, and XPS. Since the CNT bundles were covalently locked in a rigid network, an increase in mechanical properties is observed. The process remarkably improves the specific tensile strength by 40% and traditional tensile strength by 230%. These improvements are not only attributed to the process of polymer infiltration and solvent densification, but are also directly related to simultaneous functionalization and inter-tube linking, as observed by SEM images. This reaction employed required no catalyst, and releases no byproducts, showing promise in large scale reinforcement of CNTF.

Furthermore, we extended the investigation on the proposed BCB-induced crosslinking of CNTF to find the optimum process condition. By varying the PS content in the random copolymer and applying to the CNTF, we found that “Dilute” BCB in the polymer was favored. Best mechanical properties of the crosslinked CNTF was yielded from copolymer with non-reactive PS content of 80%. The

concentration of the polymer solution for infiltration into CNTF was optimized to 0.05% wt or 0.1% wt in toluene, corresponding to between 3% wt and 7% wt of infiltrated polymer inside the CNTF, respectively. SEM imaging of the surface structure of thermally treated CNTF revealed lower bundle size than the sample prior to heating. For the PS infiltrated CNTF, the smooth layer of polymer covering the CNT bundles toggled into polymer agglomerates. Both of them could be responsible for the drop in tensile strength.

In addition of chemical treatment, the effect of e-beam irradiation and associated functionalization was investigated on CNF and CNT yarns. Irradiation of CNT fiber in air lead to changes in morphology of the fiber. Stiffness of the fiber was enhanced yet the strength was lowered after irradiating with e-beam at 300 kGy. Adjustment on the irradiation process could potentially lead to increased strength of CNT yarns. A preliminary study on e-beam induced functionalization of PAN/PAA polymers on CNF powders concluded that intermediate concentration (40 % v/v) of monomer solution is most desired for effective functionalization, supported by TGA and XPS. Subsuquently, similar e-beam functionalization was applied on CNT yarns. The covalent functionalization on the CNT surface was confirmed by Raman spectra, and formation of PAN/PAA polymer on CNT was suggested by XPS and visualized by SEM. The presence of grafted polymer in the CNT fiber effectively enhanced load transfer. Specifically, the strength of PAA grafted CNT was improved by 77%.

Finally, combining the BCB chemistry with e-beam functionalization at increasing doses indicate that the modulus increased and the strength dropped, similar to observations in CNTF only irradiated. This investigation demonstrated the vast potential of e-beam on altering the carbon nanostructures, especially if combined with chemical functionalizations.

VITA

Xinyi Lu was born in Dalian, China in 1990, and spent her childhood in several places, including Yokohama (Japan), and Bochum (Germany). After returning to her hometown, she studied at Yuming High School and then attended the Dalian University of Technologies, for her Bachelors of Science degree in chemical engineering, with focus on polymer science and technologies. After she graduated from DUT in June 2012, She joined the graduate program at UT the following fall to pursue her doctorate degree in Polymer Chemistry under the direction of Dr. Jimmy Mays. Her research expertise is in functionalization of carbon nanostructures and anionic polymerization. In May 2017, she completed the requirements for doctoral degree in chemistry.